

THE EFFECT OF HIGHER MODES ON EARTHQUAKE FATIGUE DAMAGE  
TO STEEL MOMENT FRAMES

by

Navid Nastar

---

A Dissertation Presented to the  
FACULTY OF THE GRADUATE SCHOOL  
UNIVERSITY OF SOUTHERN CALIFORNIA  
In Partial Fulfillment of the  
Requirements for the Degree  
DOCTOR OF PHILOSOPHY  
(CIVIL ENGINEERING)

May 2008

Copyright 2008

Navid Nastar

# DEDICATION

TO MY FATHER AND MOTHER

## **ACKNOWLEDGEMENTS**

The author would like to thank Professor James C. Anderson and Professor Gregg E. Brandow for their expertise and continuous support at all stages of this research. Without their guidance, completing this work would not have been possible. Thanks are also due to Professor Robert L. Nigbor for being a tremendous source of support and inspiration for the author during his graduate work at USC. The author also wants to thank Mr. Peter Maranian of Brandow and Johnston, Inc. for his interest in the project and for providing helpful resources throughout the course of study. Lastly, the author would like to acknowledge Mr. James Partridge, president of Smith-Emery Company, for kindly providing the low-cycle fatigue test results and related reference materials.

# TABLE OF CONTENTS

DEDICATION	ii
ACKNOWLEDGEMENTS	iii
LIST OF TABLES	vi
LIST OF FIGURES	vii
ABSTRACT	xii
CHAPTER 1: INTRODUCTION	1
CHAPTER 2: BACKGROUND	6
CHAPTER 3: DESCRIPTION OF THE ANALYTICAL CASE STUDIES	12
3.1 Description of the Investigated Buildings	12
3.2 Damage Observed During the Northridge Earthquake	16
3.2.1 Ten-Story Building	16
3.2.2 Two-Story Building	
3.3 Analytical Studies	21
CHAPTER 4: TIME-HISTORY ANALYSIS	23
4.1 Ground Motion	23
4.2 Ten-Story Building	30
4.2.1 Linear Modal Time-History Analysis	35
4.2.1.1 Damping	39
4.2.1.2 Mass	39
4.2.1.3 Stress Histories and Contribution of Each Mode to Total Stress	41
4.2.1.3.1 Beam Stress	42
4.2.1.3.2 Column Stress	46
4.2.2 Non-Linear Direct Integration Time-History Analysis	49
4.2.2.1 Effect of Material Properties	49
4.2.2.2 Linear vs. Non-Linear Time-History Results	52
4.3 Two-Story Building	57
4.3.1 Linear Modal Time-History Analysis	59
4.3.1.1 Stress Histories and Contribution of Each Mode to Total Stress	59
4.3.1.1.1 Beam Stress	60
4.3.1.1.2 Column Stress	63

CHAPTER 5: FATIGUE ANALYSIS	66
5.1 Fatigue Analysis Procedure	66
5.2 S-N Curve	68
5.2.1 Available Fatigue Test Data	68
5.2.1.1 Tests by Fisher et al.	68
5.2.1.2 Tests by Partridge et al.	71
5.2.1.3 Tests by Kuwamura et al.	73
5.2.2 Stress Concentration Factor	77
5.2.2.1 Available Test Data	78
5.2.2.2 Steel Manuals	78
5.2.2.3 Finite Element Study	81
5.2.2.4 Established Stress Concentration Factor	86
5.2.3 Established S-N Curve for Fatigue Analysis	87
5.3 Cycle Counting Procedure	90
5.3.1 Ten-Story Building	90
5.3.2 Two-Story Building	107
5.4 Cumulative Fatigue Analysis	112
5.4.1 Ten-Story Building	112
5.4.2 Two-Story Building	120
CHAPTER 6: CONCLUSIONS	124
6.1 Conclusions	125
6.2 Future Studies	128
BIBLIOGRAPHY	130
APPENDIX A: TEN-STORY BUILDING DRAWINGS	134
APPENDIX B: TWO-STORY BUILDING DRAWINGS	149

## LIST OF TABLES

Table 5.1	Results of the cumulative fatigue analyses on beams of the ten-story building	112
Table 5.2	Results of the cumulative fatigue analyses on columns of the ten-story building	115
Table 5.3	Results of the cumulative fatigue analyses on beams of the two-story building	121
Table 5.4	Results of the cumulative fatigue analyses on columns of the two-story building	122

## LIST OF FIGURES

Figure 3.1	Site of the two investigated buildings	13
Figure 3.2	Ten-story building	13
Figure 3.3	Two-story building	14
Figure 3.4	Investigated frames of the ten-story building	15
Figure 3.5	Investigated frame of the two-story building	15
Figure 3.6	Typical moment frame connection damage	18
Figure 3.7	Damage observed in the two-story building after the Northridge Earthquake	19
Figure 4.1	Location of the investigated buildings	24
Figure 4.2	Location of the USC 03 station along with all other stations in the region (USGS, CDMG, USC and DWP networks) which recorded the Northridge main event	25
Figure 4.3	Corrected acceleration, velocity, and displacement records in East direction, Northridge main event recorded at USC 03 station	26
Figure 4.4	Corrected acceleration, velocity, and displacement records in South direction, Northridge main event recorded at USC 03 station	28
Figure 4.5	Moment frame on gridline F.5 in East-West direction	31
Figure 4.6	Moment frame on gridline D in East-West direction	32
Figure 4.7	1 <sup>st</sup> mode shape	33
Figure 4.8	2 <sup>nd</sup> mode shape	34
Figure 4.9	3 <sup>rd</sup> mode shape	34

Figure 4.10	Roof displacement result of linear modal time-history analysis (3% damping for all modes)	35
Figure 4.11	Contribution of the 1 <sup>st</sup> mode of vibration to the roof displacement (3% damping for all modes)	36
Figure 4.12	Contribution of the 2 <sup>nd</sup> mode of vibration to the roof displacement (3% damping for all modes)	36
Figure 4.13	Contribution of the 3 <sup>rd</sup> mode of vibration to the roof displacement (3% damping for all modes)	37
Figure 4.14	Acceleration (East) recorded at roof by CDMG station	38
Figure 4.15	Displacement (East) recorded at roof by CDMG station	38
Figure 4.16	Roof response matching	40
Figure 4.17	Roof matched response	41
Figure 4.18	An example of modal stress accumulation	42
Figure 4.19	Beam stress history (contribution of all modes)	43
Figure 4.20	Beam stress history (contribution of the 1 <sup>st</sup> mode)	44
Figure 4.21	Beam stress history (contribution of the 2 <sup>nd</sup> mode)	44
Figure 4.22	Beam stress history (contribution of the 3 <sup>rd</sup> mode)	45
Figure 4.23	Column stress history (contribution of all modes)	47
Figure 4.24	Column stress history (contribution of the 1 <sup>st</sup> mode)	47
Figure 4.25	Column stress history (contribution of the 2 <sup>nd</sup> mode)	48
Figure 4.26	Column stress history (contribution of the 3 <sup>rd</sup> mode)	48
Figure 4.27	The effect of material properties on the result of nonlinear analysis	50
Figure 4.28	The effect of material properties on the result of nonlinear analysis	51

Figure 4.29	The effect of material properties on the column stress history calculated from the non-linear direct integration time-history analysis	51
Figure 4.30	Comparison between the linear and nonlinear analysis results	52
Figure 4.31	Column stress (equivalent M/S stress) history calculated from the nonlinear time-history analysis	53
Figure 4.32	Moving-window Fourier transform of the CDMG roof acceleration record	54
Figure 4.33	Ratio of maximum beam stress (M/S) from linear analysis to the material yield stress	55
Figure 4.34	Ratio of maximum beam stress (M/S) from linear analysis to the material yield stress	55
Figure 4.35	Demand to capacity ratios in the ten-story building result of linear modal time-history analysis using SAP 2000	56
Figure 4.36	Moment Frame on gridline 14 in North-South direction	57
Figure 4.37	1 <sup>st</sup> mode shape	58
Figure 4.38	2 <sup>nd</sup> mode shape	59
Figure 4.39	2 <sup>nd</sup> Floor beam stress history (contribution of all modes)	60
Figure 4.40	2 <sup>nd</sup> floor beam stress history (contribution of the 1 <sup>st</sup> and 2 <sup>nd</sup> modes)	61
Figure 4.41	Roof beam stress history (contribution of all modes)	62
Figure 4.42	Roof beam stress history (contribution of the 1 <sup>st</sup> and 2 <sup>nd</sup> modes)	62
Figure 4.43	2 <sup>nd</sup> floor column stress history (contribution of all modes)	63
Figure 4.44	2 <sup>nd</sup> floor column stress history (contribution of the 1 <sup>st</sup> and 2 <sup>nd</sup> modes)	64
Figure 4.45	Roof column stress history (contribution of all modes)	65

Figure 4.46	Roof column stress history (contribution of the 1 <sup>st</sup> and 2 <sup>nd</sup> modes)	65
Figure 5.1	S-N curves for different beam details	69
Figure 5.2	S-N curves for welded and coverplated beams	70
Figure 5.3	Fatigue crack at the end of cover plate fillet weld toe	70
Figure 5.4	Low-cycle fatigue test setup	72
Figure 5.5	Low-cycle fatigue test results	73
Figure 5.6	Low-cycle fatigue test setup and specimen detail	75
Figure 5.7	Comparison between the available low-cycle fatigue tests	76
Figure 5.8	Fatigue test results	77
Figure 5.9	Stress concentration factors observed in Fisher's tests	79
Figure 5.10	Finite element model of the Pre-Northridge connection without continuity plates	82
Figure 5.11	Result of the finite element study of the model without continuity plates	83
Figure 5.12	Finite element model of the Pre-Northridge connection with continuity plates	84
Figure 5.13	Result of the finite element study of the model with continuity plates	85
Figure 5.14	Established S-N curve for fatigue analysis	88
Figure 5.15	Rainflow histograms for beams of the ten-story building	91
Figure 5.16	Rainflow histograms for columns of the ten-story building	99
Figure 5.17	Rainflow histograms for beams of the two-story building	108
Figure 5.18	Rainflow histograms for columns of the two-story building	110

Figure 5.19	Cumulative fatigue at beams of the ten-story building (1 <sup>st</sup> mode vs. all modes)	114
Figure 5.20	Cumulative fatigue at columns of the ten-story building (1 <sup>st</sup> mode vs. all modes)	115
Figure 5.21	Rainflow histogram blow-up for the 6 <sup>th</sup> floor beam	116
Figure 5.22	Rainflow histogram blow-up for the 7 <sup>th</sup> floor column	117
Figure 5.23	Cumulative fatigue at the column above, the column below and the beam at each floor (all modes)	118
Figure 5.24	Sum of cumulative fatigue values at the column above, the column below and the beam at each floor (all modes)	119
Figure 5.25	Sum of cumulative fatigue values at the column above, the column below and the beam at each floor (1 <sup>st</sup> mode vs. all modes)	119
Figure 5.26	Cumulative fatigue at beams of the two-story building (1 <sup>st</sup> mode vs. all modes)	121
Figure 5.27	Cumulative fatigue at columns of the two-story building (1 <sup>st</sup> mode vs. all modes)	122
Figure 5.28	Sum of cumulative fatigue values at the column above, the column below and the beam at each floor (1 <sup>st</sup> mode vs. all modes)	123
Figure 6.1	Comparison between cumulative fatigue distribution and observed damage in the ten-story building	125
Figure A.1	Ten-story building framing plans	134
Figure A.2	Ten-story building frame elevations	141
Figure B.1	Two-story building framing plans	149
Figure B.2	Two-story building frame elevations	151

## **ABSTRACT**

Following the Northridge Earthquake (1994), the SAC steel project was initiated to investigate the causes of widespread damage observed in the connections of steel moment frame buildings. The published results of these studies concentrated on local connection defects that potentially initiated the observed cracks. However, damage to some buildings could not be reconciled by use of this failure mechanism. This led to renewed interest in the effects of low-cycle fatigue combined with the higher modes of vibration increasing the cumulative fatigue at critical connections and consequently creating the observed connection failures.

The current study is focused on the effect of low-cycle fatigue in the connection damage observed in steel moment frames and the contribution of the higher modes of vibration to these failures. A comprehensive fatigue analysis procedure is developed based on the Palmgren-Miner method. Low-cycle fatigue behavior of Pre-Northridge connections are studied, and S-N curves established for the high-cycle fatigue range are extended to the low-cycle region using the limited test results that are available.

A series of linear and non-linear time-history analyses are performed on two buildings damaged by the Northridge Earthquake. These buildings have two and ten stories, respectively, and used steel moment frames as the lateral load resisting system in both directions. Fatigue analyses are performed at critical locations of the

moment frames using the established procedure, and the contribution of higher modes in cumulative fatigue is evaluated. Finally, the pattern of cumulative fatigue at critical connections and the observed damage are compared.

Results of this analytical study indicate that the effect of low-cycle fatigue and higher modes of vibration can be significant in the connection damage resulting from the Northridge Earthquake. Although the first mode created a high percentage of cumulative fatigue in the connections of the two-story building, the cumulative fatigue and damage pattern in the ten-story building shows that the contribution of higher modes in the beam and column stress histories significantly increased the cumulative fatigue relative to the first mode. This results in various types of connection damage similar to that observed in the steel moment frames during the Northridge Earthquake.

## **CHAPTER 1: INTRODUCTION**

One of the major aftermaths of the Northridge Earthquake of January 17, 1994, was the widespread connection damage that posed a major question regarding the behavior of field-welded, field-bolted moment frame connections, also known as Pre-Northridge connections.

Before the Northridge Earthquake, Steel Moment Resisting Frames (SMRFs) were believed to have ductile behavior that would achieve high-cycle fatigue. As a result, fatigue was not considered to be a failure mode for these connections during a seismic event.

After the Northridge Earthquake and the widespread connection failure in steel moment frame buildings, it was concluded that many connections failed at what appears to be relatively few cycles. Observations after the Northridge Earthquake indicated that these connections failed at both a relatively low stress level and at only a few cycles of vibration.

Appearance of the cracks which in most cases started from the weld at the bottom flange of the beam and on some occasions propagated into the column flange or even column web (as in the case of the two-story building discussed later in this document in which cracks expanded all the way through the column web), undermined the

confidence in the ductile behavior of the steel moment frames [37]. According to a report by Youssef et al. in 1995, brittle fracture in and around the groove weld connecting the beam flanges to the column flange was observed in more than 150 steel moment frame buildings after the Northridge Earthquake [37].

As a result of these failures, many researchers tried to gain a better understanding of the causes of damage observed in the connections of the steel moment frames. Due to the complexity of the problem, the SAC steel project was initiated by FEMA as a joint venture between Structural Engineers Association of California (SEAOC), Applied Technology Council (ATC), and Consortium of Universities for Research in Earthquake Engineering (CUREE). Since the response of the structures is often dominated by the first mode, the SAC project was never focused on the potential effects of higher modes. Consequently, all the performed SAC tests represented the first mode type of motions.

The majority of published results of this nationwide project ([10], [11], [12], [13], [14], [15], [16], [17], [18], [19], and [20]) concentrated on local connection defects that potentially initiated the observed cracks. For instance, the existence of the weld access hole (web cope hole) and discontinuity of the bottom flange weld were shown to be the cause of porosity and slag inclusions in the weld at the center of the beam and potentially one of the main reasons for crack initiation. Also, leaving the backup bar after the beam flange to column flange full penetration welds were completed

(which was the common practice in Pre-Northridge connections) showed to be a source of porosity and slag inclusions and eventually contributed to the initiation of cracks at the weld area [4].

Although remarkable research under the SAC project was performed to address the above issues, damage to some buildings could not be reconciled by use of these failure mechanisms. This led to renewed interest in studying the effects of low-cycle fatigue combined with the higher modes of vibration that can increase the cumulative fatigue at critical connections, and as a result, potentially create the observed connection failures.

Through an investigation of the role of the higher modes in the fatigue damage, the current study focuses on the contribution of higher modes of vibration to the damage observed in steel moment connections during the Northridge Earthquake. In other words, the contribution of higher mode motions to the stress histories at the connection beams and columns is investigated, as are cyclic fatigue type damages. In essence, this study shows that a large number of cycles at higher frequency and at significant but lower stress levels than the primary mode could be a major cause of increasing the cumulative fatigue at the connections of steel moment frames, potentially creating connection failures similar to those observed in the moment connections during the Northridge Earthquake.

As a part of this study, two buildings damaged by the Northridge Earthquake have been investigated. These buildings were two and ten stories, respectively, and used steel moment frames as the lateral load resisting system in both directions.

Chapter two of this document describes the definition of fatigue failure and summarizes the research done in the area of fatigue behavior of steel moment connections and the concept of low-cycle fatigue.

In chapter three of the current document, the analytical case studies are explained and the investigated buildings are described. Also, the observed damage in these buildings is studied.

Chapter four contains a series of linear and non-linear time-history analyses and includes a very thorough analytical study on the stress histories at the critical locations of the buildings. Furthermore, the contribution of each mode of vibration to total stress is investigated.

Chapter five establishes a comprehensive fatigue analysis procedure, which was developed using the *Palmgren-Miner method*. In addition, low-cycle fatigue behavior of Pre-Northridge connections are studied in this chapter, and S-N curves established for the high-cycle fatigue range are extended to the low-cycle region using the limited test results that are available. Fatigue analyses are performed at

critical locations of the moment frames using the established procedure, and the contribution of higher modes in cumulative fatigue is evaluated.

Finally, chapter six summarizes the results of the study and compares the pattern of cumulative fatigue at critical connections to the observed damage. Also, conclusions of this study are included in this section.

## **CHAPTER 2: BACKGROUND**

Although structural steel is an excellent building material that has positive characteristics which make it behave well in many conditions, there are still concerns with its fatigue behavior and possible cyclic fatigue failures of steel components in the scientific community.

The topic of cyclic fatigue has been thoroughly addressed by researchers in the areas of fracture mechanics and material science, resulting in some good publications in these areas. In one of the best books in the field [9], Norman E. Dowling explains the concept and applications of low and high cycle fatigue failures. Most of the examples in this book deal with material steel, which is specifically the focus of the current study. Likewise, Rolfe and Barsom cover the concept of fatigue in a thorough manner in their book [7], which is a classic book on the topic.

Historically, the birth of fracture mechanics goes back to 1920s and studies by Griffith. He studied the fracture behavior of silica glass and focused on the effect of defects in lowering the fracture strength of silica glass. He expressed his theories based on the conservation of energy in a closed system (first law of thermodynamics) [27]. The next steps were taken by Irwin (1948) [24] and Orowan (1945) [28] who worked on the fracture of steel and considered the plastic work done during the fracture.

In general, fatigue is a type of fracture failure which occurs when a material is subjected to cyclic or repeated loading [27], [9]. In other words, structural members subjected to cyclic loading may fail at stress levels lower than expected as a result of the fatigue phenomenon. Fatigue failure can be represented in three simplified steps [27]:

1. Crack initiation: the material transition from the virgin condition to the formation of macro crack.
2. Crack propagation: stable growth of the crack after the crack initiation phase.
3. Final fracture: unstable, rapid growth of the crack.

If there are pre-existing defects in the material, the crack initiation step could be eliminated, causing the total fatigue life to decrease. The three steps explained above could be represented in the form of [27]:

$$N_f = N_i + N_p$$

In the above equation,  $N_f$  represents the number of cycles to failure,  $N_i$  is the number of cycles for crack initiation, and  $N_p$  shows the number of cycles for crack propagation. When the number of cycles to failure is expected to be relatively large (typically larger than  $10^3$  cycles), the concept of *high-cycle fatigue* is often used to

represent the situation. On the other hand, when the number of cycles is not large (typically less than  $10^3$  cycles) the condition will be referred to as *low-cycle fatigue* [27].

During earthquakes, steel moment connections could be subject to low-cycle fatigue. Higher mode effects which create a significant number of stress cycles at the connection (in some cases with relatively high stress levels) need to be investigated. Although demand in the beams and columns of connections could be less than the member strength, cumulative fatigue at the connections could potentially damage them during a seismic event.

Although the low-cyclic fatigue failure has been well researched and documented in the last decades, this issue has not been translated properly into the structural engineering practice and commonly used design manuals [27].

SEAOC Seismology Committee, FEMA 350 task group, strongly recommends that further research to be done on the issue of low-cycle fatigue [38].

The FEMA 350 commentary cites low-cycle fatigue as the main cause of failure in some laboratory connection tests but does not give any information or any possible recommendations on the issue.

Some of the SAC task groups addressed the low-cycle fatigue issue in their individual reports. For instance, the work done by Ricles et al. in 2000 [37] has a chapter on low-cycle fatigue with a proposed method for predicting crack initiation and extension over the life cycle of a connection utilizing finite element analysis [37], [38].

Barsom (2000) [6], concludes that fatigue is the failure mechanism of the connection. This report was never distributed to the practicing engineers, as only selected SAC committee members received it.

The report by Krawinkler et al. (1983) [26] cites low-cycle fatigue as the failure mechanism of the Pre-Northridge connections. The concept of “cumulative damage” is discussed in this document. The author indicates that each connection remembers the past events, and these past seismic events consume part of the predictable and quantifiable life of a connection.

In a follow-up to his 1983 report, Krawinkler introduces the cumulative damage testing criteria method for establishing cyclic life of a connection in the ATC-24 report [5].

Furthermore, in his confidential report to SAC “Development of Loading Histories for Testing of Steel Beam-to-Column Assemblies” in August 2000, Krawinkler again

suggests the cumulative damage testing per ATC-24 to determine the performance of the connection.

Bertero and Popov (1965) [8], discusses the *low-cycle fatigue* as a potential cause of failure in the steel members through a series of tests on beam specimens with large deformations. Their tests shows that fatigue, which in the case they studied was mainly caused by local buckling of flanges, was the failure mode of the specimens. They emphasize that fatigue life of a structural component can not be solely estimated by the fatigue characteristics of the material. Other factors need to be considered for determination of the low-cycle fatigue endurance of a structural member like type and size of a member, states of stress and strain across and along the critical region of a member, and most importantly the magnitude and history of alternating stress and strain.

Popov and Pinkey's (1969) paper [33], indicates that buckling and the cumulative fatigue associated with it are the main modes of failure for the rolled beams.

In their interesting paper submitted to the 10<sup>th</sup> World Conference in Earthquake Engineering, Kuwamura and Suzuki (1992) [25] conclude that the Pre-Northridge connection has a finite cyclic life and that *low cycle fatigue* is the failure mode for this connection.

Partridge et al. (2000) [31] show that fatigue is the principal failure mechanism of the Pre-Northridge connection. In this paper, constant cyclic tests were performed on 10 beam-column connections. This paper along with other publications by Partridge, Allen, Richard, and Radau ([30], [32], [34], [35], and [36]) strongly demonstrate that the Pre-Northridge connection failure during the Northridge Earthquake was the result of *low-cycle fatigue*.

As described in this chapter, the *low-cycle fatigue* issue has been widely addressed in the literature before and after the Northridge Earthquake; however, the methodology of implementing the fatigue considerations in the state-of-the-art design practices has not been properly developed.

## **CHAPTER 3: DESCRIPTION OF THE ANALYTICAL CASE STUDIES**

### **3.1 Description of the Investigated Buildings**

Two buildings which experienced significant damage in their steel moment frames during the Northridge Earthquake were chosen for this study. Both buildings used steel moment frames with Pre-Northridge connections in both major directions (North-South and East-West) as the main lateral resisting system. These buildings were ten and two stories, respectively, and located in Chatsworth, CA, 91311. Figure 3.1 shows the site of the buildings. Also, figures 3.2 and 3.3 illustrate photos of the ten and two-story buildings, respectively.

The original design of both buildings was performed by Brandow and Johnston, Inc. After the Northridge Earthquake, Brandow and Johnston, Inc. performed the structural inspection for possible damages and the subsequent repair project. As a result, the original design documents including structural calculations and drawings, mill test results, shop drawings, inspection results, and damage data were available for use in this study, in addition to the proposed repair methods and procedures. Appendices A and B contain a complete set of drawings for the ten-story and two-story buildings, respectively.



Figure 3.1: Site of the two investigated buildings.  
[[http://www.ngdc.noaa.gov/seg/hazard/slideset/18/18\\_380\\_slide.shtml](http://www.ngdc.noaa.gov/seg/hazard/slideset/18/18_380_slide.shtml)]



Figure 3.2: Ten-story building (photo courtesy of James C. Anderson).



Figure 3.3: Two-story building (photo courtesy of James C. Anderson).

Fortunately, the ten-story building was instrumented by California Department of Mines and Geology (CDMG) at the roof level. As described in chapter four of this document, this record has been used to calibrate and validate the analytical model used for the current study. The roof record taken during the Northridge Earthquake was provided for this research by Dr. Tony Shakal of California Geological Survey.

Figures 3.4 and 3.5 show the investigated frames in the ten-story and two-story buildings, respectively. The selection of these frames was based on a careful study of the damage observed in these buildings after the Northridge Earthquake. Red lines show the beam and columns of the connections under investigation.

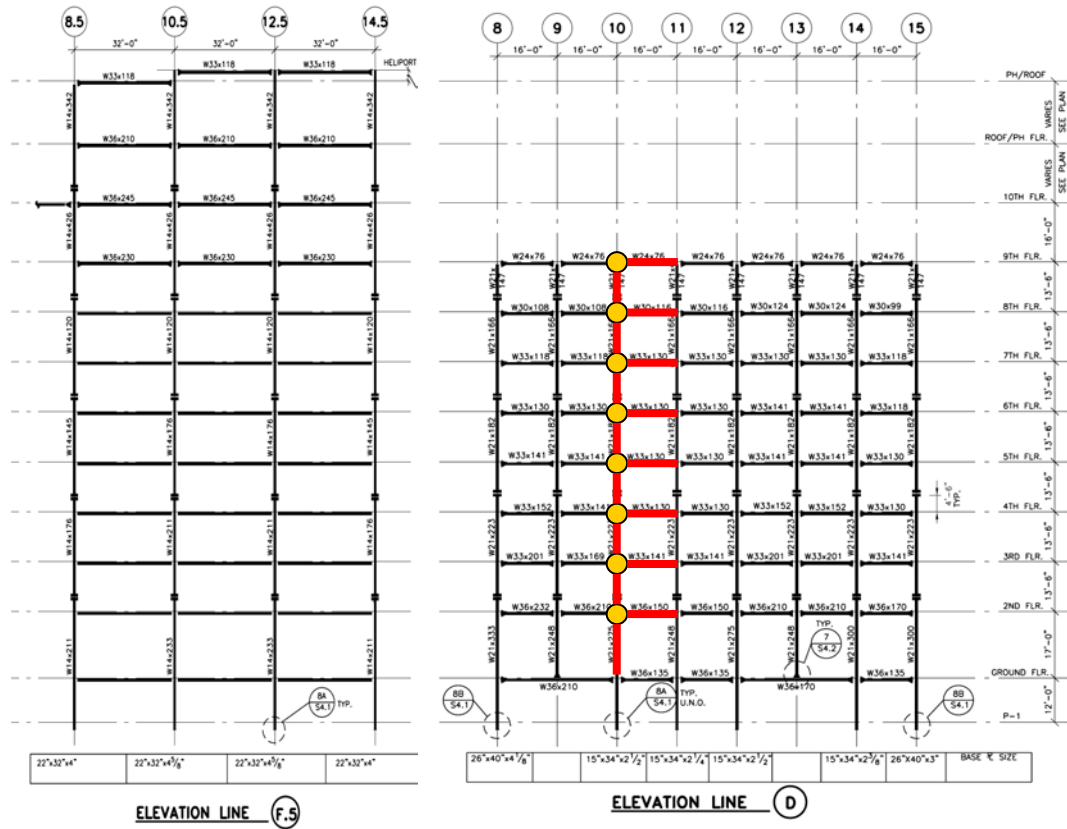


Figure 3.4: Investigated frames of the ten-story building. [Brandow and Johnston, Inc. drawings]

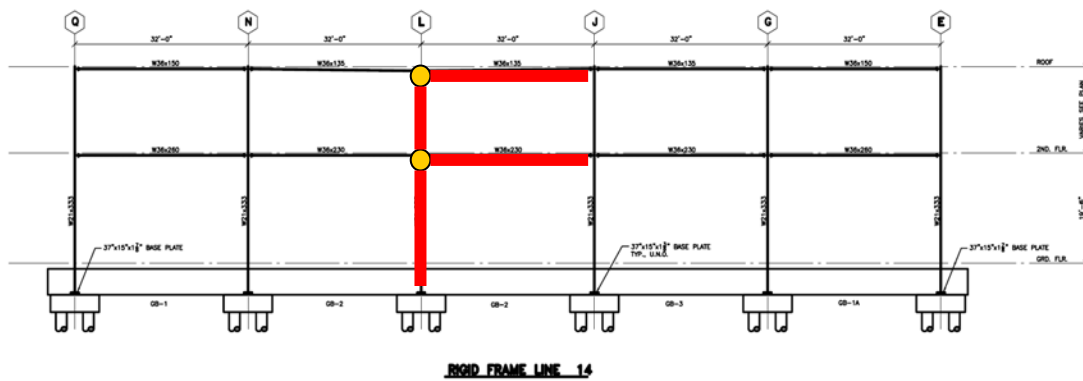


Figure 3.5: Investigated frame of the two-story building. [Brandow and Johnston, Inc. drawings]

## **3.2 Damage Observed During the Northridge Earthquake**

### **3.2.1 Ten-Story Building**

Observations after the Northridge Earthquake showed that no major damage occurred in the moment frame on gridline F.5. Also, they demonstrated that gridline 10 of moment frame D could be a good representation of the typical damages that occurred in this building. As shown in Figure 3.4, connections from 2<sup>nd</sup> floor through the 9<sup>th</sup> floor on gridline 10 were studied carefully for the level of stress they experienced. Furthermore, the contribution of each mode to the total stress was carefully investigated. Finally, fatigue analysis was performed to calculate the cumulative fatigue and the effect of higher modes on it. Figure 3.4 also depicts in red the beams and columns on which this analytical study has been performed.

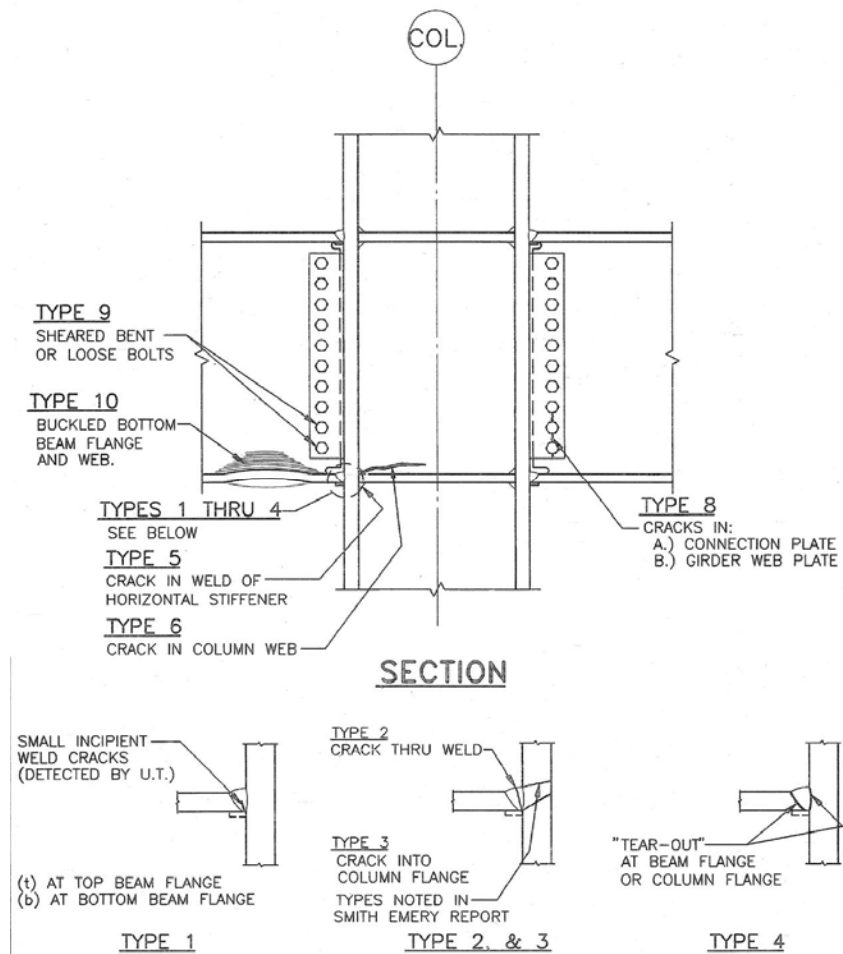
Figure 3.6 shows the typical damage observed in Pre-Northridge steel moment frame connections after the Northridge Earthquake. Post-Northridge inspection results show that most of the damage in Frame D gridline 10 happened at 5<sup>th</sup>, 6<sup>th</sup>, and 7<sup>th</sup> floors. The 6<sup>th</sup> floor experienced the most severe damage represented by types 2 and 3 in the bottom of the connection. This means the connection had cracks that went through the weld and column flange (Types 2b and 3b). The 5<sup>th</sup> floor experienced only type 2 damage in the bottom of the connection, and cracks were just observed in

the bottom flange weld (Type 2b). The damage at the 7<sup>th</sup> floor was minor, and only small cracks in the weld root zone of the bottom flange were observed (Type 1b).

### **3.2.2 Two-Story Building**

Inspection after the Northridge Earthquake indicated that severe damage occurred at gridline L at the 2<sup>nd</sup> floor. This connection and the investigated beams and columns have been shown in Figure 3.5. Damage observed at the connections of this frame was similar in nature to the damage previously observed in the ten-story building. However, the damage at the 2<sup>nd</sup> floor connection on gridline L was significantly more severe. The damage was reported to be of type 3 and type 6 at the bottom, in the form of cracks through the column flange and their propagation into the column web. For this specific connection, the crack went horizontally all the way through the web of the column.

Photos shown in Figure 3.7 clearly illustrate the initiation of the crack from the weld area and its propagation into the column flange and eventually the column web.



DAMAGE TYPE	
1.	SMALL INCIPIENT WELD CRACK IN ROOT ZONE AND/OR PARTIAL CRACK OR DISCONTINUITY t) TOP BEAM FLANGE WELD b) BOTTOM BEAM FLANGE WELD
2.	THRU CRACK IN WELD.
3.	PARTIAL OR THRU CRACK IN COLUMN FLANGE.
4.	"TEAR-OUT" AT BEAM FLANGE OR COLUMN FLANGE.
5.	CRACK IN WELD OF HORIZONTAL STIFFENER.
6.	CRACK PROPAGATED INTO COLUMN WEB.
7.	CRACK IN REINFORCING FILLET WELD OF CONNECTION PLATE TO BEAM WEB.
8.	CRACK IN BEAM CONNECTION PLATE (VERTICAL THRU LOWER BOLT HOLES)
9.	SHEARED, BENT, OR LOOSE BOLTS.
10.	BUCKLED BOTTOM BEAM FLANGE AND WEB.

Figure 3.6: Typical moment frame connection damage. [Brandow and Johnston, Inc. drawings]



Figure 3.7: Damage observed in the two-story building after the Northridge Earthquake (Photos courtesy of Peter J. Maranian).



Figure 3.7, continued: Damage observed in the two-story building after the Northridge Earthquake (Photos courtesy of Peter J. Maranian).

### **3.3 Analytical Studies**

The purpose of these analytical studies was to break down the response of the structure into responses caused by each mode of vibration. In other words, the contribution of each mode in the overall response was investigated. As described earlier in this chapter, the critical moment frames of each building were carefully selected, and the type of damage was identified at all critical connections. Next, a series of linear and non-linear time history analyses was performed on the selected frames. The goal was to look at the stress levels under the response of each mode and try to get a better understanding of what the frame (specifically the connections) went through during the Northridge Earthquake. Basically, finding the number of cycles created by each mode of vibration separately and the stress level associated with each of them was the starting point for this study.

The ultimate intention of this research was to establish a comprehensive fatigue analysis procedure for the steel moment frames with Pre-Northridge connections. This procedure would then be used to investigate the cumulative fatigue created at each connection component and to study the effect of higher modes of vibration on calculated values. Finally, finding a pattern between the observed damage and cumulative fatigue that could reasonably justify the damage observed in the investigated frames, as well as studying the higher mode effects on the cumulative fatigue values, was of essence to this study.

The next chapter includes the time-history analyses performed on these buildings. Chapter five goes through the fatigue analyses procedures. Finally chapter six summarizes the results of the performed studies.

## **CHAPTER 4: TIME-HISTORY ANALYSIS**

This chapter contains the result of a series of linear and non-linear time-history analyses on the investigated ten-story and two-story buildings. Modeling and analysis details are explained, and stress histories at the beam and columns of the critical connections are studied. Finally, the contribution of each mode of vibration in the total stress is investigated.

### **4.1. Ground Motion**

Since the earthquake record could potentially play a major role in the final results of a time-history analysis, a thorough study was performed to select the best available earthquake record for the purposes of the current research. Figure 4.1 shows the location of the investigated buildings on the map of the Los Angeles area. According to Maporama ([www.maporama.com](http://www.maporama.com)), the latitude and longitude of the site are 34.238 and -118.567 degrees, respectively.

After investigating the available earthquake records in the area using United States Geological Survey (USGS), California Department of Mines and Geology (CDMG), University of Southern California (USC), and Department of Water and Power (DWP) networks, it was concluded that the closest record to the site was recorded at

the USC 03 station. This earthquake record was selected to be used for time-history analyses explained later in this chapter.



Figure 4.1: Location of the investigated buildings. [www.mapquest.com]

Figure 4.2 depicts the location of the USC 03 station along with all other stations belonging to USGS, CDMG, USC, and DWP, which recorded the Northridge main event. USC 03 is located at 17645 Saticoy Street, Northridge, California, with a latitude and longitude of 34.209 and -118.517 degrees, respectively.

Figure 4.3 shows the corrected acceleration, velocity, and displacement data for the

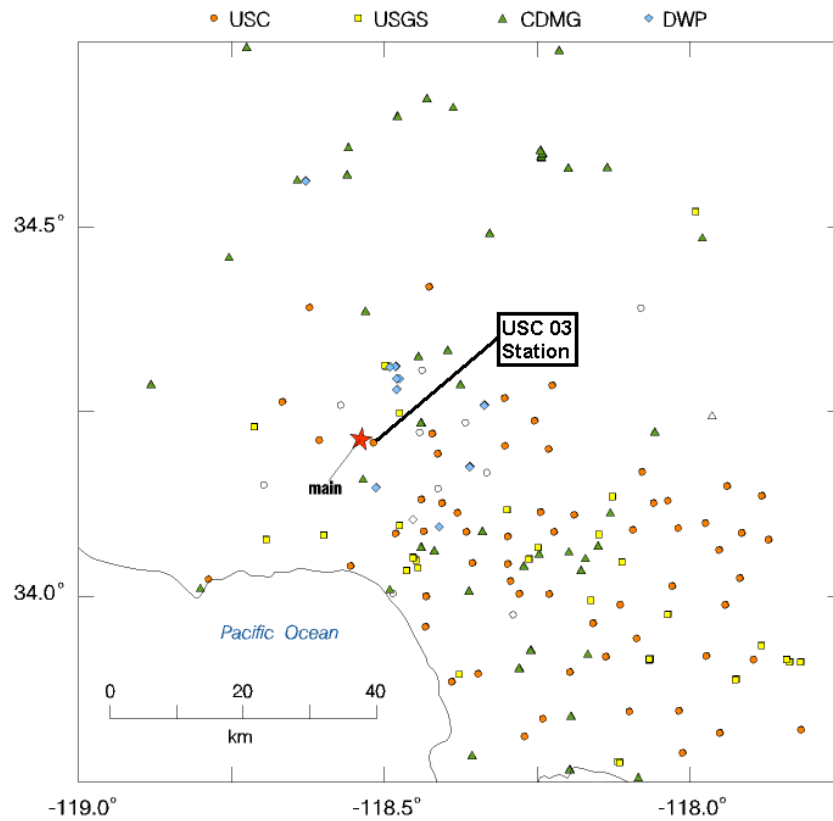


Figure 4.2: Location of the USC 03 station along with all other stations in the region (USGS, CDMG, USC and DWP networks) which recorded the Northridge main event. [[http://www.usc.edu/dept/civil\\_eng/Earthquake\\_eng/](http://www.usc.edu/dept/civil_eng/Earthquake_eng/)]

East direction presented in the form of 6021 data points with 0.01 second intervals. This corrected record was obtained from the USC Earthquake Engineering Strong Motion Group website ([http://www.usc.edu/dept/civil\\_eng/Earthquake\\_eng/](http://www.usc.edu/dept/civil_eng/Earthquake_eng/)).

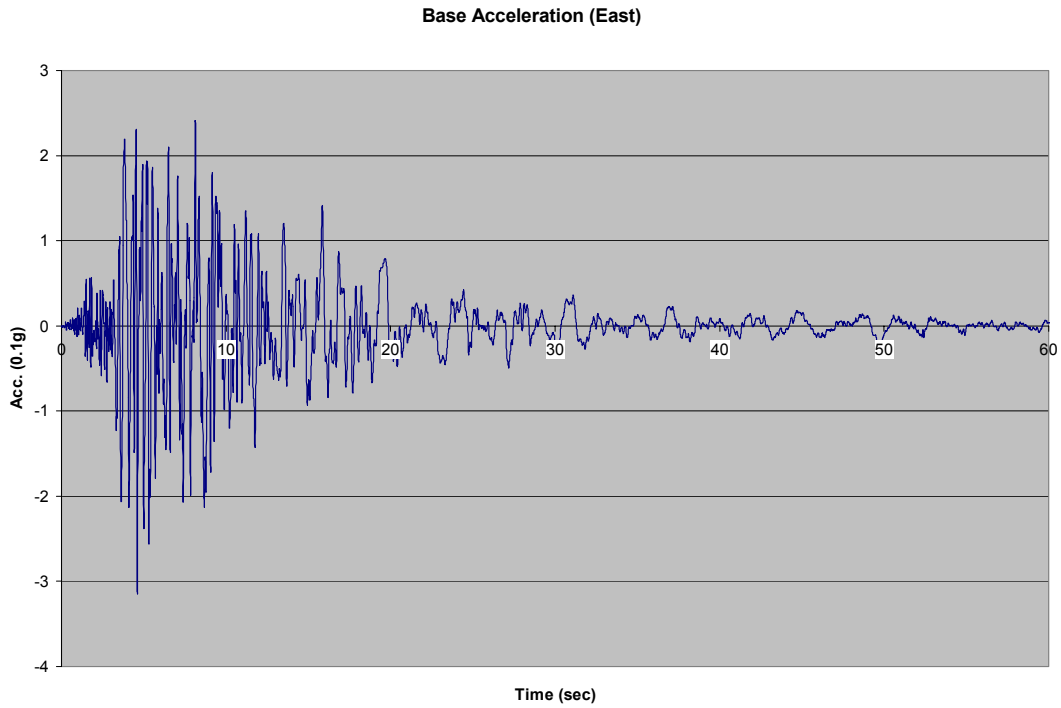
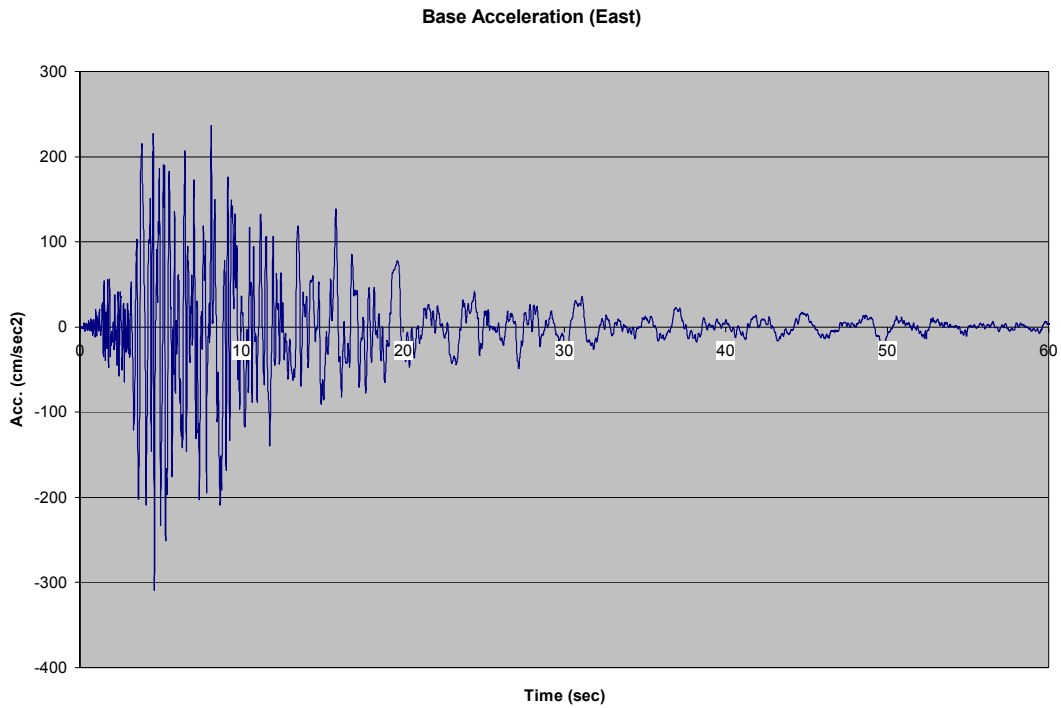


Figure 4.3: Corrected acceleration, velocity, and displacement records in East direction, Northridge main event recorded at USC 03 station.

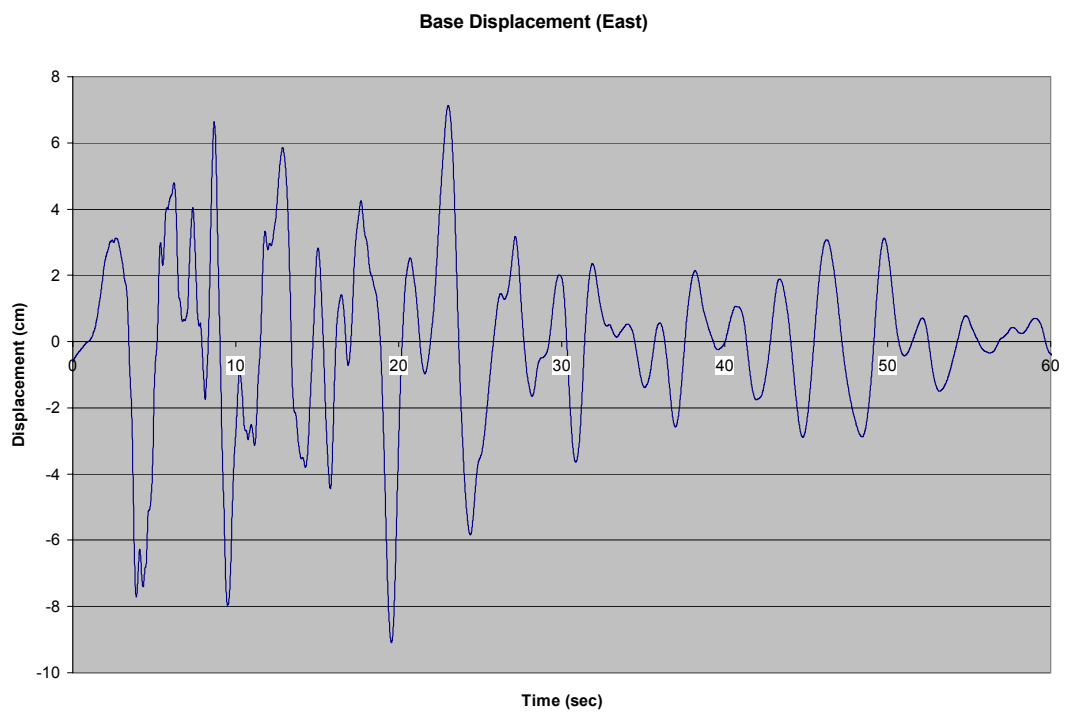
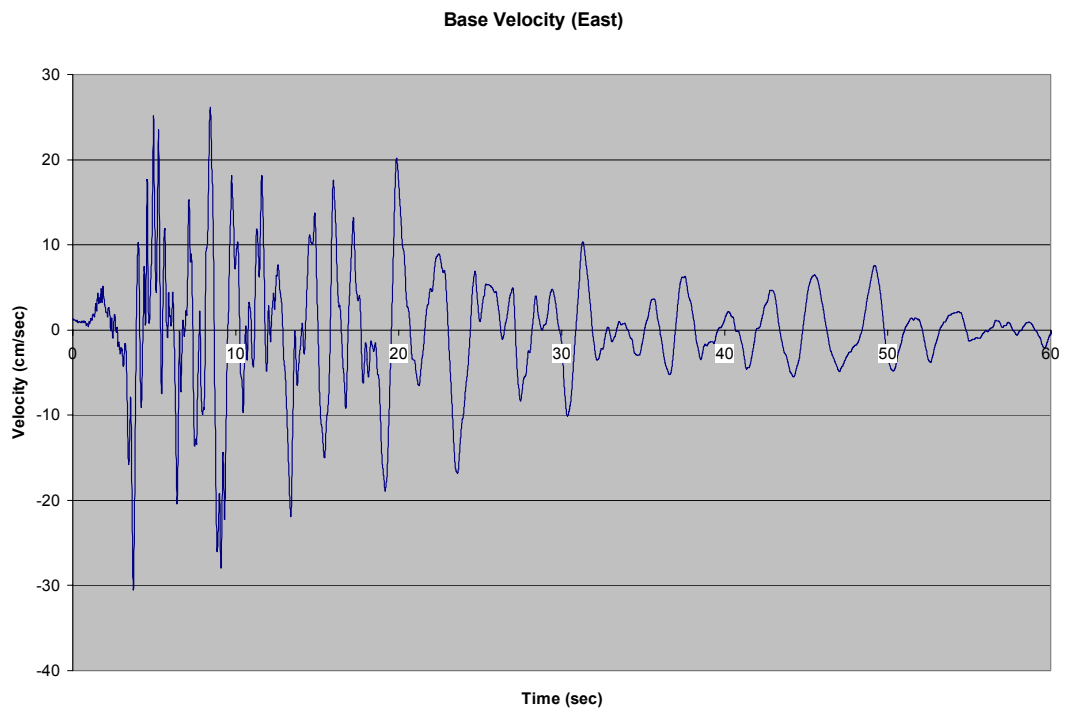


Figure 4.3, continued: Corrected acceleration, velocity, and displacement records in East direction, Northridge main event recorded at USC 03 station.

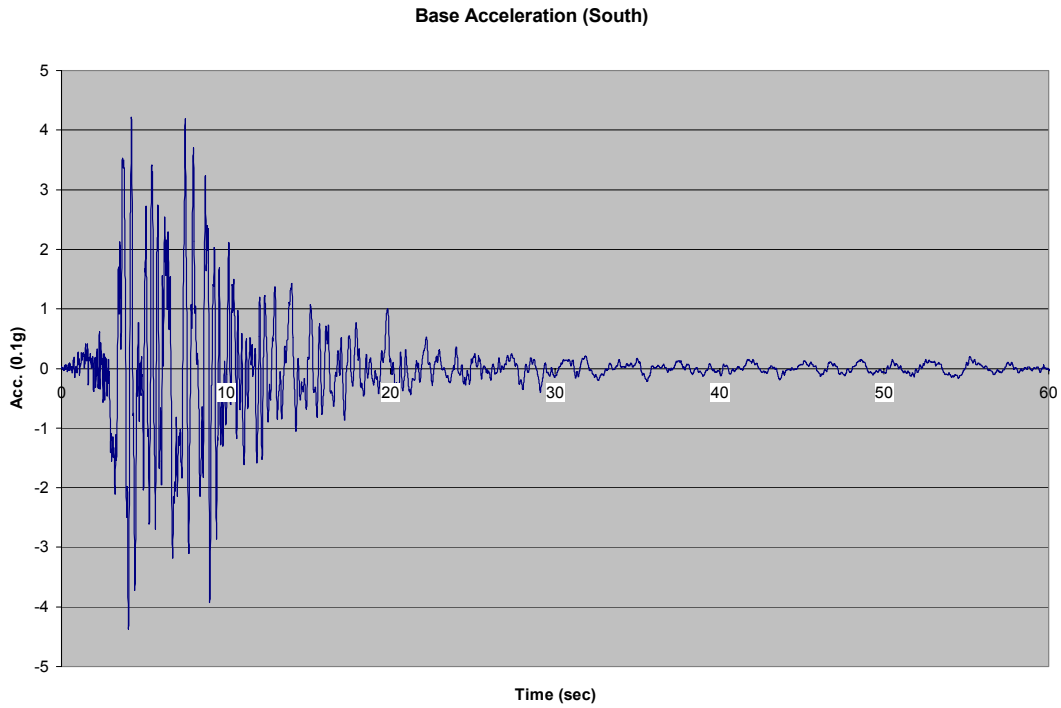
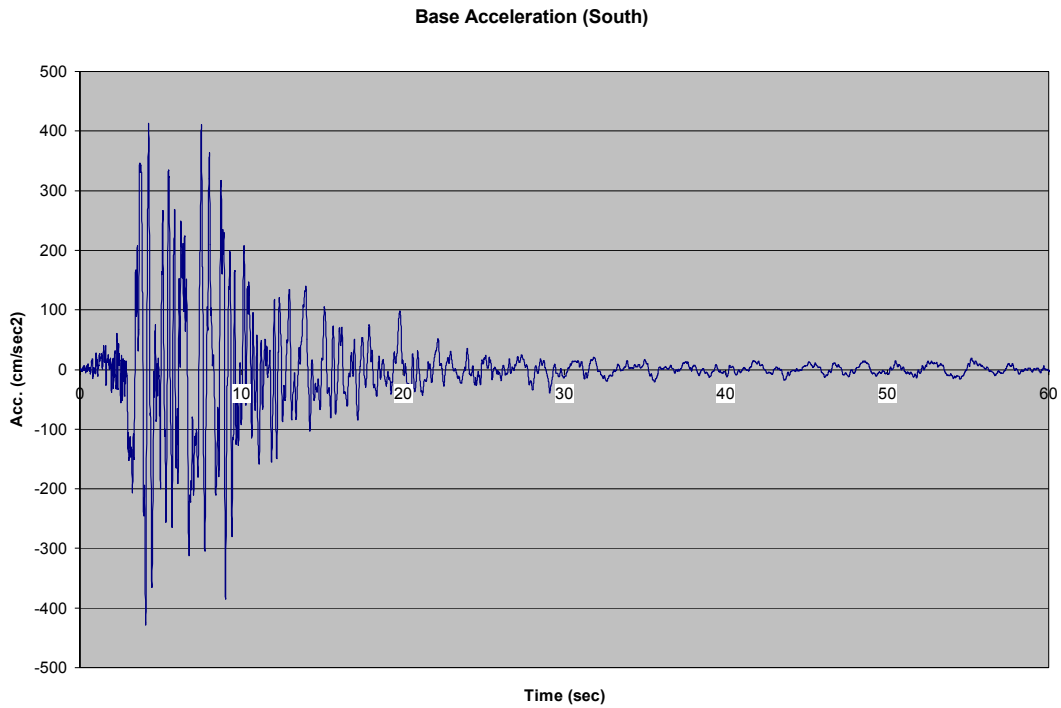


Figure 4.4: Corrected acceleration, velocity, and displacement records in South direction, Northridge main event recorded at USC 03 station.

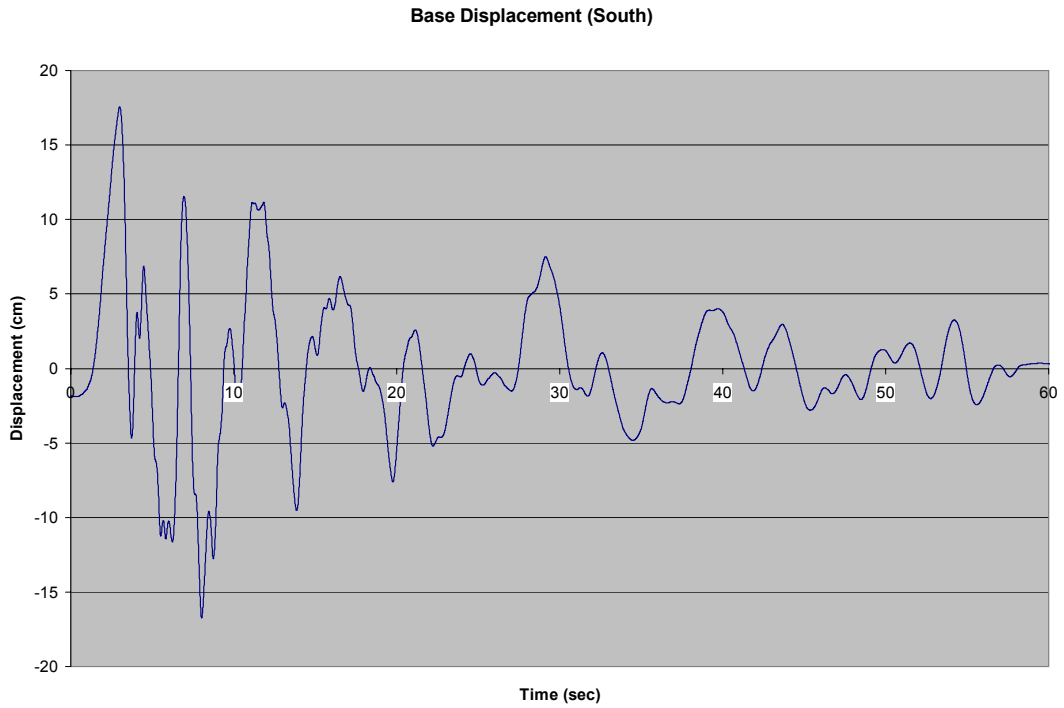
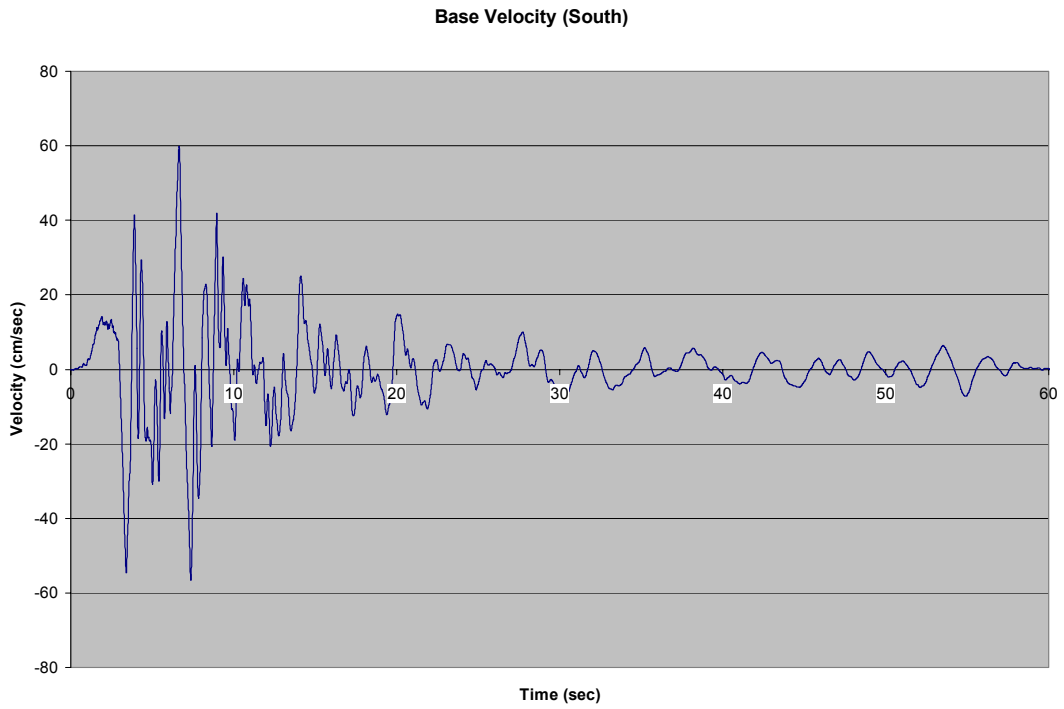


Figure 4.4, continued: Corrected acceleration, velocity, and displacement records in South direction, Northridge main event recorded at USC 03 station.

## 4.2 Ten-Story Building

In order to study the behavior of the ten-story building during the Northridge Earthquake a series of modal, linear modal time-history, and nonlinear direct integration time-history analyses was performed using SAP 2000. The 10-story building is almost symmetrical in both North-South and East-West directions. Lateral load-resisting system in each direction consists of four steel moment frames. The two selected moment frames for this study, are part of the lateral system in East-West direction which is the longitudinal direction of the building. Figures 4.5 and 4.6 show the elevation views of these two frames on gridlines F.5 and D. See Appendix A, which contains the drawings of the ten-story building, for the location of the frames. Since the building is symmetrical, these two frames together are assumed to be supporting half of the total seismic forces in East-West direction. As a result, half of the building seismic mass was assigned to the model at each level. Also, in order to make the two frames work together, weightless link elements with high axial stiffness were used to connect the frames together and to represent axial stiffness of floor slabs. These members had pinned connections at the ends.

As discussed in chapter three, gridline 10 of moment frame D is a good representative for the typical connection damages that occurred in this building. As a result, this study was focused on the beams and columns on gridline 10 as shown in red in figure 4.6.

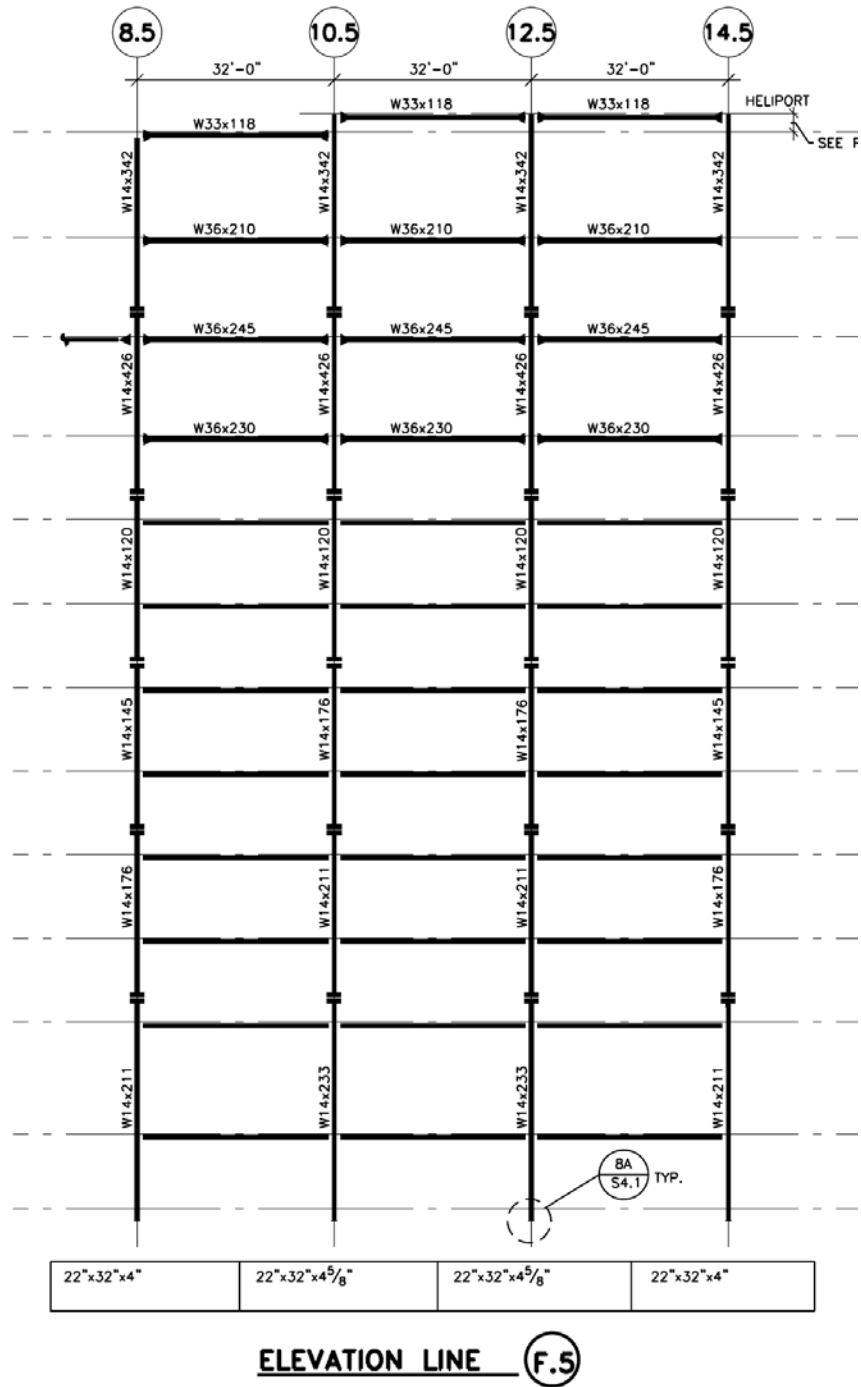


Figure 4.5: Moment frame on gridline F.5 in East-West direction.



Modal analysis was performed and the periods of the first three modes were calculated to be:

$$T_1 = 2.70 \text{ sec}$$

$$T_2 = 1.07 \text{ sec}$$

$$T_3 = 0.63 \text{ sec}$$

Figures 4.7, 4.8, and 4.9 show the first three mode shapes of the model.

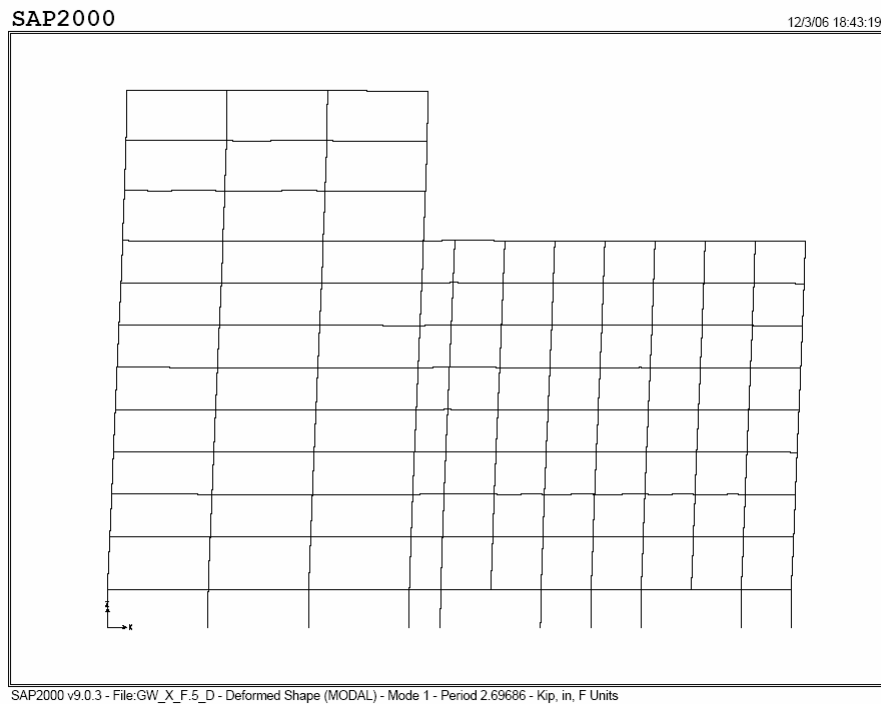
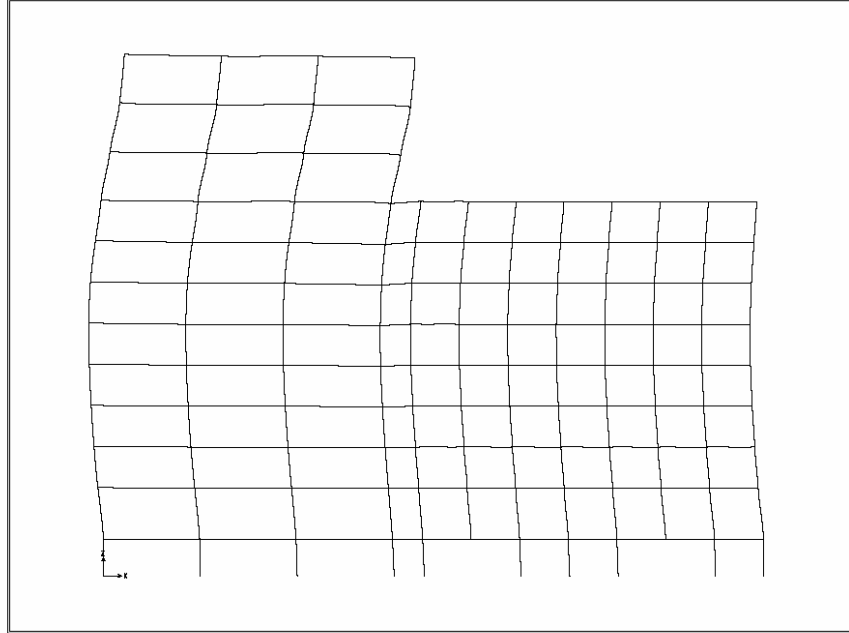
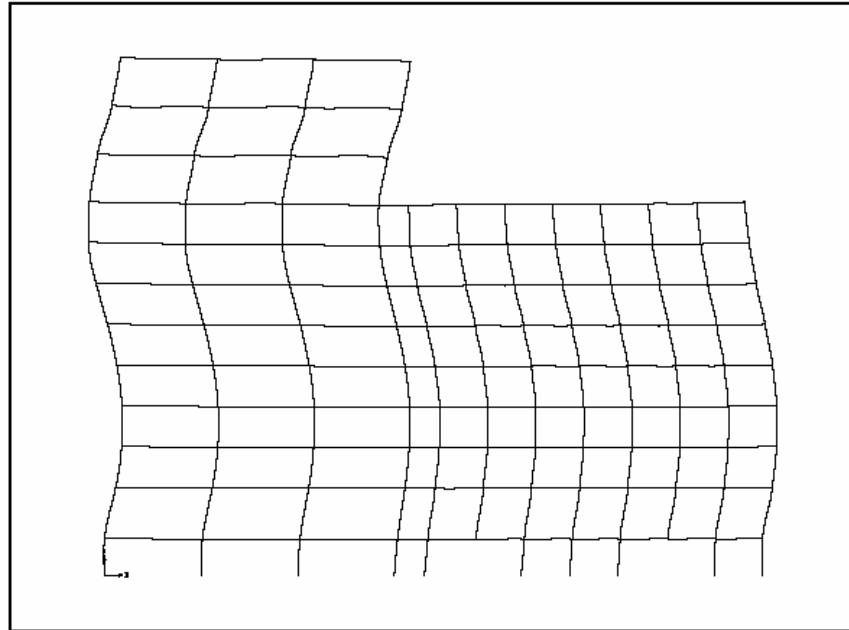


Figure 4.7: 1<sup>st</sup> mode shape.



SAP2000 v9.0.3 - File:GW\_X\_F\_5\_D - Deformed Shape (MODAL) - Mode 2 - Period 1.06514 - Kip, in, F Units

Figure 4.8: 2<sup>nd</sup> mode shape.



SAP2000 v9.0.3 - File:GW\_X\_F\_5\_D - Deformed Shape (MODAL) - Mode 3 - Period 0.62504 - Kip, in, F Units

Figure 4.9: 3<sup>rd</sup> mode shape.

### 4.2.1 Linear Modal Time-History Analysis

A linear modal time-history analysis was performed on the model. The USC 03 record was used as the ground motion as explained earlier in this chapter. Figure 4.10 shows the displacement response history of frame F.5 at the roof level calculated as a result of this analysis. Also, Figures 4.11, 4.12 and 4.13 show the contribution of each of the first three modes of vibration to the total displacement. Initial damping assumed to be 3% to calculate these displacement histories.

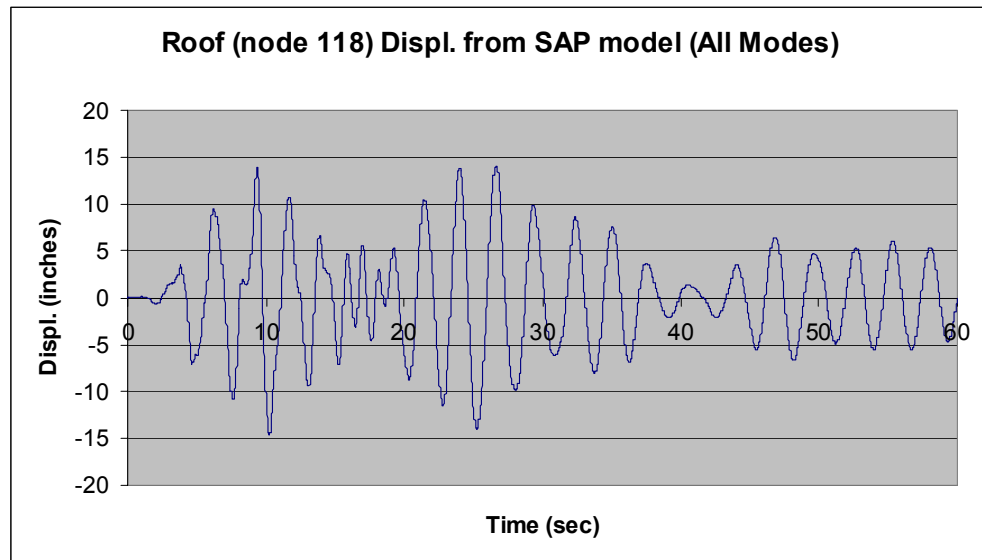


Figure 4.10: Roof displacement result of linear modal time-history analysis (3% damping for all modes).

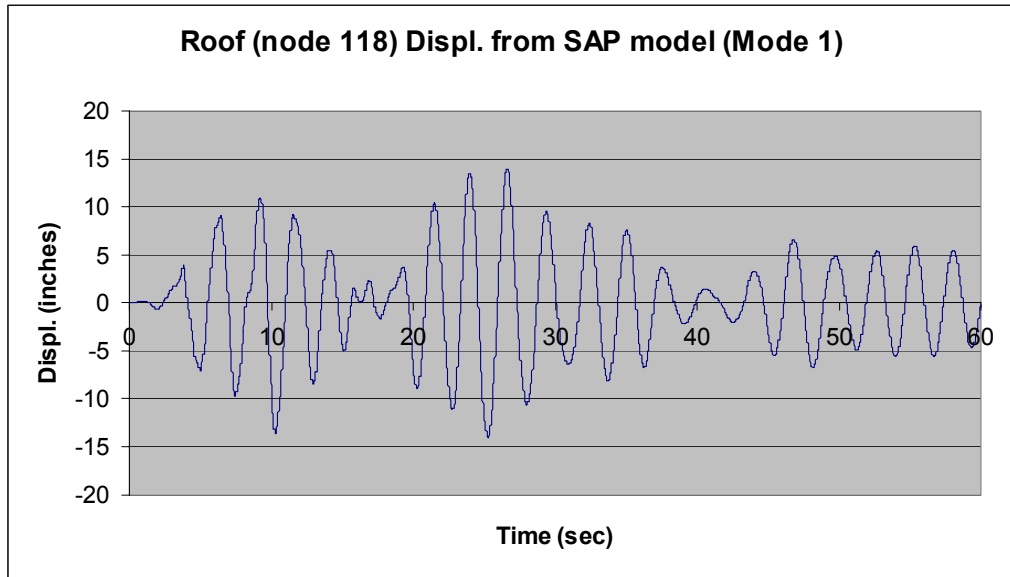


Figure 4.11: Contribution of the 1<sup>st</sup> mode of vibration to the roof displacement (3% damping for all modes).

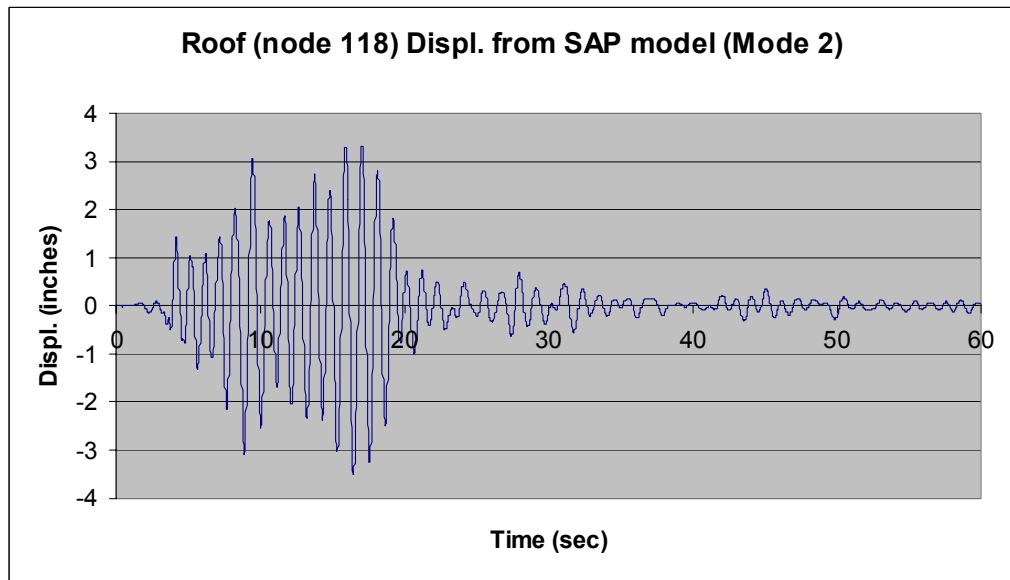


Figure 4.12: Contribution of the 2<sup>nd</sup> mode of vibration to the roof displacement (3% damping for all modes).

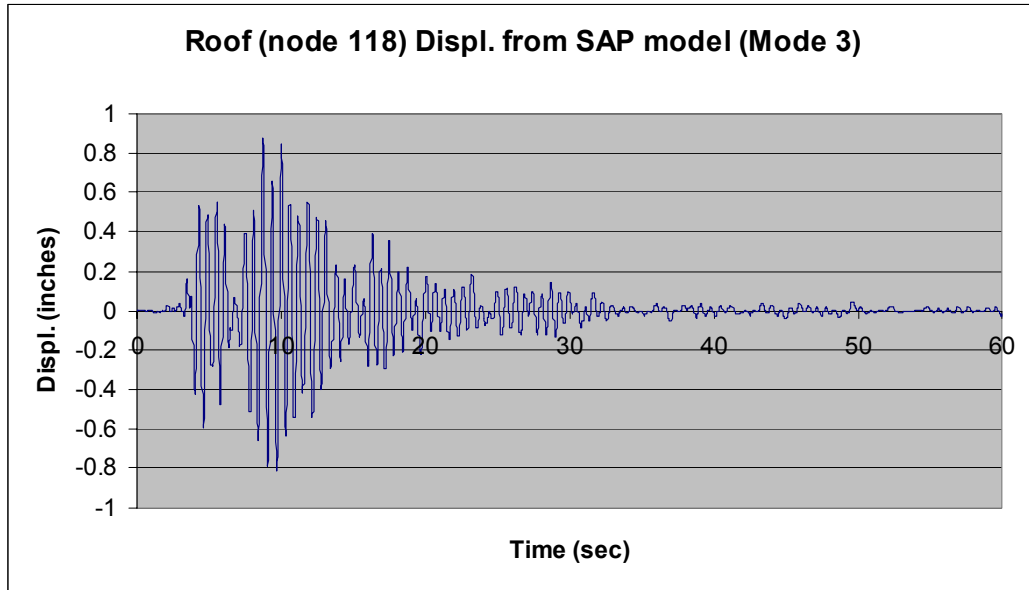


Figure 4.13: Contribution of the 3<sup>rd</sup> mode of vibration to the roof displacement (3% damping for all modes).

The main goal of this linear modal time-history analysis was to plot the stress histories at the critical locations of the frames and break them down to the contribution of each mode separately. In order to do that, it was necessary to have a reasonable degree of confidence in the model and calibrate it by adjusting the values of damping and mass assigned to it according to the behavior of the actual building. Fortunately, there was a CDMG instrument at the roof level which recorded the Northridge Earthquake main event. This record which is shown in Figures 4.14 and 4.15 was used to adjust the damping and mass used for the analysis.

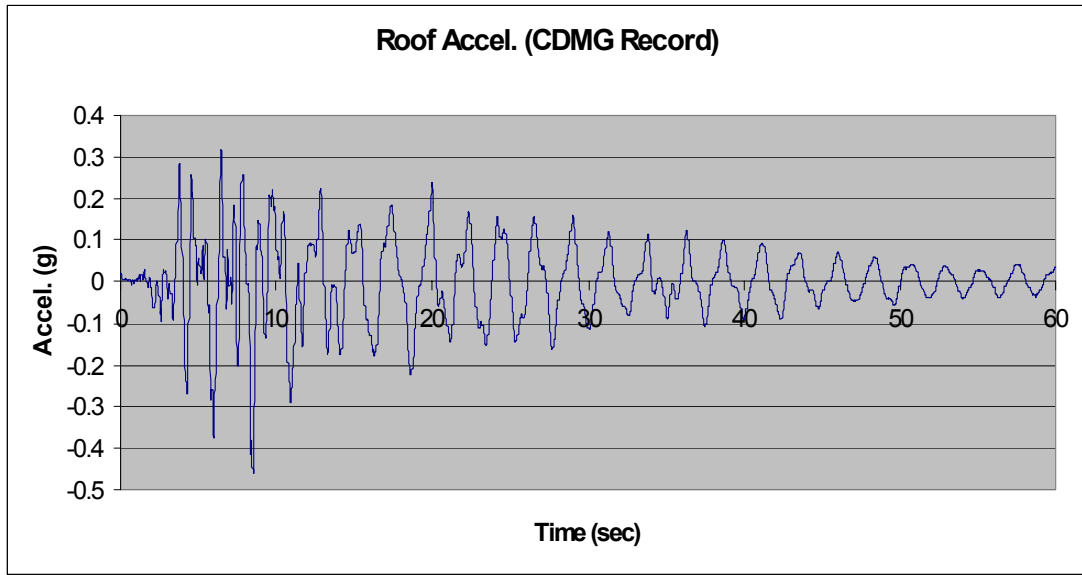


Figure 4.14: Acceleration (East) recorded at roof by CDMG station.

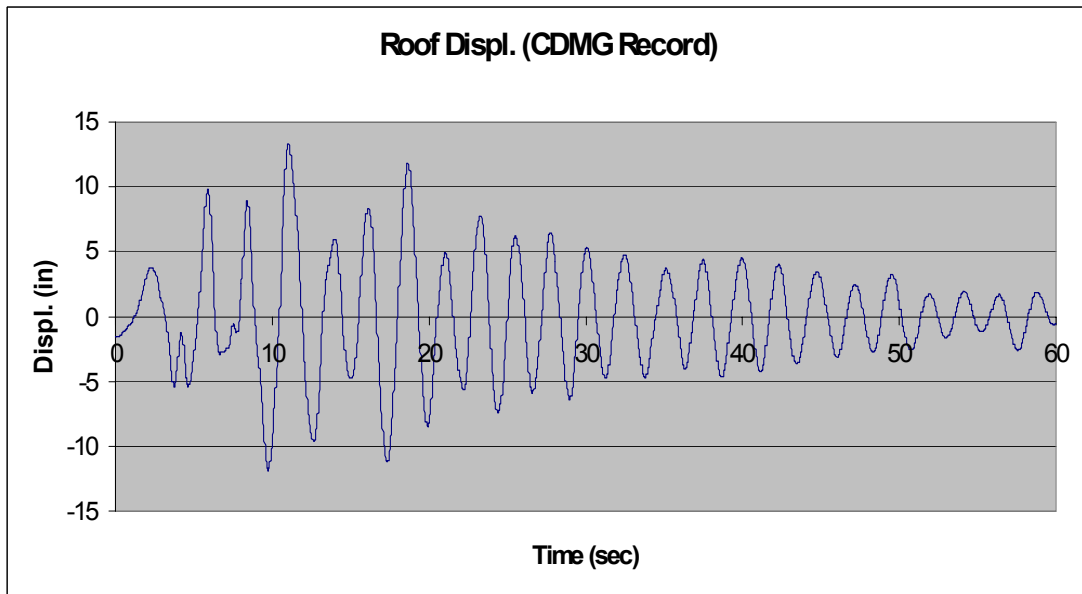


Figure 4.15: Displacement (East) recorded at roof by CDMG station.

#### **4.2.1.1 Damping**

Analysis was repeated for different damping values ranging from 1% to 5%. Comparing the results with the CDMG roof record showed that damping value of 1% seems to be the closest to reality. As a result, damping value of 1% for all modes was used in the next stages of this study. Figures 4.16 and 4.17 show the result of different analysis runs with 1% damping for all modes.

#### **4.2.1.2 Mass**

In order to be able to match the response of the model with the CDMG roof record, a series of linear modal time-history analyses was performed with damping set to 1%. Mass associated with each level was proportionally changed in order to make changes to the modal periods of the frame and consequently result in a better match between the calculated response at the roof and the recorded response by the CDMG instrument. Finally, it was concluded that the original masses (masses based on the original design documents of the buildings), which result in the first mode period of 2.7 seconds, seem to create the best match. Figures 4.16 and 4.17 show the result of this study and depict the response of the models with different assigned masses and consequently different first mode periods. As a result, in the next stages of this study,

the model with first mode period of 2.7 seconds (original building masses) was used for stress investigations.

It will be shown later on in this chapter that a moving-window Fourier transform of the CDMG roof record (figure 4.32) indicates that the first mode period of the building is 2.5 seconds. This result shows good compatibility with the first mode period of the analytical model.

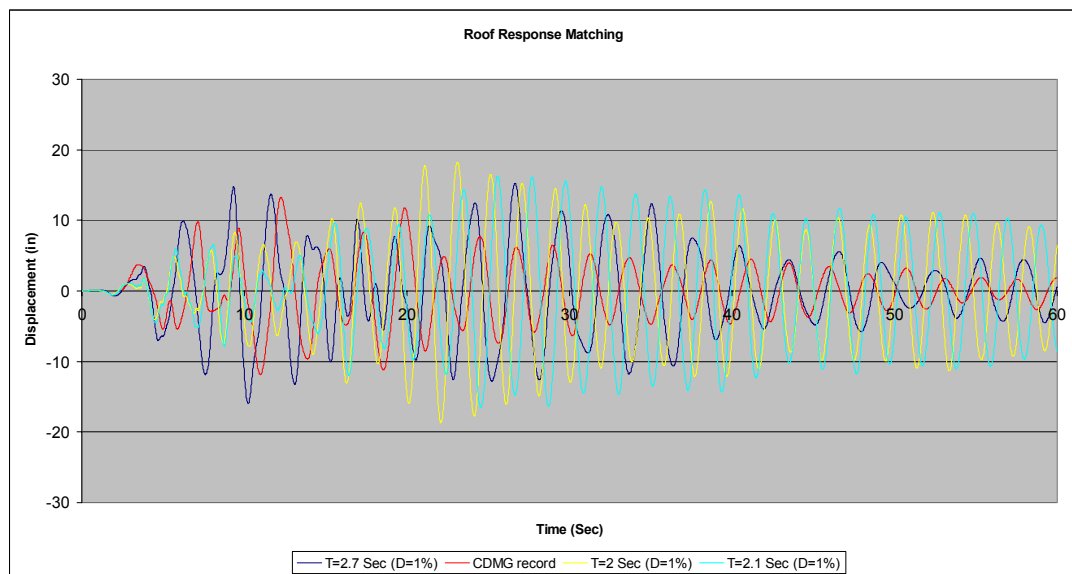


Figure 4.16: Roof response matching.

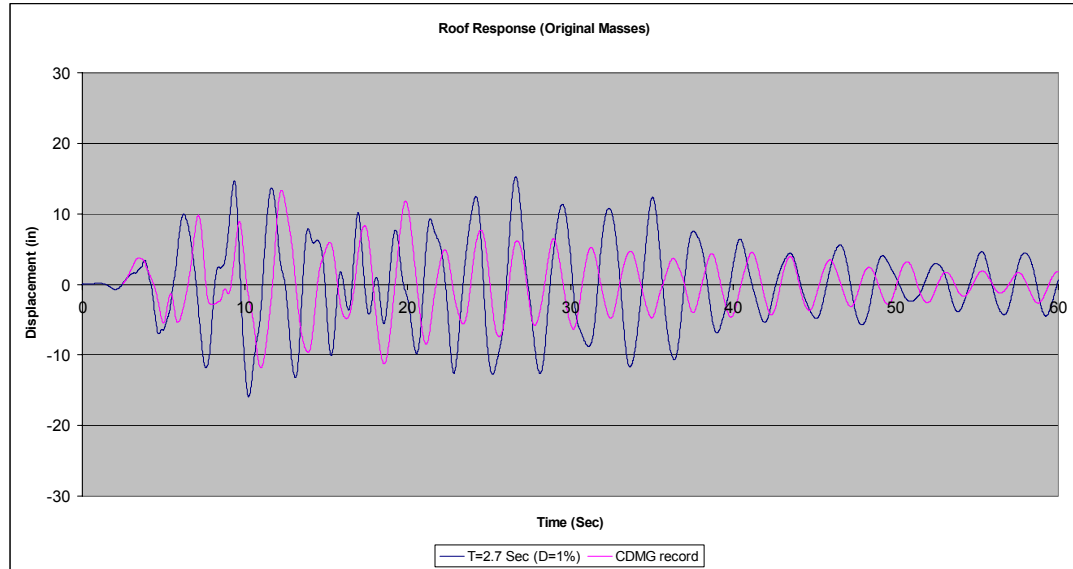


Figure 4.17: Roof matched response.

#### 4.2.1.3 Stress Histories and Contribution of Each Mode to Total Stress

The stresses at beams and columns were calculated using the calibrated model described in the previous sections of this chapter. The purpose was to indicate the total stress level and show the contribution of each mode of vibration in the stress value at each time step and finally, plotting the stress history for each mode separately. In reality each member is experiencing stress cycles created by the first mode as well as many more cycles created by higher modes of vibration. The purpose of this study was to investigate the higher mode stress cycles and their distribution along the height of the building and finally, to look for a pattern between these higher mode effects and the damage occurred at the frame connections.

Chapter five shows how these stress histories will be used to perform a series of cumulative fatigue analyses. Figure 4.18 shows a clear example of the modal stress accumulation happening at the 7<sup>th</sup> floor column located on gridline 10.

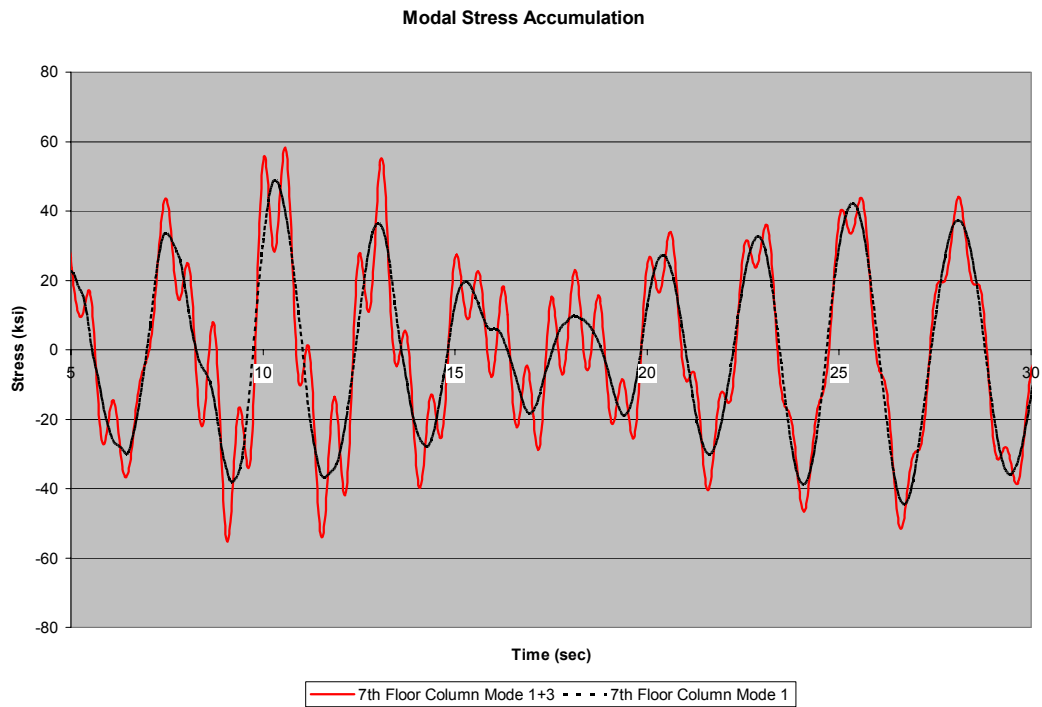


Figure 4.18: An example of modal stress accumulation.

#### 4.2.1.3.1 Beam Stress

Figure 4.19 shows the stress histories that the beams experienced as a result of the time-history analysis of the frame. The stress values plotted are calculated by

dividing the moment at the end of each member ( $M$ ) by the elastic modulus of the cross section ( $S$ ).

The plotted stress histories for different floors indicate that the maximum beam stresses are at or slightly above yield and does not show significantly higher stress values at the floors with severe connection damage (5<sup>th</sup>, 6<sup>th</sup>, and 7<sup>th</sup> floors as indicated in chapter three). In other words, maximum stress values are not high enough to justify the connection damages caused by the Northridge Earthquake. This was the motivation to study the contribution of the first three modes of vibration to the total stress. Figures 4.20, 4.21, and 4.22 show the result of this study.

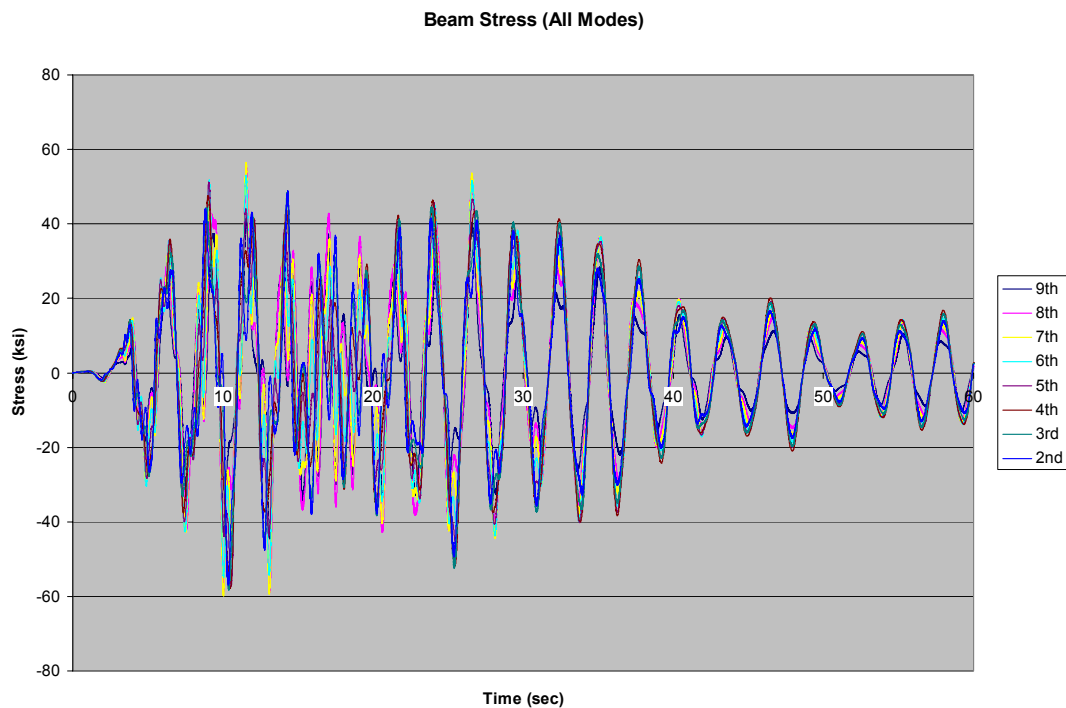


Figure 4.19: Beam stress history (contribution of all modes)

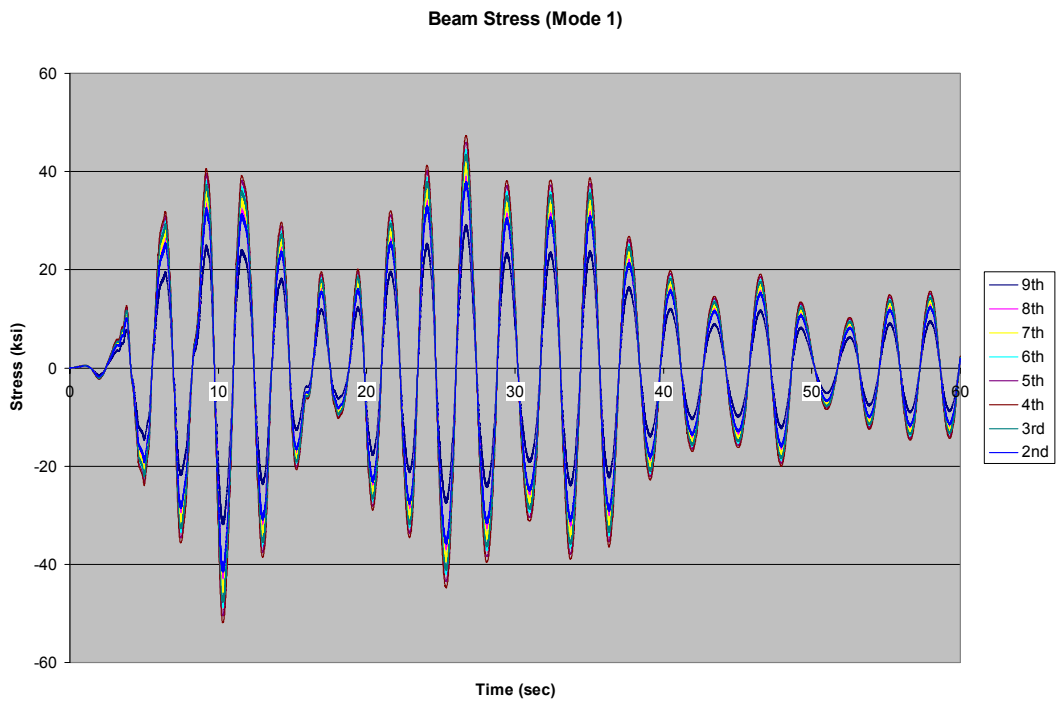


Figure 4.20: Beam stress history (contribution of the 1<sup>st</sup> mode).

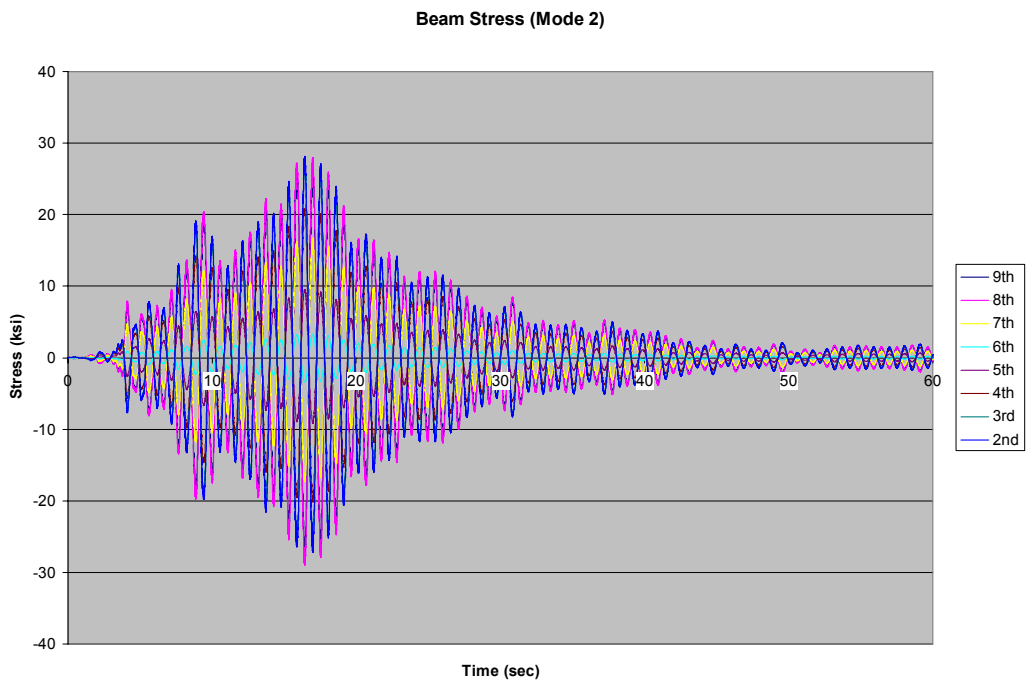


Figure 4.21: Beam stress history (contribution of the 2<sup>nd</sup> mode).

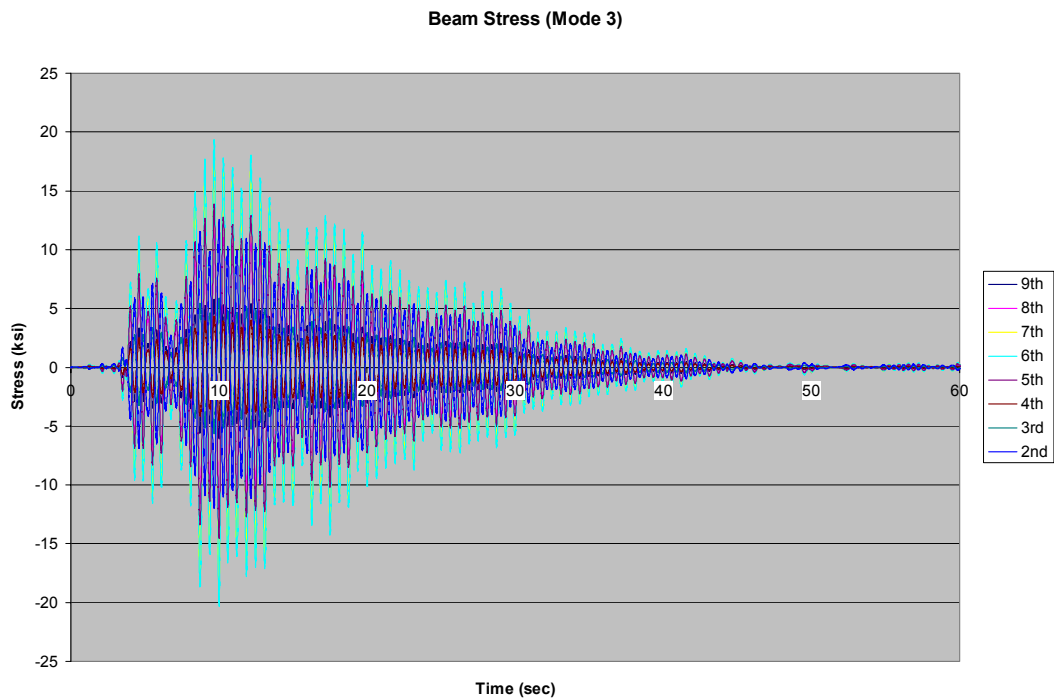


Figure 4.22: Beam stress history (contribution of the 3<sup>rd</sup> mode).

It can be clearly seen on Figure 4.22 that 5<sup>th</sup>, 6<sup>th</sup> and 7<sup>th</sup> floor beams are going through a lot of cycles with noticeable stress levels created by the 3<sup>rd</sup> mode of vibration. Knowing that these connections are the ones that experienced significant damage during the Northridge Earthquake, it can be concluded that the higher modes of vibration are potentially a major player in the connection damages occurred in the 10-story building. The 6<sup>th</sup> floor beam as shown in Figure 3.23 has the highest level of stress created by the 3<sup>rd</sup> mode and this is the floor with the most significant damage during the Northridge Earthquake. The result of cumulative fatigue studies described later on in chapters five and six of this document confirm this observation.

#### 4.2.1.3.2 Column Stress

The next step is looking at the column stress histories. Figure 4.23 shows the total column stresses. Similar to what was observed previously for beams, the total stress does not appear to justify the severe column damage observed at the 6<sup>th</sup> floor. Also the maximum column stress values are not high enough to justify the connection damages caused by the Northridge Earthquake. Figures 4.24, 4.25, and 4.26 show the stress histories created by the first three modes of vibration separately. By looking at Figure 4.26, it is obvious that the 6<sup>th</sup> and 7<sup>th</sup> floor columns (columns above and below the 6<sup>th</sup> floor moment connection that experienced severe damage in the form of crack through the weld and column flange) have gone through many cycles with significant stress levels. It can be concluded that the higher modes of vibration are potentially a major player in the connection damages that occurred in the 10-story building. The result of cumulative fatigue studies described later on in chapters five and six of this document confirm this observation.

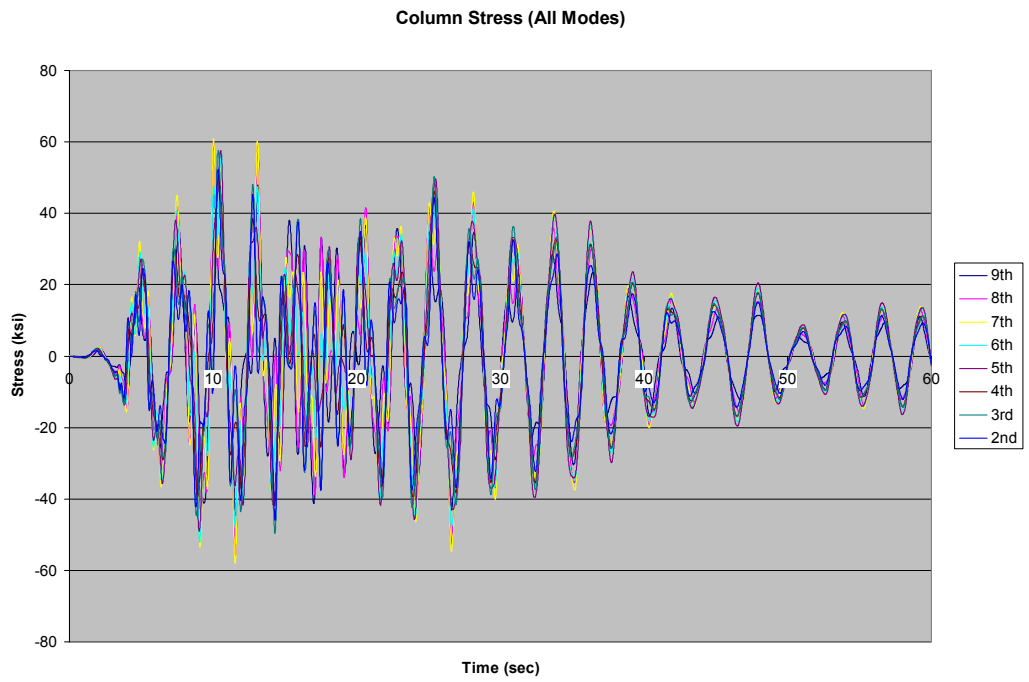


Figure 4.23: Column stress history (contribution of all modes).

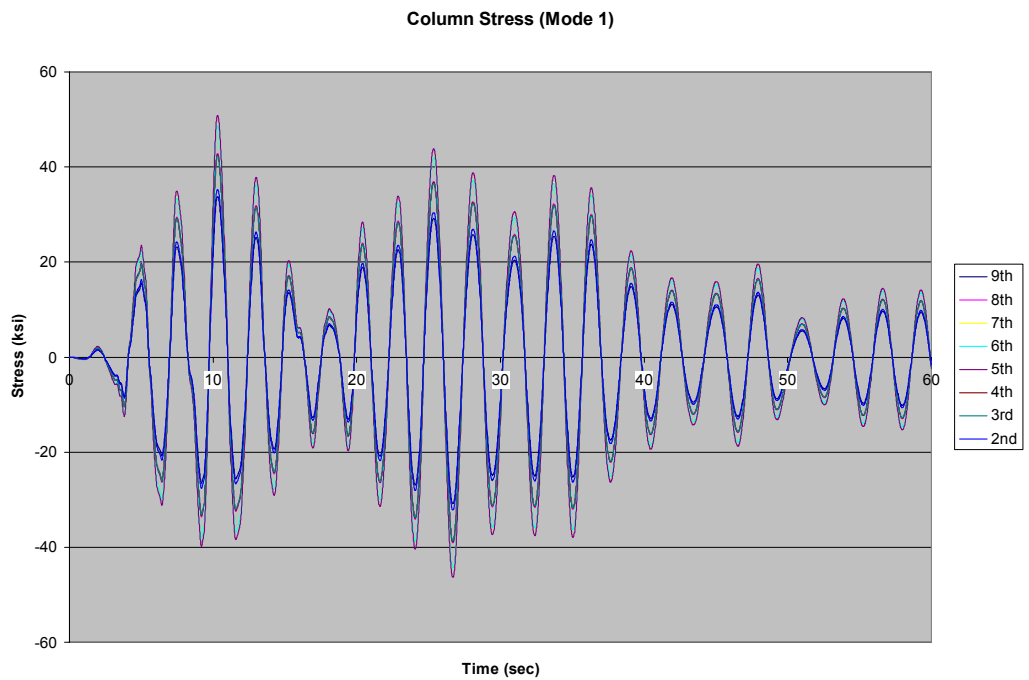


Figure 4.24: Column stress history (contribution of the 1<sup>st</sup> mode).

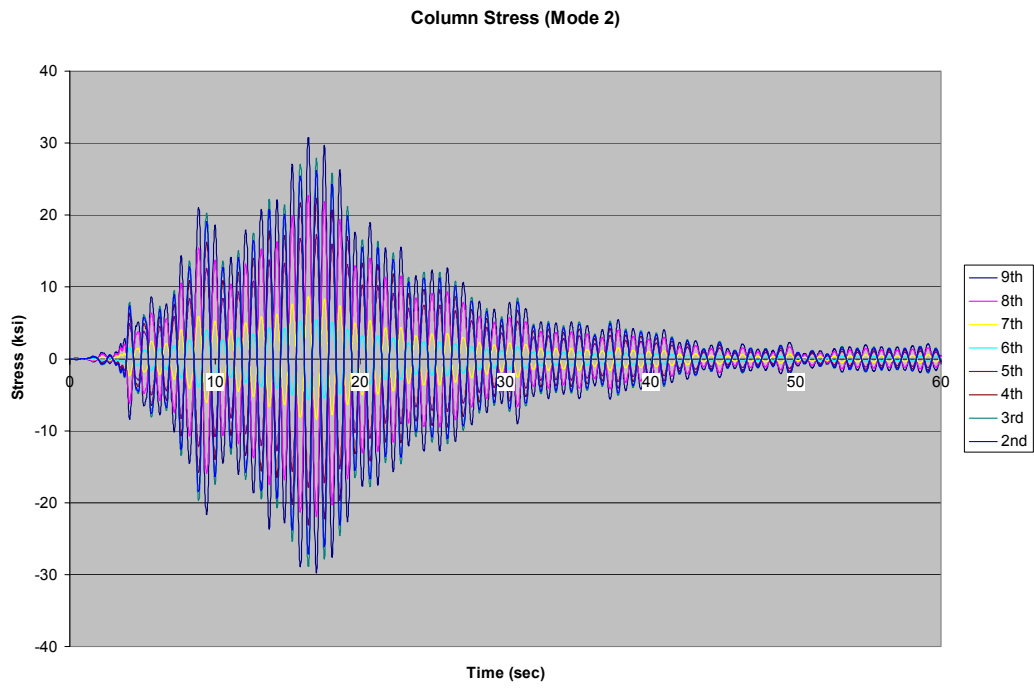


Figure 4.25: Column stress history (contribution of the 2<sup>nd</sup> mode).

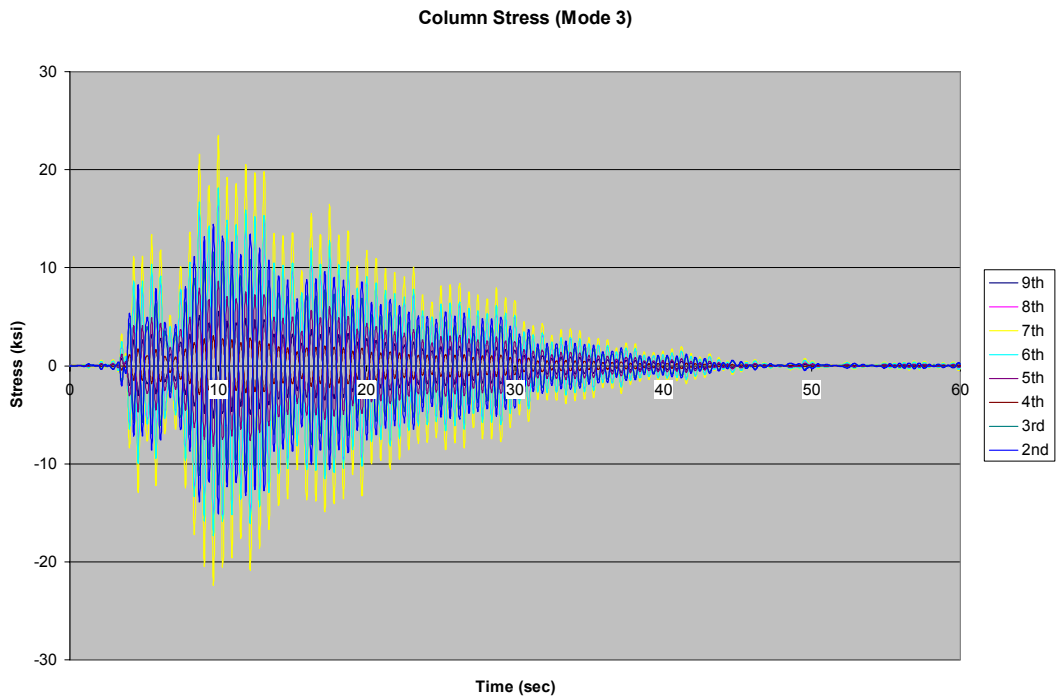


Figure 4.26: Column stress history (contribution of the 3<sup>rd</sup> mode).

## 4.2.2 Non-Linear Direct Integration Time-History Analysis

A series of non-linear direct integration time-history analyses was performed on the same model used for the linear modal time-history analysis. The purpose was to study the effect of nonlinearities in the behavior of the frames and to investigate the adequacy of the linear model for the purpose of this research project.

### 4.2.2.1 Effect of Material Properties

According to the design documents, the material used for the beams and columns had yield stresses of 36 and 50 ksi, respectively (A36 beams and A572 GR.50 columns). In this document, these material properties are referred to as *theoretical material properties*. The mill test results on the other hand, indicate that the average values of  $F_y$  and  $F_u$  for the beams and columns are as follows:

Beams:  $F_y = 50$  ksi ;  $F_u = 70$  ksi

Columns:  $F_y = 52$  ksi ;  $F_u = 75$  ksi

These values are referred to as *mill test material properties* in this document. A series of non-linear direct integration time-history analyses was performed considering different material properties for beams and columns and the analysis

results from *theoretical material properties* was compared to the results from *mill test material properties*. Figure 4.27 and 4.28 illustrate the roof displacement history calculated from these two analyses.

As shown in these figures, the displacement results are very similar. Figure 4.29 compares the stress history at the 7<sup>th</sup> floor column calculated by using the *theoretical* and *mill test material properties* in the analysis. The result shows that the column stress under this earthquake record is not very sensitive to the material properties selected for the analysis. This indicates that the behavior is primarily linear-elastic.

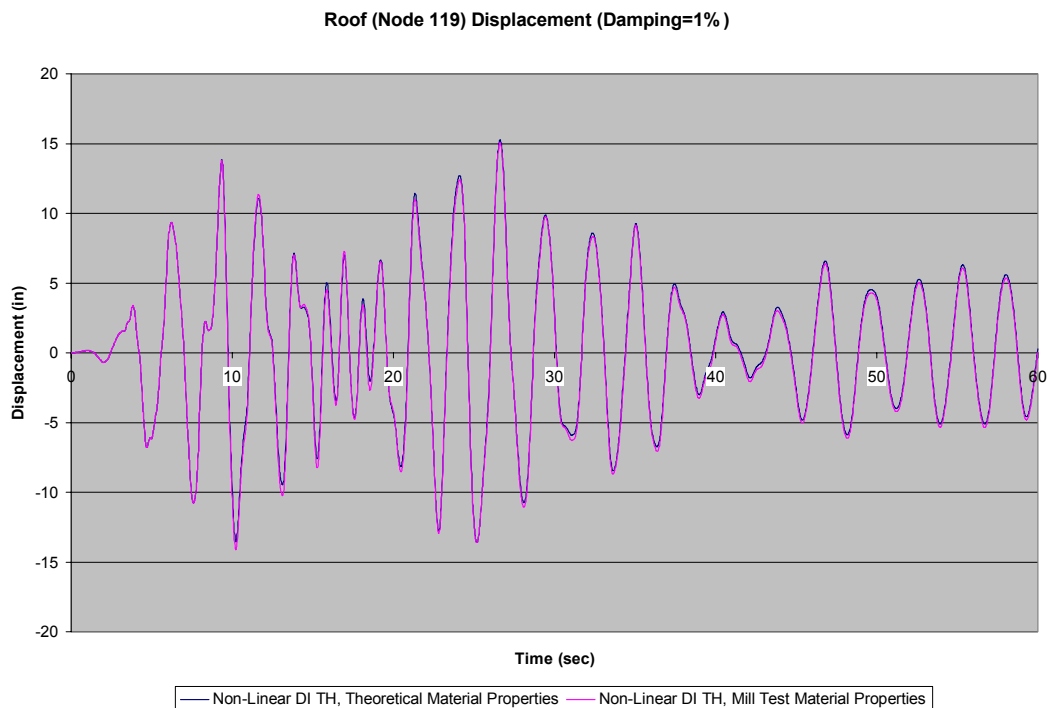


Figure 4.27: The effect of material properties on the result of nonlinear analysis.

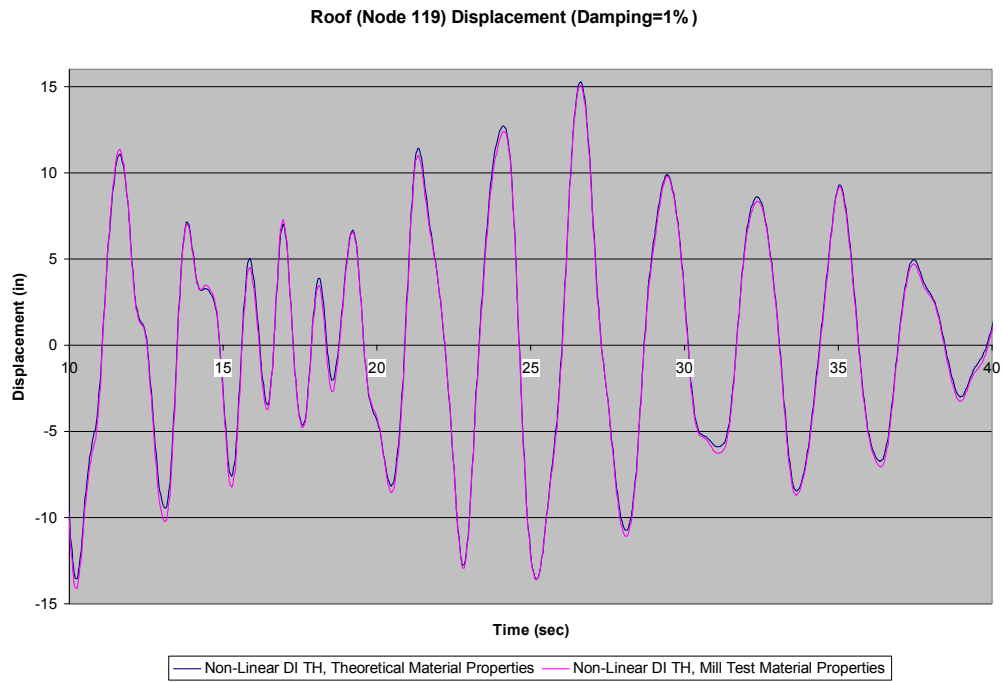


Figure 4.28: The effect of material properties on the result of nonlinear analysis.

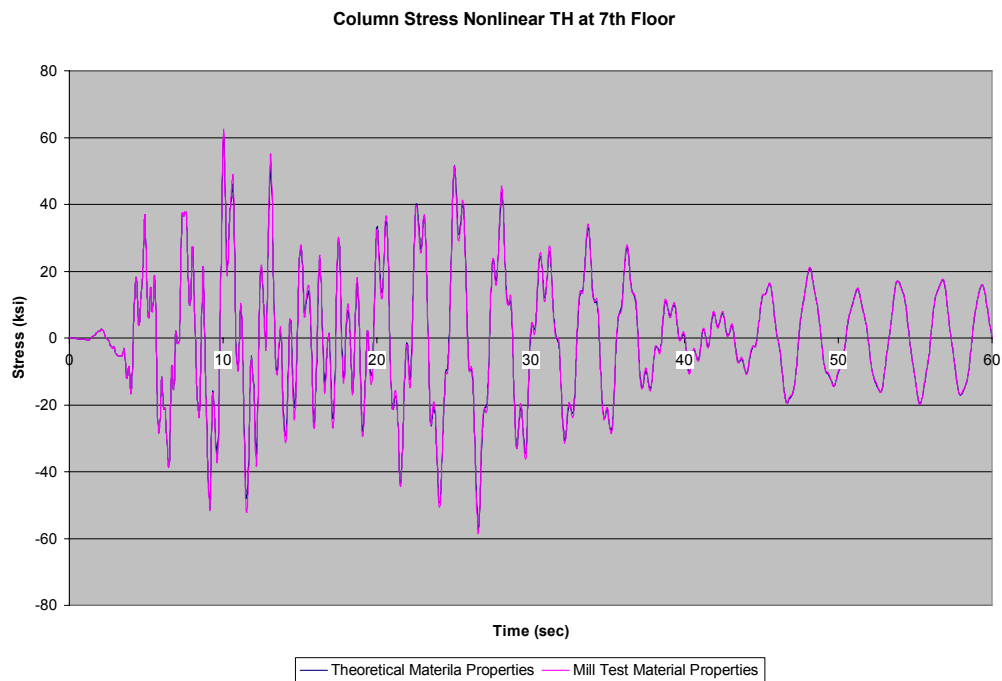


Figure 4.29: The effect of material properties on the column stress history calculated from the non-linear direct integration time-history analysis.

#### 4.2.2.2 Linear vs. Non-Linear Time-History Results

In this section, the result of the linear modal time-history analysis is compared to the non-linear direct integration time-history results. Figure 4.30 depicts the displacement histories at the roof calculated by the linear and non-linear analyses. Also, figure 4.31 illustrates the column stress histories resulted from the nonlinear direct integration time-history analysis. It should be noticed that the stress shown in this graph is calculated by dividing the moment at the end of each member (M) by the elastic section modulus (S). The reason for using the elastic section modulus (and not the plastic section modulus) is to keep the stress levels comparable to those of linear analysis. Comparing this figure with the result of the linear modal time history analysis shown on figure 4.23, indicates that the stresses are in the same range.

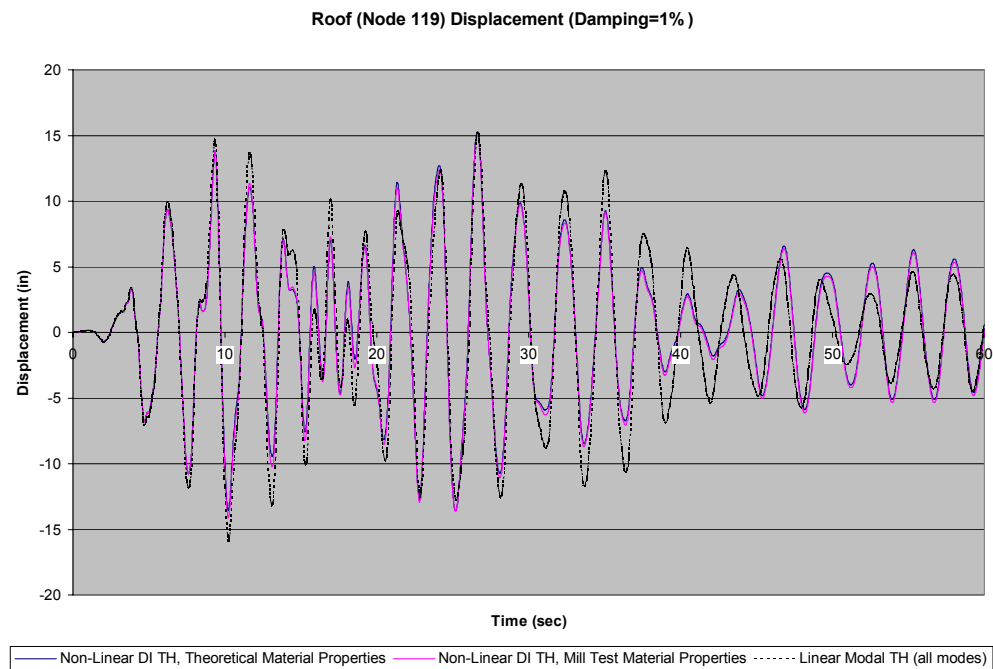


Figure 4.30: Comparison between the linear and nonlinear analysis results.

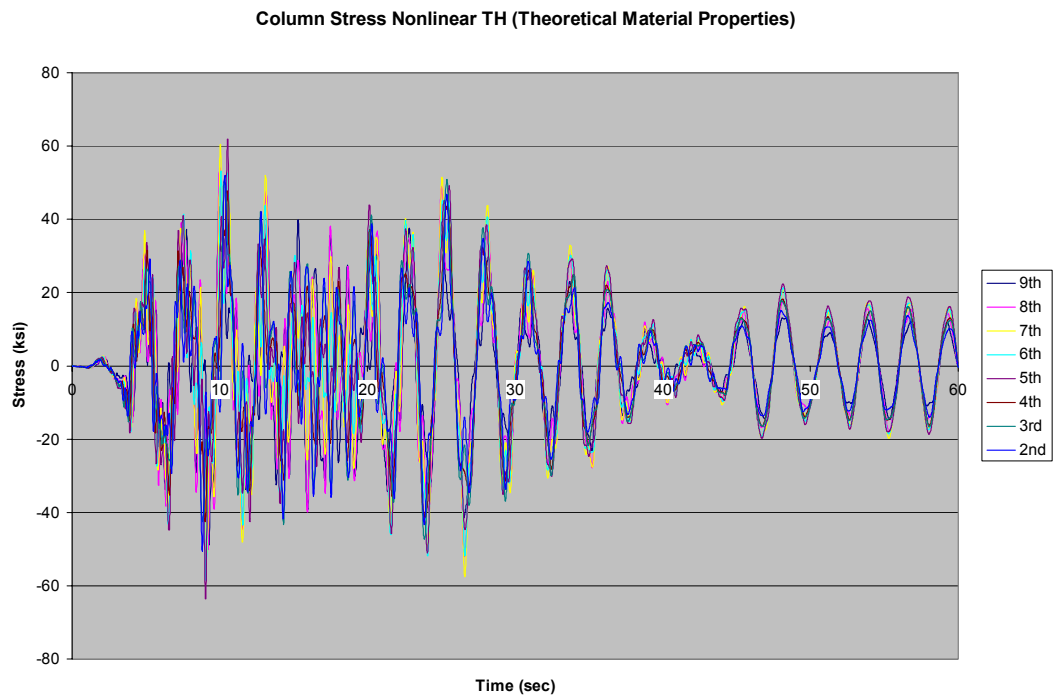


Figure 4.31: Column stress (equivalent M/S stress) history calculated from the nonlinear time-history analysis.

As indicated earlier in this chapter, the CDMG record at the roof of the building was available for this study. Result of a moving-window Fourier transform of the CDMG roof acceleration record has been shown on figure 4.32. The moving window analysis has been performed in MATLAB [www.mathworks.com]. For this analysis, ten-second blocks with 5-second overlaps have been used. The results indicate that the first mode period of the building is 2.5 seconds. This result shows good compatibility with the first mode period of the analytical model. Figure 4.32 also shows that the first mode period of the building did not change during the Northridge event. This means that there have not been significant nonlinearities in the building.

This observation is well justified by studying the maximum stresses (M/S) at the investigated beams and columns. This study has been performed on maximum stresses resulting from the linear modal time-history analysis. As shown in figures 4.33 and 4.34, the maximum stresses are not significantly larger than the yield value. This combined with the fact that higher than yield stresses happened in very few cycles (figures 4.19 and 4.23), give more validity to the linear modal time history analysis. As a result, building nonlinearities have not been significant during the Northridge Earthquake and use of the linear modal time-history analysis is adequate for the purposes of this study. Low demand to capacity ratios as shown in figure 4.35 indicate that response is mainly linear-elastic and confirms the previous observations.

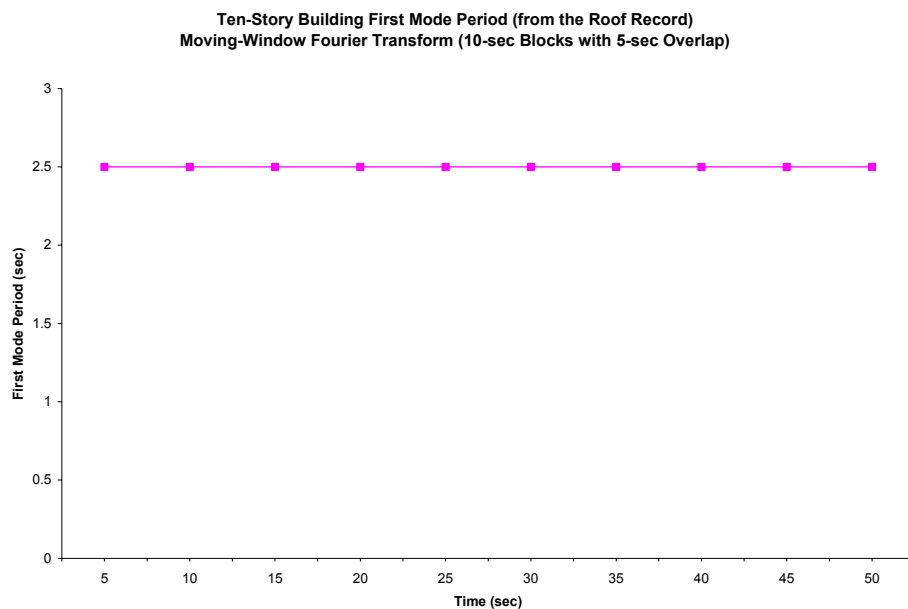


Figure 4.32: Moving-window Fourier transform of the CDMG roof acceleration record.

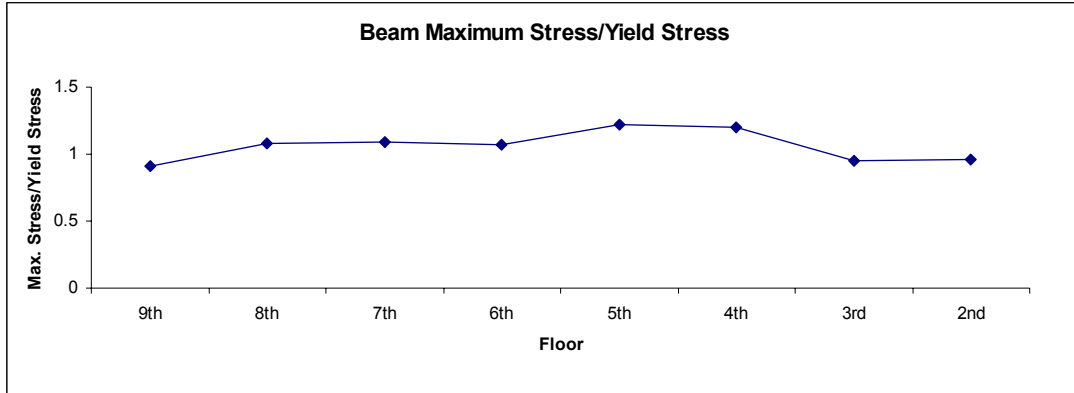


Figure 4.33: Ratio of maximum beam stress (M/S) from linear analysis to the material yield stress.

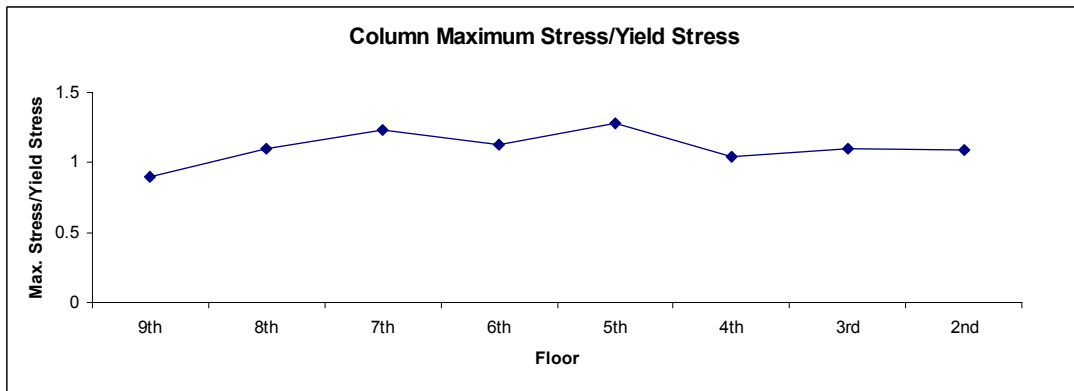


Figure 4.34: Ratio of maximum column stress (M/S) from linear analysis to the material yield stress.

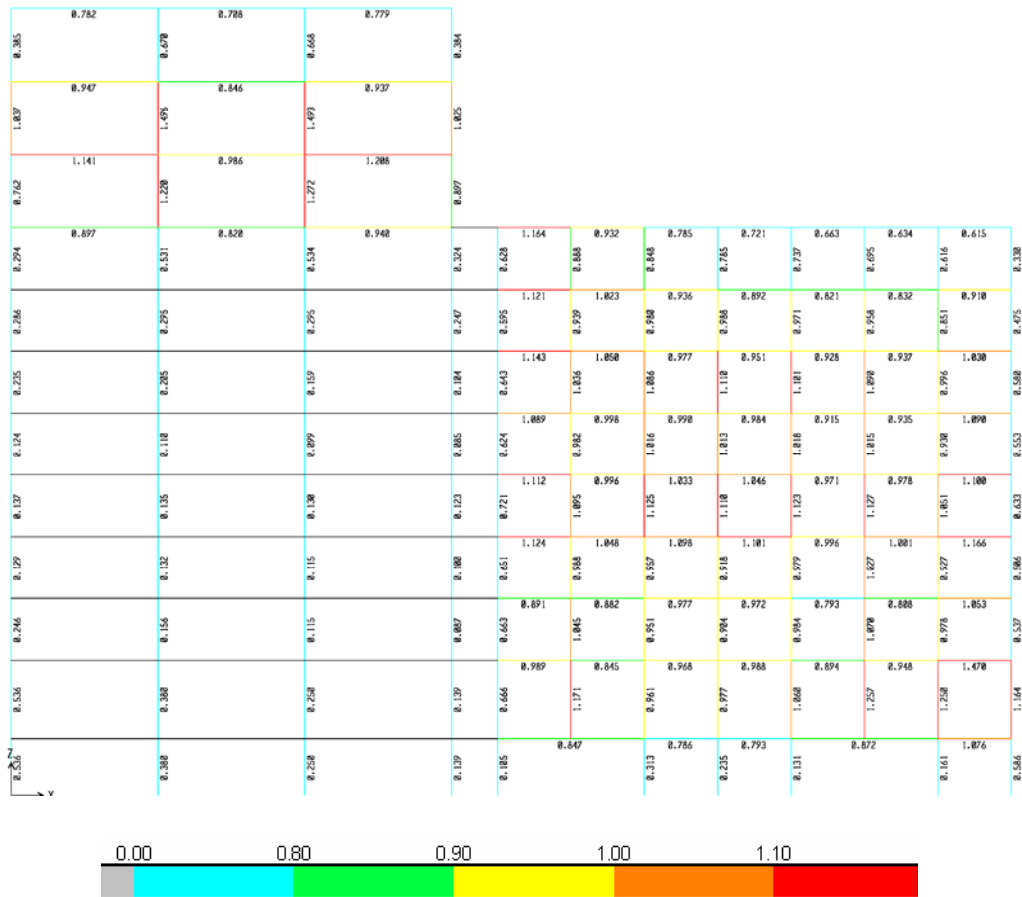


Figure 4.35: Demand to capacity ratios in the ten-story building result of linear modal time-history analysis using SAP 2000.



Modal analysis was performed and the periods of the first two modes were calculated to be:

$$T_1 = 0.60 \text{ sec}$$

$$T_2 = 0.18 \text{ sec}$$

Figures 4.37 and 4.38 show the first two mode shapes of the model.

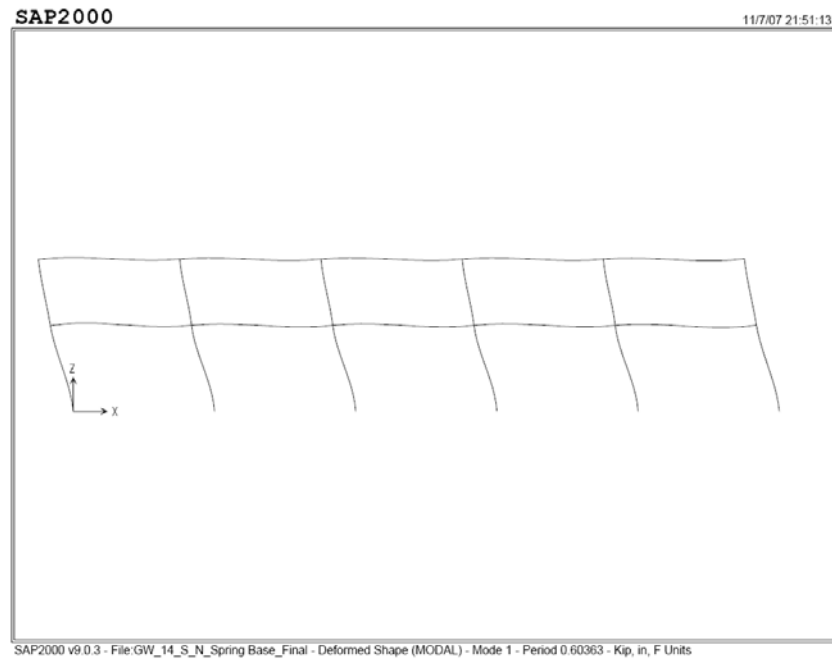


Figure 4.37: 1<sup>st</sup> mode shape.

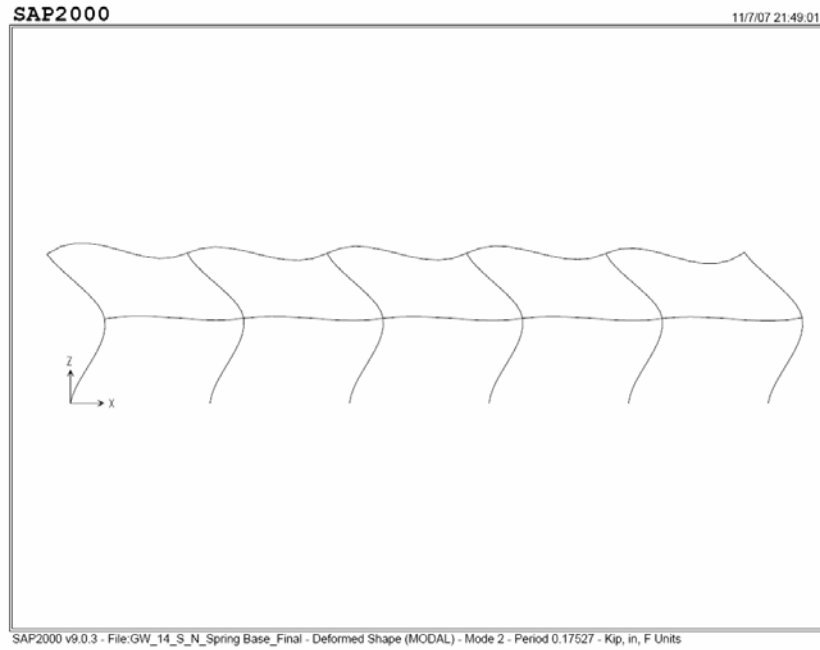


Figure 4.38: 2<sup>nd</sup> mode shape.

### 4.3.1 Linear Modal Time-History Analysis

A linear modal time-history analysis was performed on the frame. The USC 03 record in South direction (as shown in section 4.1) was used as the ground motion.

#### 4.3.1.1 Stress Histories and Contribution of Each Mode to Total Stress

As described earlier for the ten-story building, a similar study was performed on beam and column stresses of the two-story building. The goal was to investigate the

contribution of higher modes (in this case 2<sup>nd</sup> mode) to the total stress created at the investigated beams and columns.

#### 4.3.1.1.1 Beam Stress

Figure 4.39 shows the total stress history at the 2<sup>nd</sup> floor beam and figure 4.40 illustrates the contribution of each of the first two modes in the beam stress.

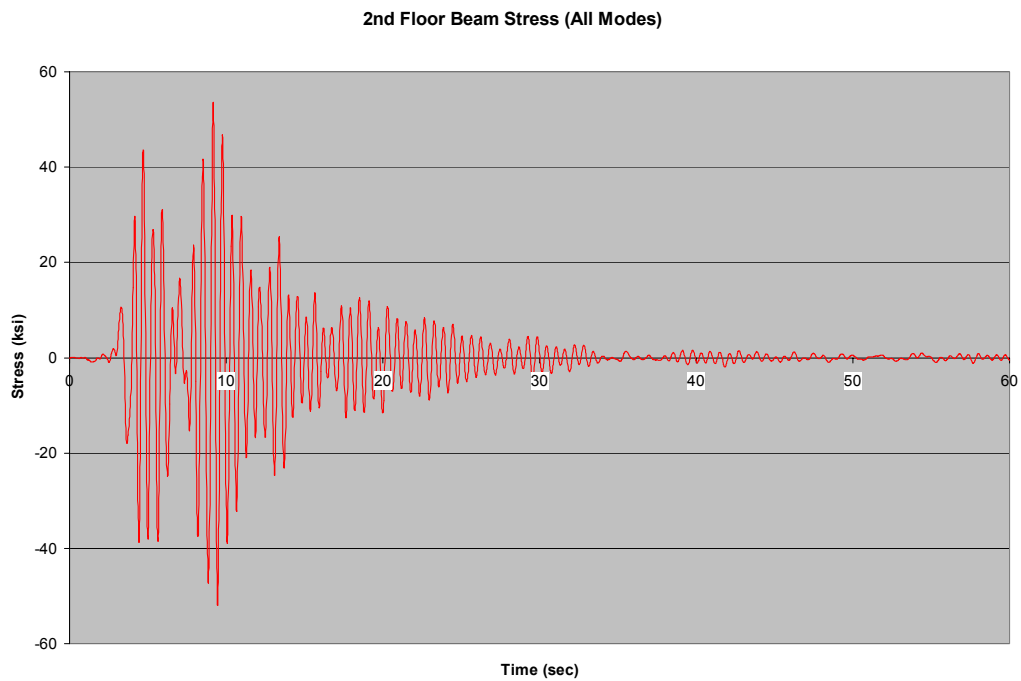


Figure 4.39: 2<sup>nd</sup> Floor beam stress history (contribution of all modes).

As seen on Figure 4.40, there is not much contribution from 2<sup>nd</sup> mode in the total beam stress and the 1<sup>st</sup> mode is somehow dominating the response.

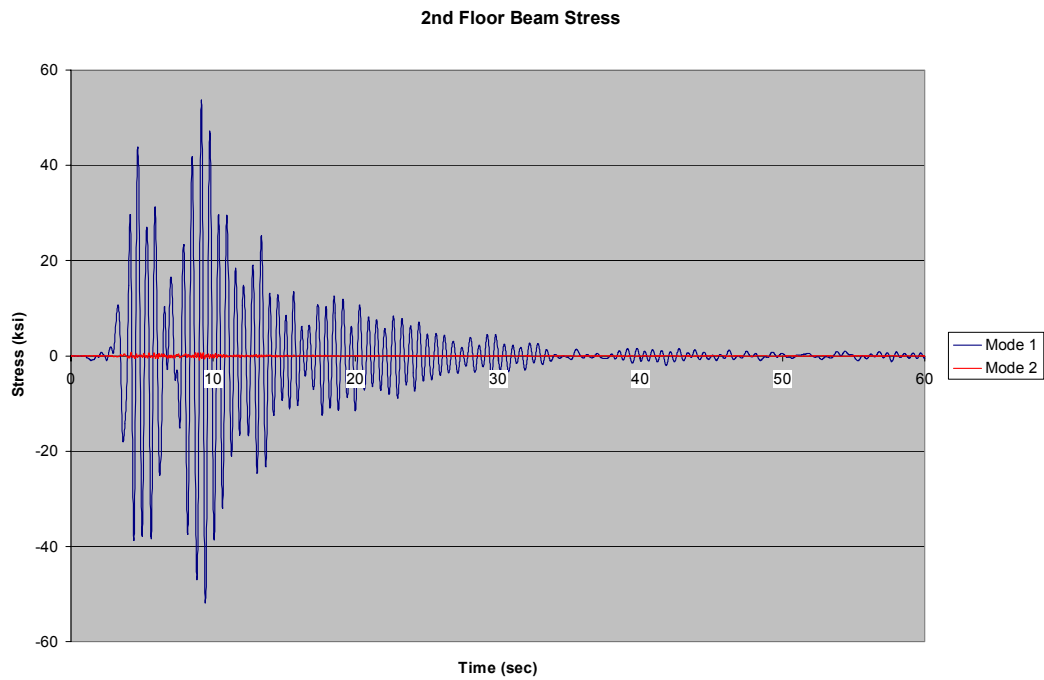


Figure 4.40: 2<sup>nd</sup> floor beam stress history (contribution of the 1<sup>st</sup> and 2<sup>nd</sup> modes).

Same observation can be made at the roof beam. Figures 4.41 and 4.42 show the roof beam stress histories.

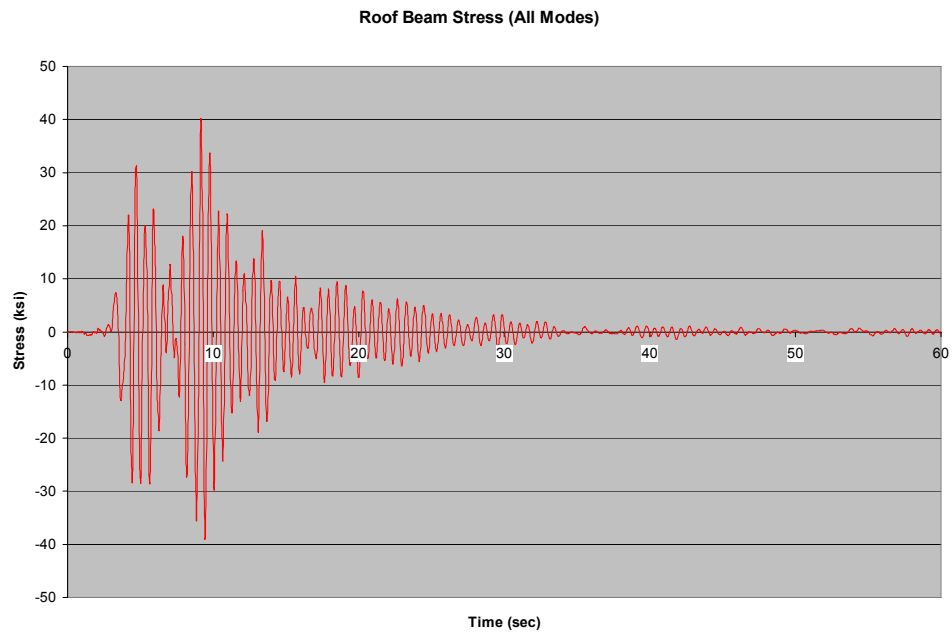


Figure 4.41: Roof beam stress history (contribution of all modes).

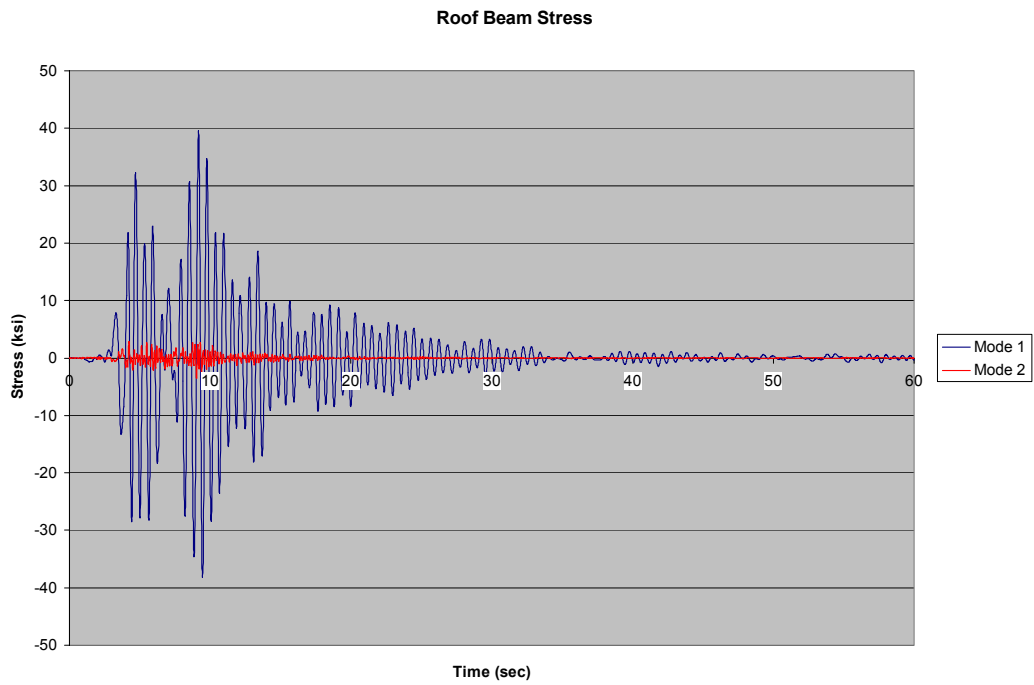


Figure 4.42: Roof beam stress history (contribution of the 1<sup>st</sup> and 2<sup>nd</sup> modes).

### 4.3.1.1.2 Column Stress

The 2<sup>nd</sup> floor column stress histories, shown on Figures 4.43 and 4.44, indicate that there is not a significant contribution from the 2<sup>nd</sup> mode of vibration to the total stress. In other words, the first mode creates a significant share of the total stress.

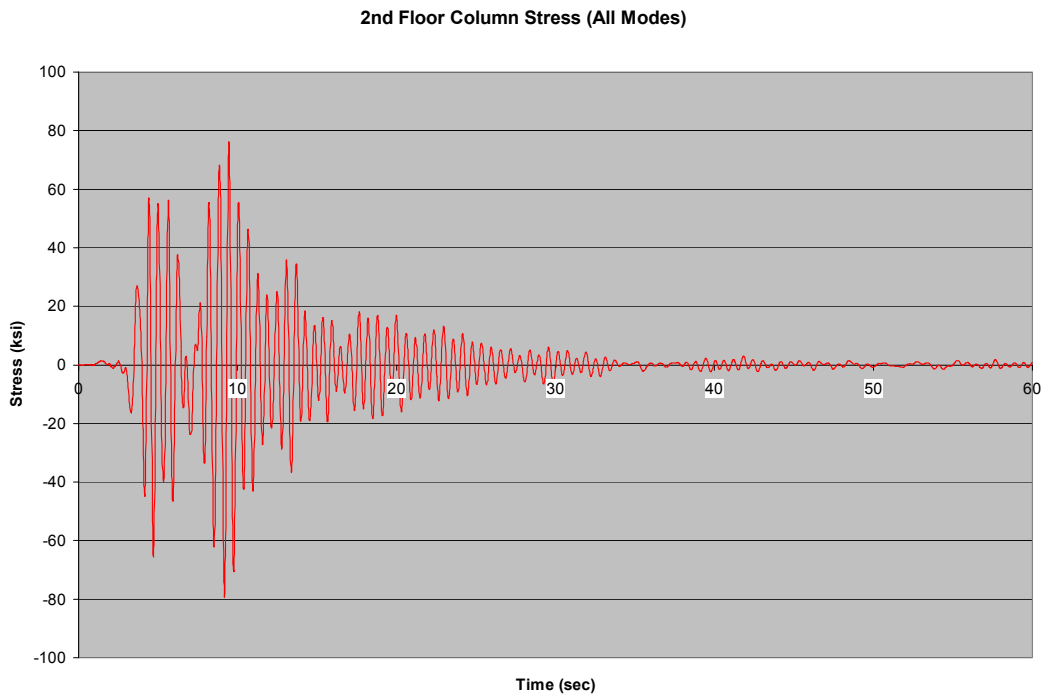


Figure 4.43: 2<sup>nd</sup> floor column stress history (contribution of all modes).

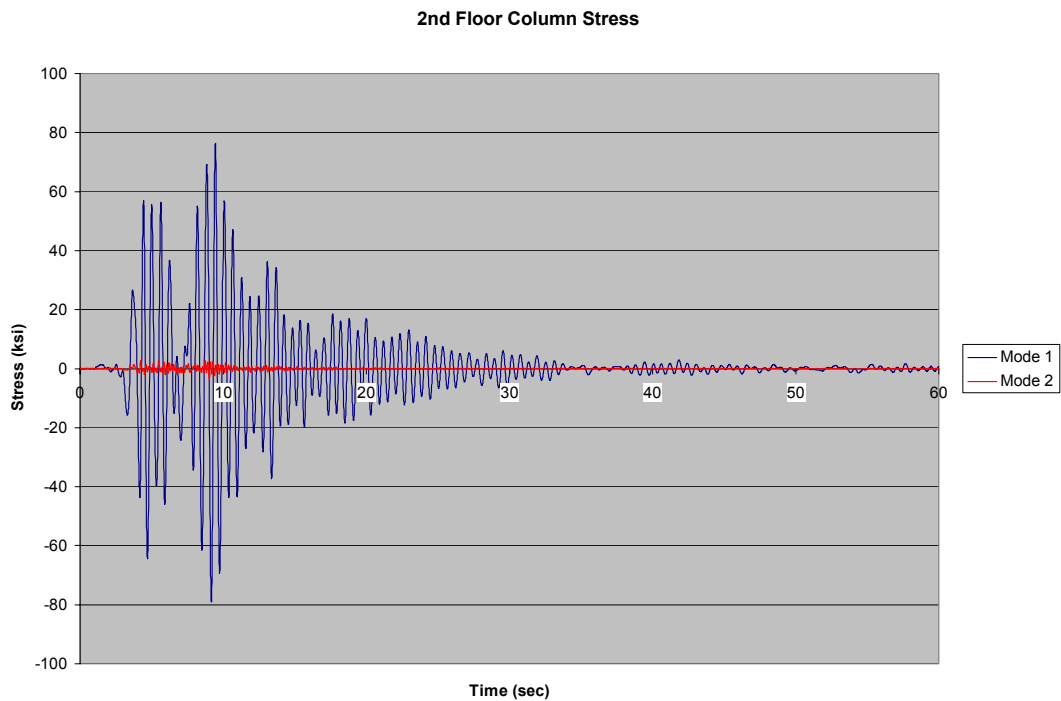


Figure 4.44: 2<sup>nd</sup> floor column stress history (contribution of the 1<sup>st</sup> and 2<sup>nd</sup> modes).

Same conclusion can be made from the stress histories shown on figures 4.45 and 4.46. The observations of the beam and column stress histories indicate that the higher mode effects do not appear to be significant for the investigated two-story building. It can be concluded that the first mode of vibration is potentially the major contributor in the connection damages occurred in this building. The result of cumulative fatigue studies described later on in chapters five and six of this document confirm this theory.

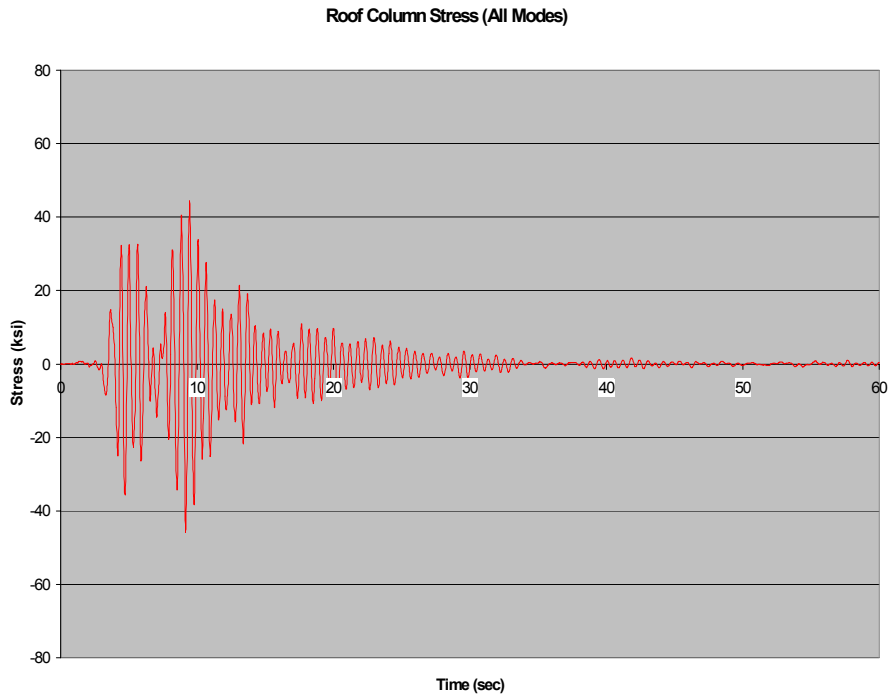


Figure 4.45: Roof column stress history (contribution of all modes).

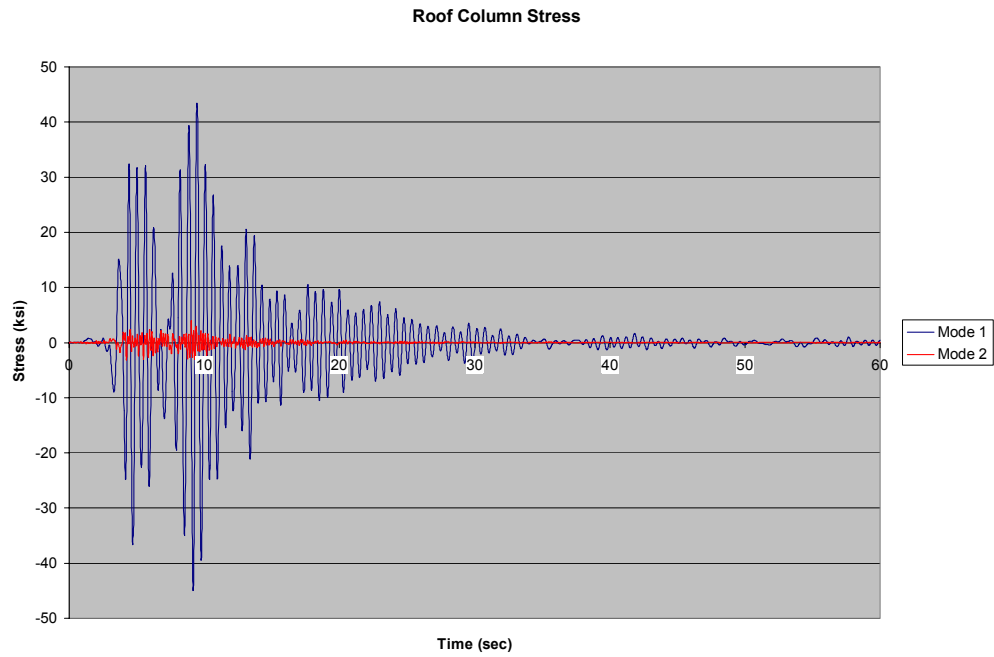


Figure 4.46: Roof column stress history (contribution of the 1<sup>st</sup> and 2<sup>nd</sup> modes).

## CHAPTER 5: FATIGUE ANALYSIS

This chapter contains the procedure and the results of a series of fatigue analyses performed on the investigated ten-story and two-story buildings. Cumulative fatigue is calculated and the effect of higher modes on cumulative fatigue is investigated.

### 5.1 Fatigue Analysis Procedure

Since stresses at the investigated beams and columns do not have a constant harmonic amplitude, the selected fatigue assessment procedure needs to be applicable to variable stress ranges. The study of different fatigue assessment methods resulted in using the *linear damage rule* that is widely used in civil engineering practice. This method, which is known as *Palmgren-Miner rule* was first proposed by Palmgren in 1924. Two decades later, Miner further developed the procedure in 1945. [9], [23], [39]

This method assumes that the damage fraction resulting from each particular stress range is a linear function of the number of cycles at that stress range. As a result, the total fatigue damage in the detail is the sum of the damage from all different stress levels that are applied to it. This can be written as the following equation. [9], [23], [39]

$$\sum \frac{n_i}{N_i} = 1$$

Where  $n_i$  and  $N_i$  are defined as follows:

$n_i$ : Number of cycles at stress level  $i$  (from time-history analysis).

$N_i$ : Number of cycles to failure at stress level  $i$  (from S-N curve).

Based on the results of the time-history analyses explained in chapter four, the number of cycles at each stress level ( $n_i$ ) can be computed through a cycle counting process. As described later in this chapter, the *rainflow method* [9], [23], [39] is selected as the cycle counting procedure for the beam and column stress histories.

The number of cycles to failure at each stress level ( $N_i$ ) is another parameter in the fatigue equation. Fatigue life of the investigated detail at each stress level is needed to determine this parameter. As a result, establishing a fatigue life curve for the investigated Pre-Northridge moment connection appears to be essential for this study. This curve is technically known as *S-N curve* and illustrates the stress versus the number of cycles to failure. The following section of this document includes the steps taken to establish an *S-N curve* suitable for this study.

## **5.2 S-N Curve**

The current research tried to use all applicable technical resources and fatigue test results available at the time of this work. Since the available fatigue tests for the investigated beam-column connection detail are limited, a probabilistic approach is not possible. Therefore, the S-N curve developed later in this chapter, and consequently the fatigue analysis results, are based on the available test data at the time of this study.

### **5.2.1 Available Fatigue Test Data**

A thorough study has been performed on the fatigue tests available at the time of this research. Independent tests have been done on low-cycle and high-cycle regions that are investigated in this section.

#### **5.2.1.1 Tests by Fisher et al.**

Investigations conducted by Fisher et al. (1977) [22] are mainly used for the high-cycle region of the S-N curve. Figure 5.1 illustrates the results of these tests for *rolled beams*, *welded beams*, and *beams with end welded cover plate*.

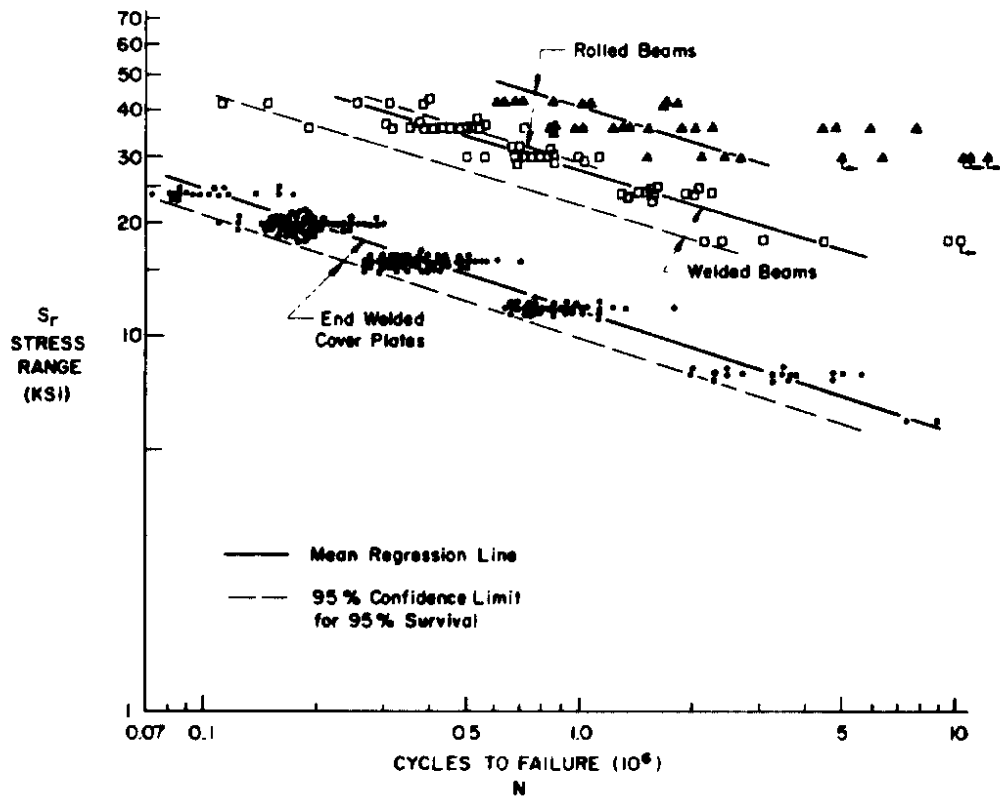


Figure 5.1: S-N curves for different beam details. [22]

These tests results have been widely used in establishing most of the fatigue design criteria currently used in United States. Since the high-cycle fatigue is significant in bridge structures, the criteria developed from these tests are widely used in fatigue design and assessment of bridges [1]. “Fatigue and Fracture in Steel Bridges” [21] includes a series of case studies by Fisher on the fatigue in steel bridges. Also, in a document published by Fisher et al. (1998) [23], the authors present more fatigue test results in the high-cycle region. Figure 5.2 depicts the S-N curves presented in that document for *welded and coveplated beams*.

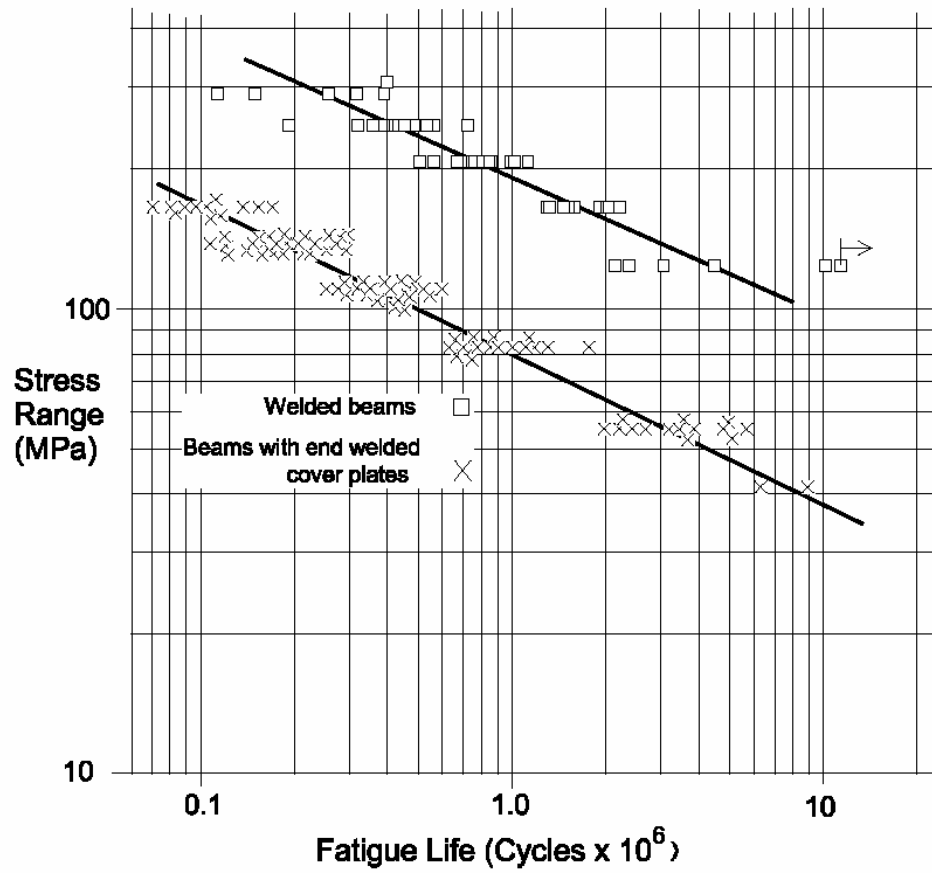


Figure 5.2: S-N curves for welded and coverplated beams. [23]

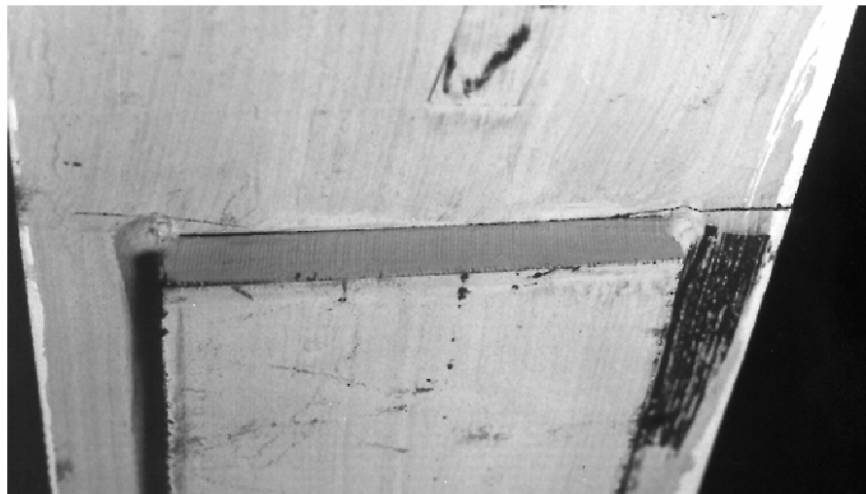


Figure 5.3: Fatigue crack at the end of cover plate fillet weld toe. [23]

The results shown in this figure, completely match the S-N curves in figure 5.1. The fatigue crack, which is the main mode of failure for *coverplated beam* specimens, has been illustrated in figure 5.3.

The current study uses the appropriate *stress concentration factors* in these test results in order to apply them to the investigated Pre-Northridge connection detail. This will be further explained in the following pages.

#### **5.2.1.2 Tests by Partridge et al.**

Ten full scale fatigue tests have been performed in the low-cycle region. Figure 5.4 shows the setup for these tests. Identical W14x155 columns and W18x40 beams have been used for this experimental study. Backup bars were left in place in the first two tests and were removed for the rest of the experiments. Figure 5.5 shows the results of the study by Partridge et al. [31] based on the test data.

The current study mainly uses these test results for the low-cycle region. Relevant *stress concentration factor* has been used to account for the back-up bar which is further clarified later in this chapter.

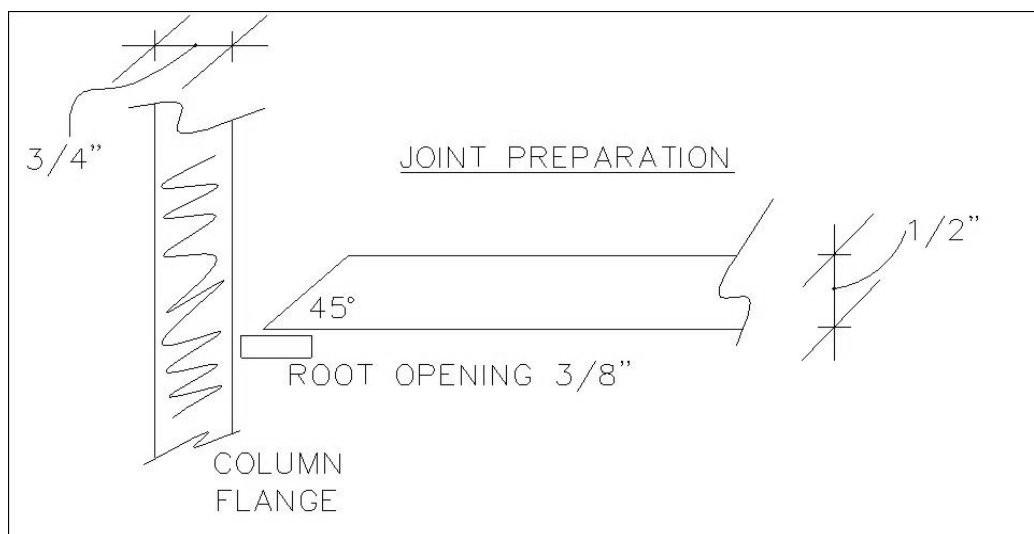
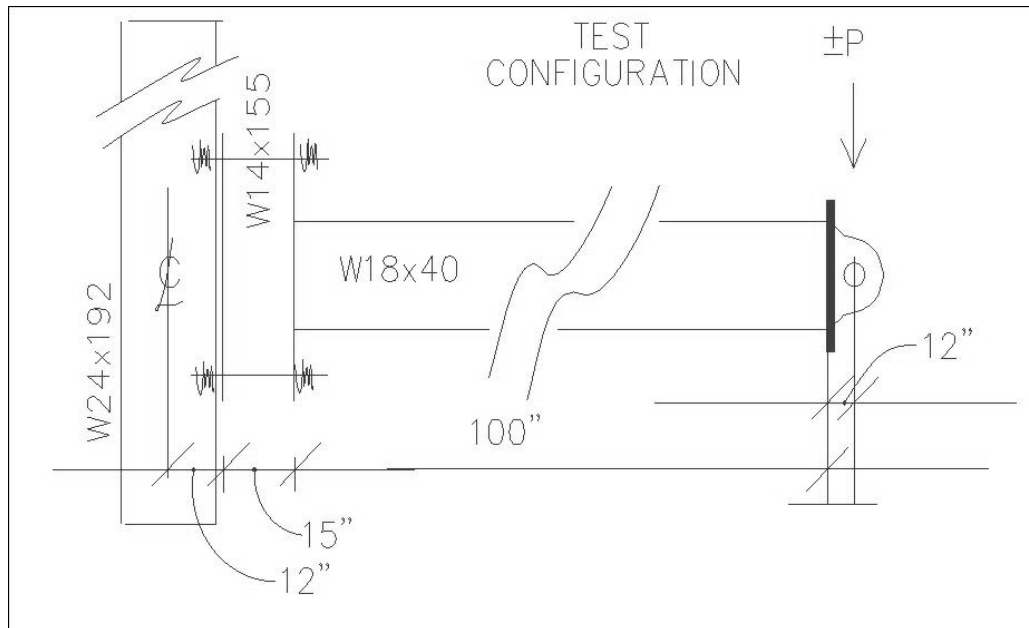


Figure 5.4: Low-cycle fatigue test setup (courtesy of James Partridge).

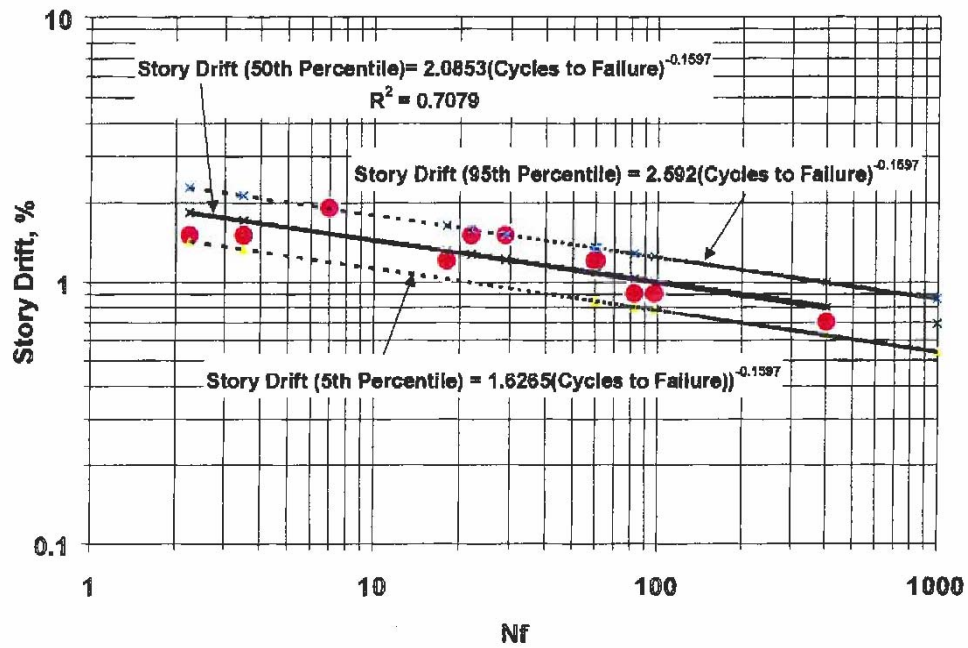


Figure 5.5: Low-cycle fatigue test results. [31]

### 5.2.1.3 Tests by Kuwamura et al.

A series of low-cycle fatigue tests on welded joints with high-strength steel members has been performed in Japan by Kuwamura et al. The result of their studies was published in a paper in the proceedings of *the Tenth World Conference on Earthquake Engineering* [25].

A new type of high-strength steel was used for these tests. The properties of this new material were as follows:

$$F_y = 62.5 \text{ ksi}$$

$$F_u = 85.3 \text{ ksi}$$

Test specimen comprised an H-shape member with 200mm x 100mm x 9mm x 9mm dimensions. Backup bars were removed for all tests. Tests were displacement controlled and it was concluded that fatigue failure happened at all the specimens.

Figure 5.6 illustrates the test setup and specimen details of these tests. The results of this study are used to verify the tests done by Partridge et al. [31]. The material used in the Japanese tests is significantly different from the regular steel used in the studies by Partridge et al. As a result, for comparison and verification purposes, the test stress values are normalized relative to the yield stress of the material. In other words, the maximum equivalent elastic stress is calculated for all tests by dividing the maximum moment (M) by the elastic section modulus (S). This value is then normalized by dividing it by the yield stress of material. The result of this comparison can be observed in figure 5.7.

It is concluded that the investigated tests appear to be significantly consistent. This validates the results of the tests by Partridge et al.

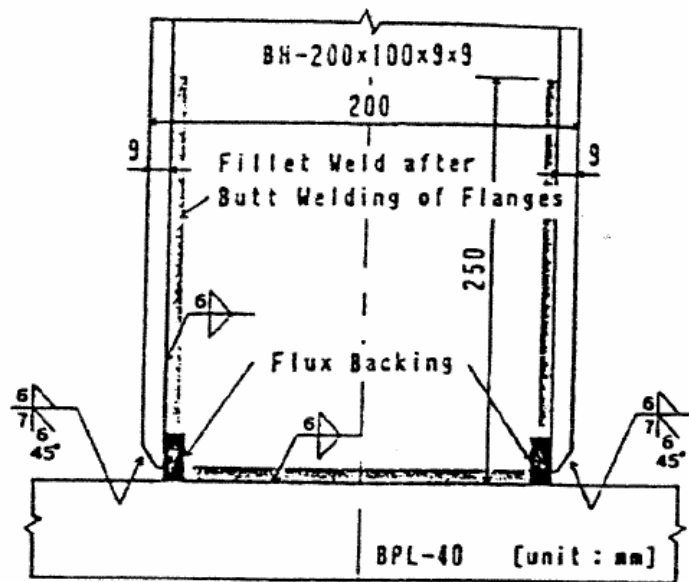
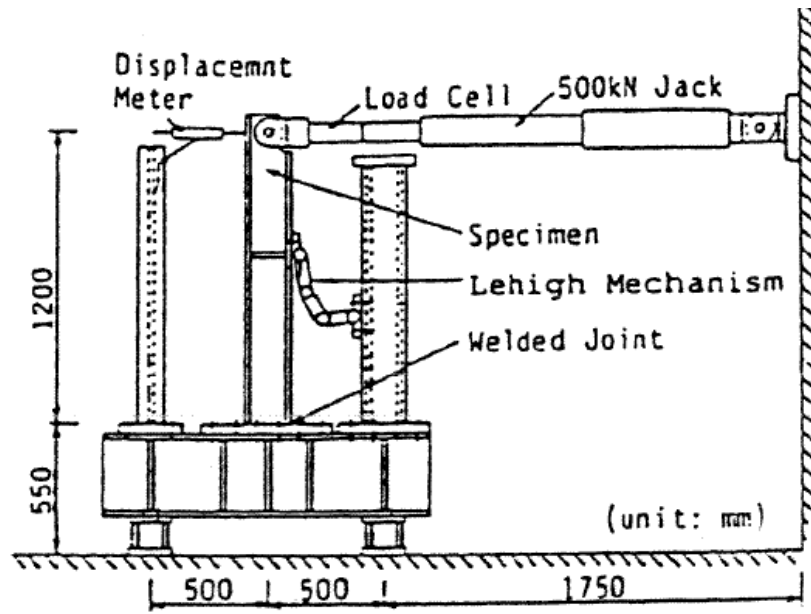


Figure 5.6: Low-cycle fatigue test setup and specimen detail. [25]

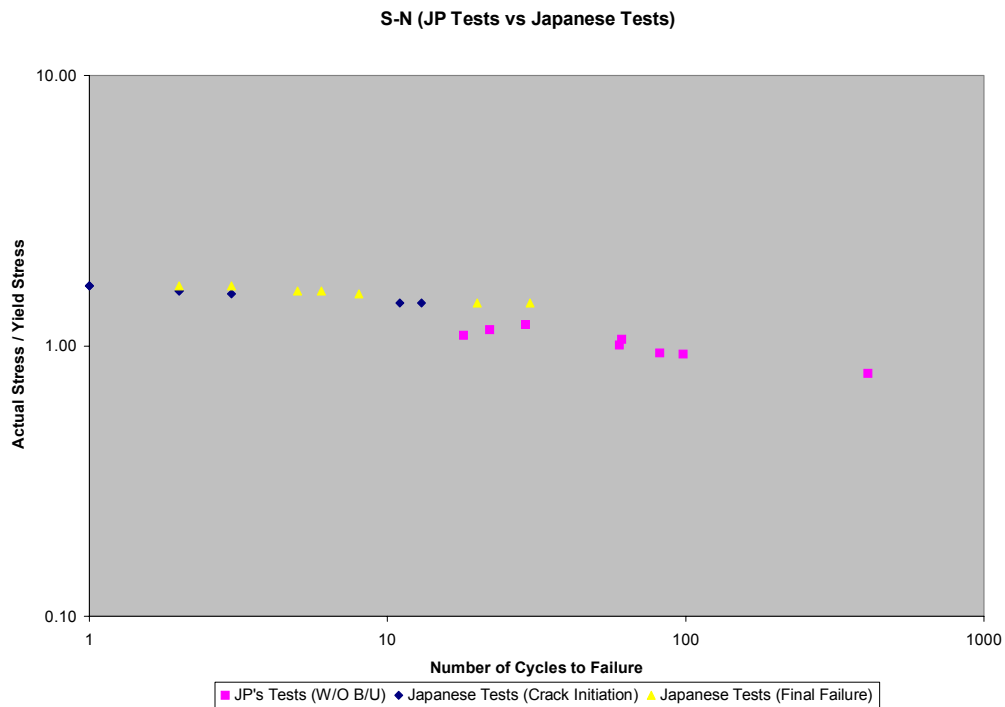


Figure 5.7: Comparison between the available low-cycle fatigue tests.

As a conclusion of the agreement between the results, the tests by Partridge et al. are selected to be used in the current study as the basis of S-N curve in low-cycle region.

Figure 5.8 depicts the fatigue test data selected for the current study. It can be observed that data points from the tests by Fisher et al. have been plotted in the high-cycle region. In the low-cycle area, eight data points plotted in pink show the tests by Partridge et al. on the Pre-Northridge connection specimens without backup bar. These points can be represented by the line shown in yellow.

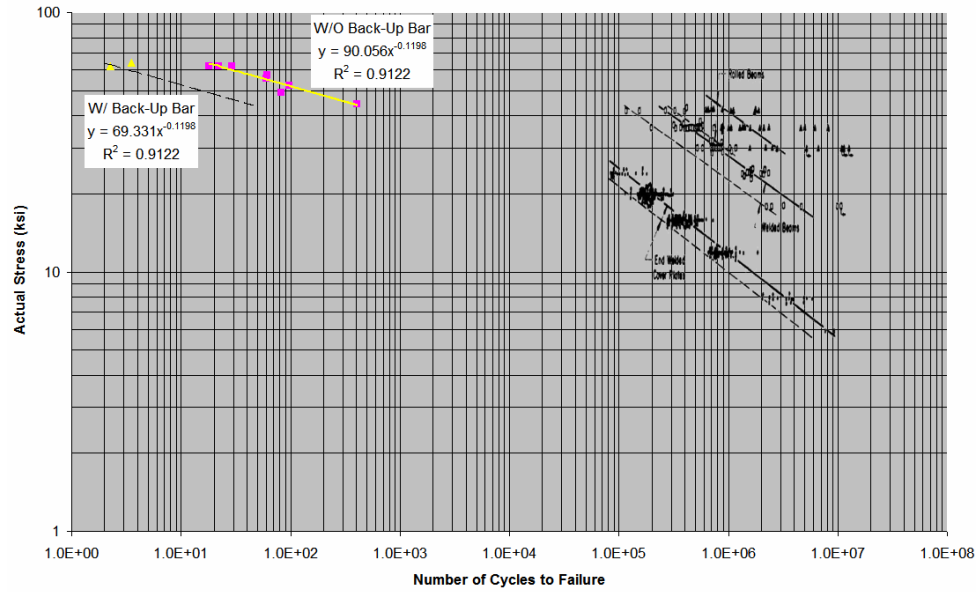


Figure 5.8: Fatigue test results.

Also, the two yellow data points shown in figure 5.8 represent the two tests performed on specimens with backup bar. The dotted line shown in the graph represents the low-cycle fatigue curve for the Pre-Northridge specimens with backup bar. The *stress concentration factor* associated with backup bar is described in the next section.

### 5.2.2 Stress Concentration Factor

The *stress concentration factor*, which will be referred to as SCF in this document, is defined as the ratio of the maximum stress caused by stress concentrations to the

analytical stress (M/S). SCF is a critical element in establishing the *S-N curve* and as a result careful study is performed to estimate the relative SCF for the investigated Pre-Northridge moment connection.

#### **5.2.2.1 Available Test Data**

Comparing the overlapping area of solid and dotted lines in the low-cycle region of figure 5.8 indicates that based on tests by Partridge et al. the value of SCF is estimated to be 1.3 (for backup bars).

In the high-cycle region, tests by Fisher et al. indicate that SCF associated with *welded beams* and *beams with end welded cover plates* are respectively 1.5 and 3.5 relative to *rolled beams*. Figure 5.9 shows how these values are estimated.

#### **5.2.2.2 Steel Manuals**

In this section, the SCFs estimated from the available test results are verified using the well established fatigue criteria in widely accepted steel manuals. “AISC Steel Construction Manual” [2] and British “Steel Designers’ Manual” [29] (which is the

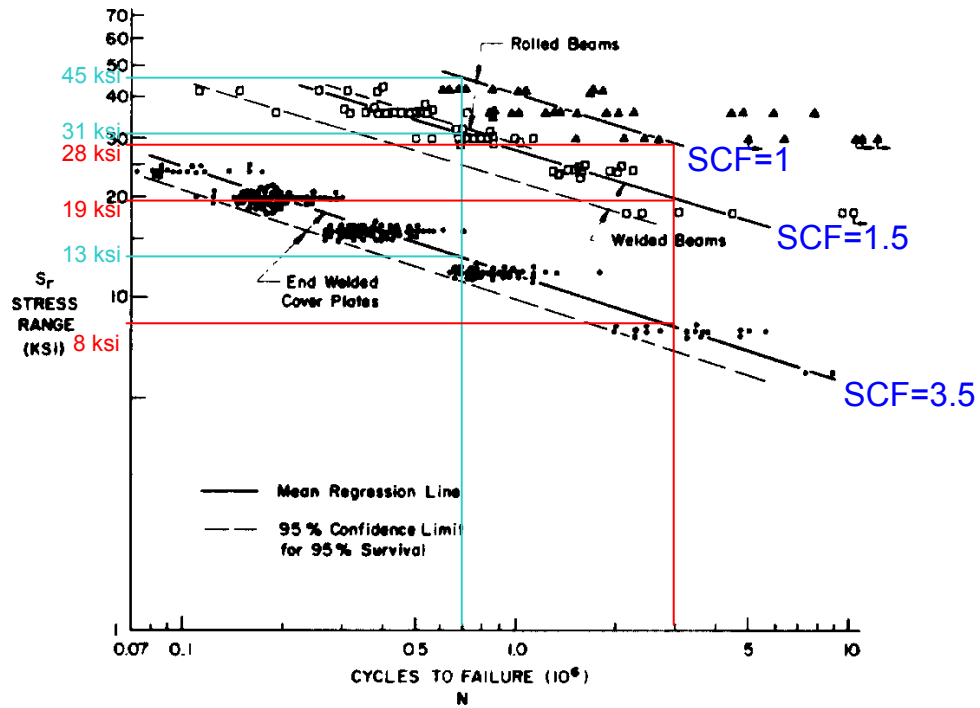


Figure 5.9: Stress concentration factors observed in Fisher's tests.

main reference for steel construction and design in Great Britain) have been selected for this verification study.

Observations from "AISC Steel Construction Manual" [2] are as follows:

- SCF of *base metal* is assumed to be 1 and all other SCFs are calculated relative to *base metal*.

- SCF of *rolled beams* is calculated to be 1.5.
- SCF of *beams with welded end cover plates* is calculated to be 5.3.
- SCF of *welded joints* (caused by weld) is calculated to be 2.4.
- SCF of *beams with welded end cover plates* relative to *rolled beams* is calculated to be  $5.3/1.5 = 3.53$ . This confirms the SCF estimated from tests by Fisher et al. which suggests a SCF of 3.5 (see figure 5.9) [22], [23].
- SCF of *welded joints* relative to *rolled beams* is calculated to be  $2.4/1.5 = 1.6$ . This confirms the SCF estimated from tests by Fisher et al. which suggests a SCF of 1.5 (see figure 5.9) [22], [23].

Observations from the British “Steel Designers’ Manual” [29] are as follows:

- SCF of *welded joints* relative to *rolled beams* is calculated to be 1.67. This confirms the SCFs presented in “AISC Steel Construction Manual” (SCF of *welded joints* relative to *rolled beams* =  $2.4/1.5 = 1.6$ ).

- SCF of *welded joints with backup bar* relative to *welded joints* (caused by backup bar) is calculated to be 1.3. This perfectly confirms the backup bar SCF estimated from the tests by Partridge et al. (1.3).

### **5.2.2.3 Finite Element Study**

A series of linear static finite element analyses was performed on the Pre-Northridge moment connection. ANSYS was used as the finite element software for this study. The purpose was to investigate the SCF caused by geometry of the detail. Two typical details of the Pre-Northridge moment connection, with and without continuity plates, were investigated.

Figure 5.10 shows the finite element model of the connection without continuity plates and figure 5.11 shows the result of the analysis. This study indicates that the SCF is 1.92 for the Pre-Northridge connection without continuity plates. This SCF is calculated as the ratio of maximum stress observed as the result of the finite element analysis to the maximum bending stress in the beam (M/S).

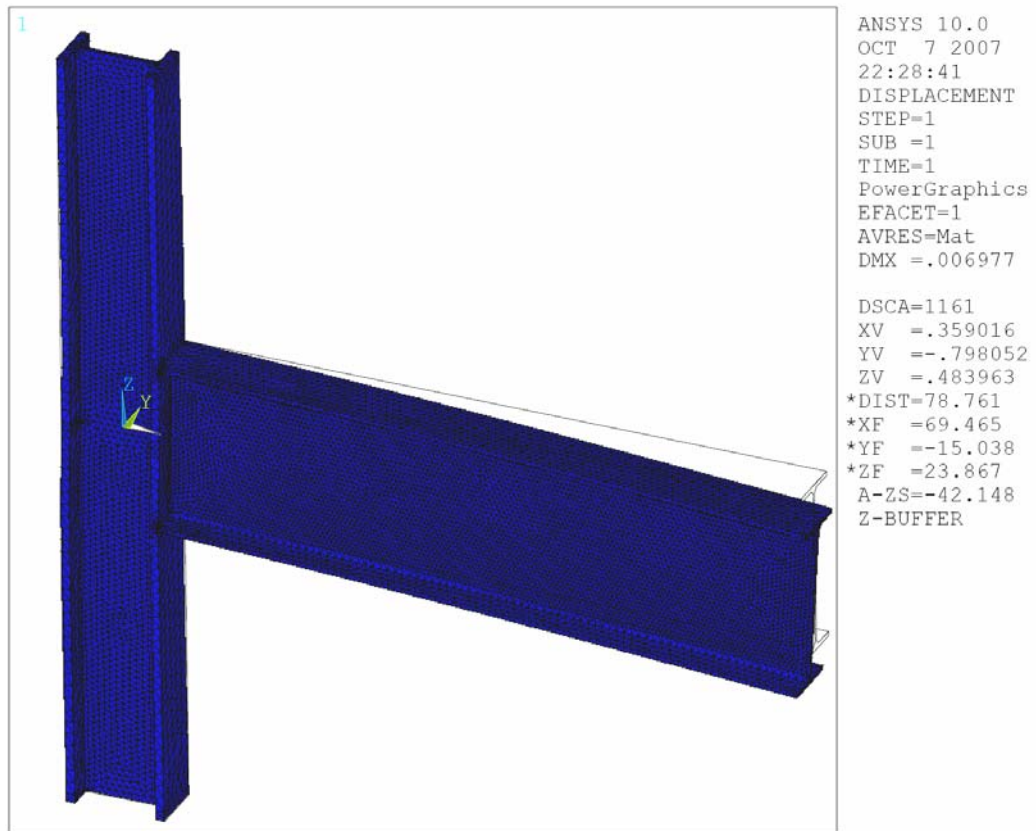


Figure 5.10: Finite element model of the Pre-Northridge connection without continuity plates.

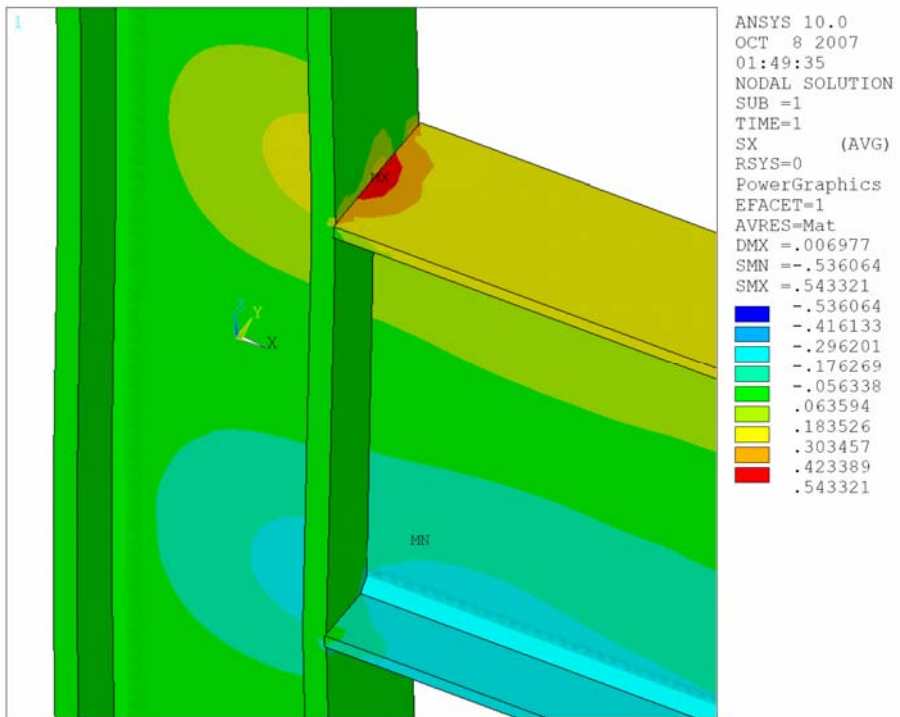
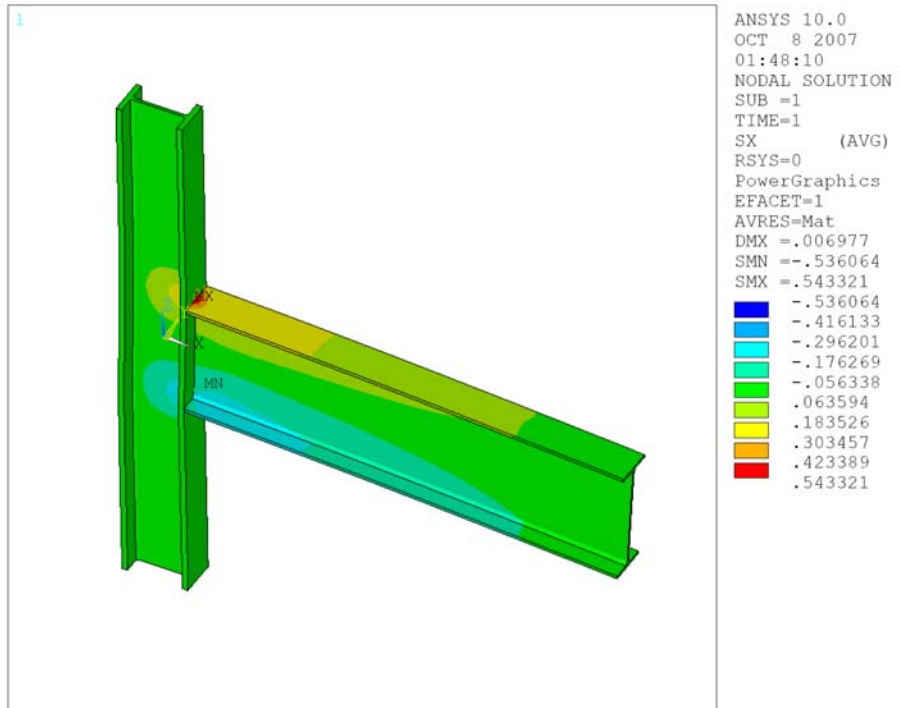


Figure 5.11: Result of the finite element study of the model without continuity plates.

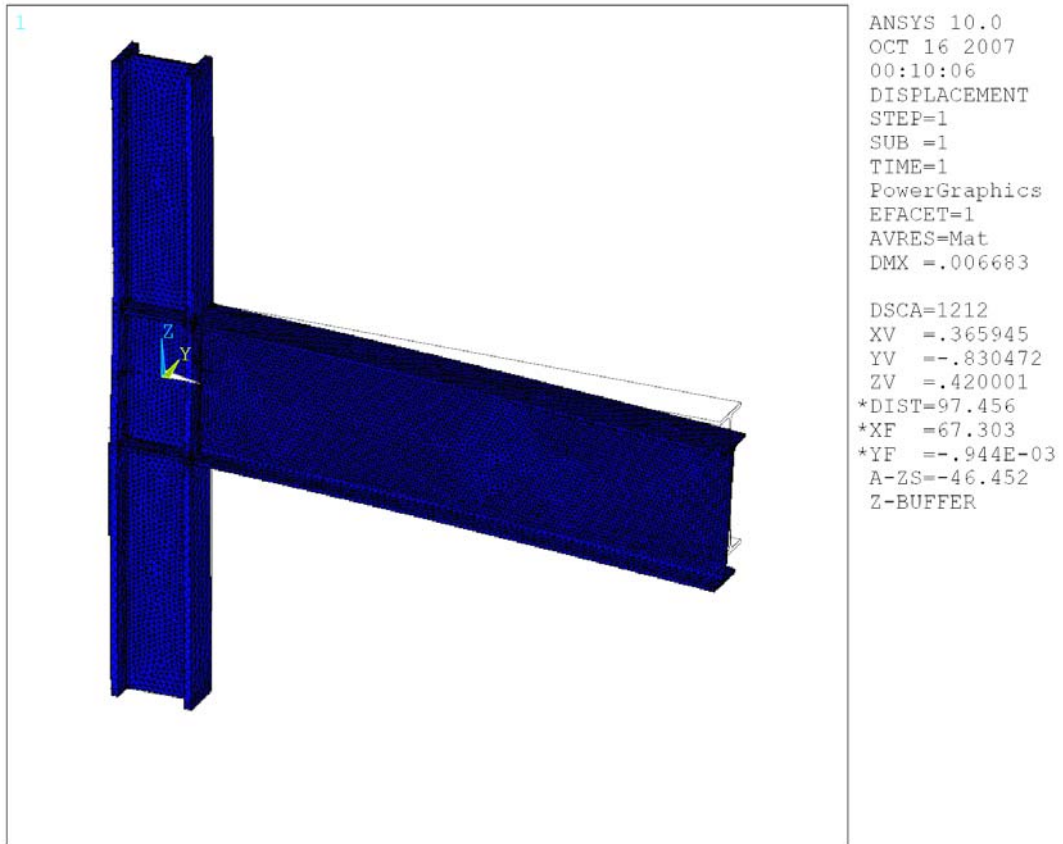


Figure 5.12: Finite element model of the Pre-Northridge connection with continuity plates.

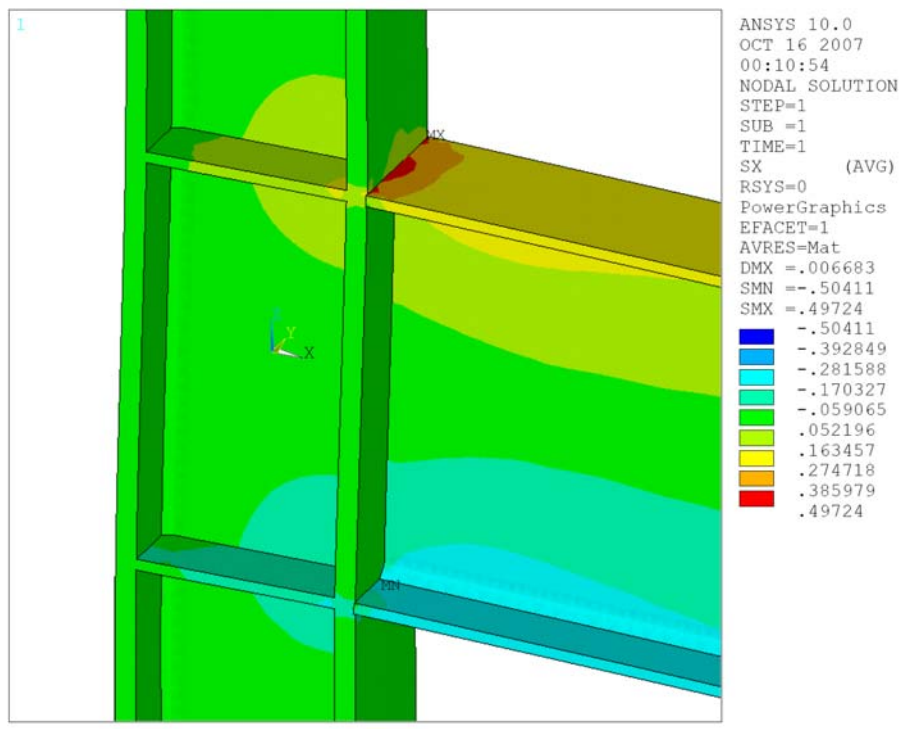
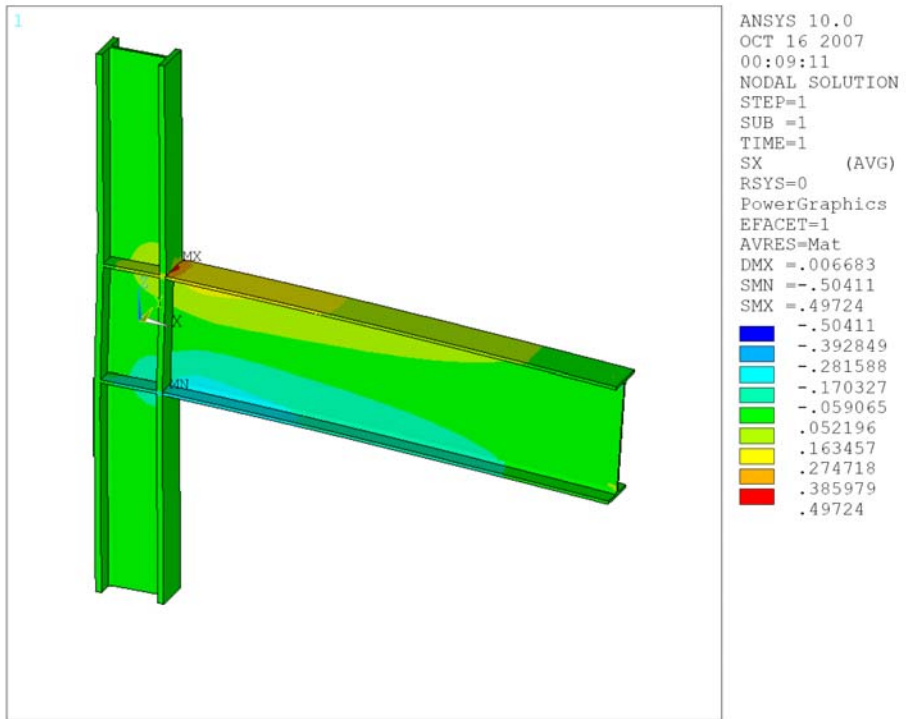


Figure 5.13: Result of the finite element study of the model with continuity plates.

Figure 5.12 shows the finite element model of the connection with continuity plates and figure 5.13 shows the result of the analysis. This study indicates that the SCF is 1.75 for the Pre-Northridge connection with continuity plates. This SCF is calculated as the ratio of maximum stress observed as the result of the finite element analysis to the maximum bending stress in the beam ( $M/S$ ).

Since the connections of the investigated buildings have continuity plates, the value of 1.75 is chosen for the purposes of this study.

#### **5.2.2.4 Established Stress Concentration Factor**

The results of the study of SCFs can be summarized as follows:

- SCF caused by geometry of the connection (relative to  $M/S$  stress) has been shown to be 1.75 (finite element analysis).
- SCF caused by weld has been calculated to be 2.4.
- SCF caused by backup bar has been calculated to be 1.3.
- SCF caused by rolling effects has been calculated to be 1.5.

As a result the SCF in the high-cycle region can be written as:

$$\text{SCF (relative to rolled beams)} = 1.75 * 2.4 * 1.3 = 5.5$$

This value that compares with “AISC Steel Construction Manual” [2] value (5.3) for beams with welded cover plates is used later in this chapter for establishing S-N curve.

### 5.2.3 Established S-N Curve for Fatigue Analysis

After establishing the SCF for the investigated detail, available test results can be used to establish the S-N curve. Figure 5.14 shows the established S-N curve for the fatigue analyses performed later in this study. The equation of the established S-N curve is calculated to be the following:

$$\text{For } S > 19.7 \text{ (} N < 36175 \text{)} \quad ; \quad S = 69.3N^{-0.1198}$$

$$\text{For } S < 19.7 \text{ (} N > 36175 \text{)} \quad ; \quad S = 658.4N^{-0.326}$$

where;

N: is the number of cycles to failure,

S: is stress (M/S) in ksi.

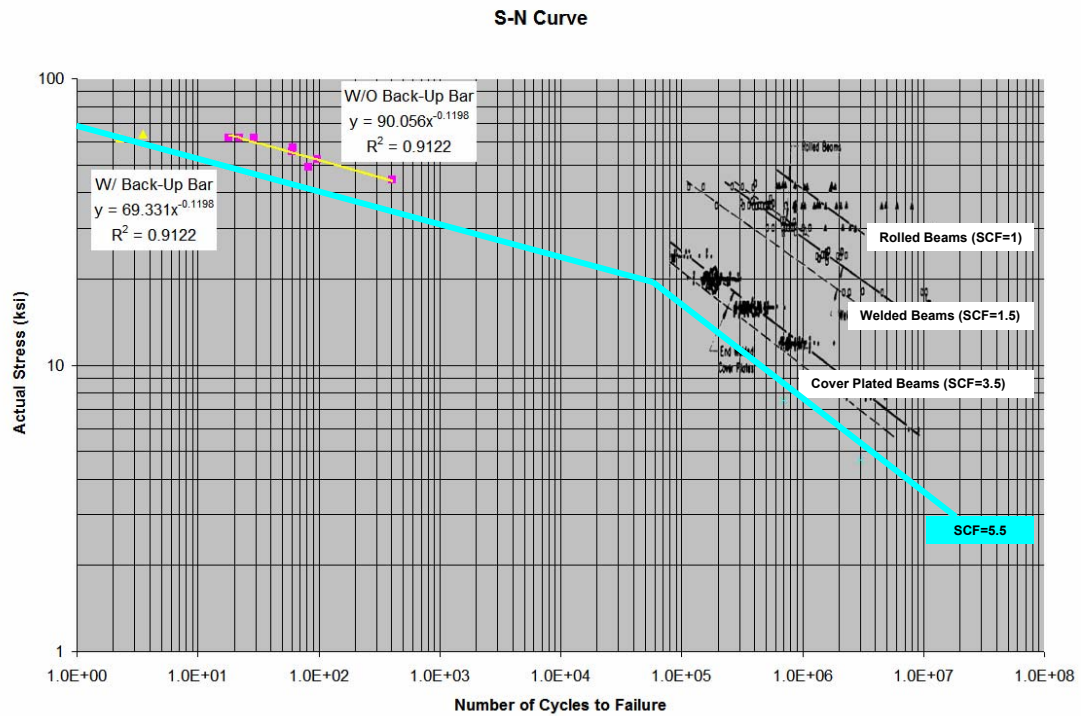


Figure 5.14: Established S-N curve for fatigue analysis.

The following need to be considered in regards to the established S-N curve:

- Mode shape and its effects will be captured by the global model (time-history analysis).
- Higher mode distributions will change the global behavior and will be automatically captured in M/S stress output at the end of critical members.

- In *low-cycle fatigue* range, getting from M/S to actual concentrated stresses does not appear to be critical since the test results are plotted against M/S stress (and not the maximum concentrated stress). However, understanding of the magnitude of SCF created by Backup bar is a must. This study shows that this value is 1.3.
- In *low-cycle fatigue* range, since the stress field in tests by Partridge et al. is identical to actual conditions of Pre-Northridge connection, using the SCF of 1.3 (relative to specimen without backup bar) to account for backup bar effects appears to be appropriate. This has been cross checked with the British Steel Designers' Manual.
- In *high-cycle fatigue* range, SCF relative to *rolled beams* test data (tests by Fisher et al.) has been calculated to be approximately 5.5. S-N curves developed by Fisher et al. can be used after implementing this factor.
- Available tests for the investigated detail are limited and as a result a probabilistic approach is not possible. Developed S-N curve is based on the available test data at the time of this study.

### 5.3 Cycle Counting Procedure

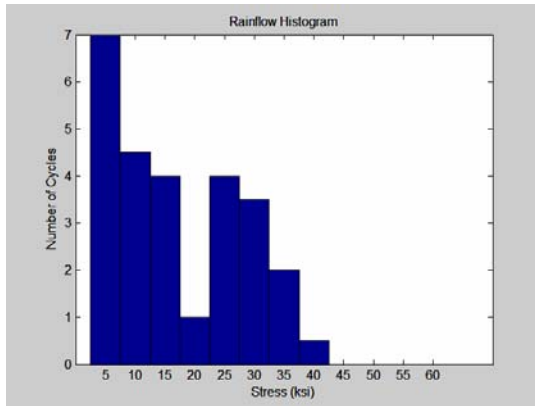
Due to the complexity of the stress histories at the investigated beams and columns, the cycle counting method used needs to be applicable to irregular histories. Dowling (1993), who is one of the research leaders in this area, believes that the best approach is to use a procedure called *rainflow cycle counting*. [9] This method was developed by Professor T. Endo in Japan around 1968 and is currently widely used for fatigue cycle counting applications in structural engineering. [9], [39], [23]

*Rainflow cycle counting* is used in this study as the cycle counting procedure. Details of this method are out of the scope of this document and can be found in references [9], [39], and [23]. The *MATLAB* [www.mathworks.com] computer program is used and the *rainflow* function is obtained from www.mathworks.com for performing the *rainflow cycle counting* procedure.

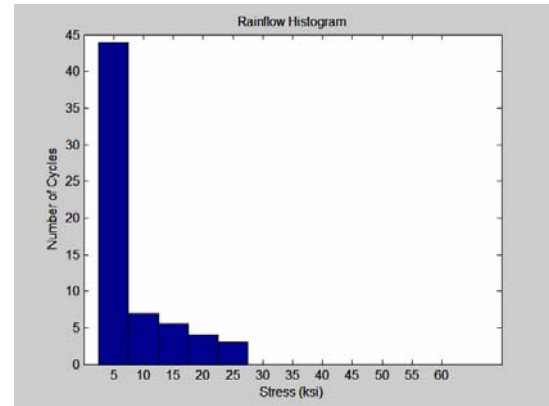
#### 5.3.1 Ten-Story Building

Figure 5.15 shows the results of the *rainflow cycle counting* for the beams of the investigated ten-story building. Also, Figure 5.16 illustrates the *rainflow* histograms for the columns.

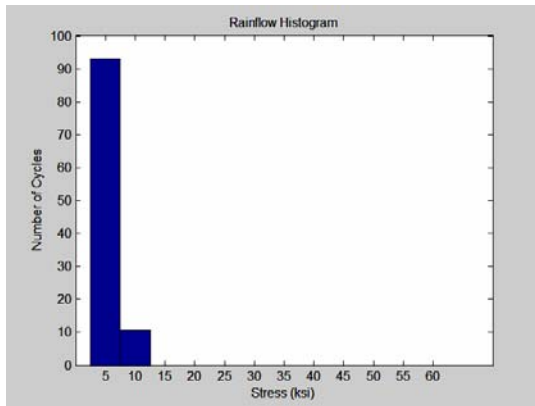
## 2<sup>nd</sup> Floor Beam



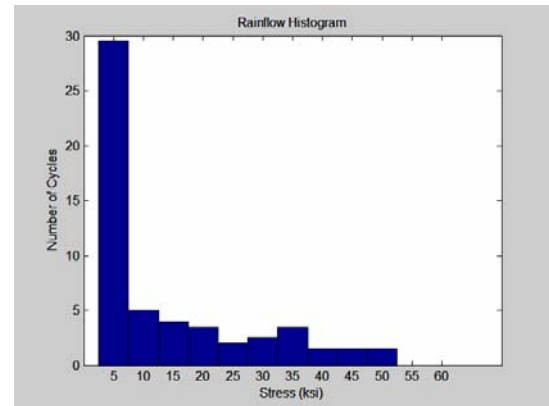
1<sup>st</sup> Mode



2<sup>nd</sup> Mode



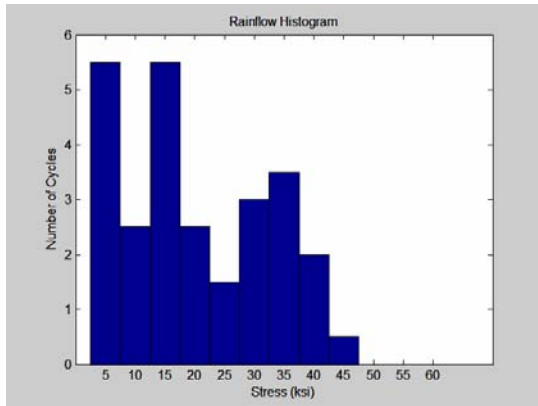
3<sup>rd</sup> Mode



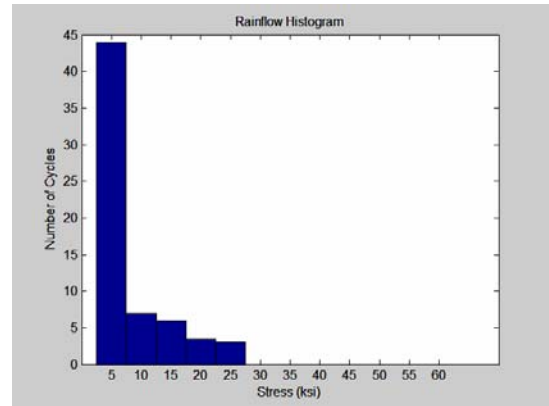
All Modes

Figure 5.15: Rainflow histograms for beams of the ten-story building.

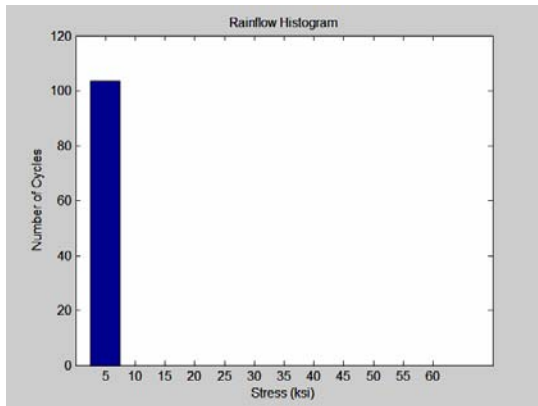
### 3<sup>rd</sup> Floor Beam



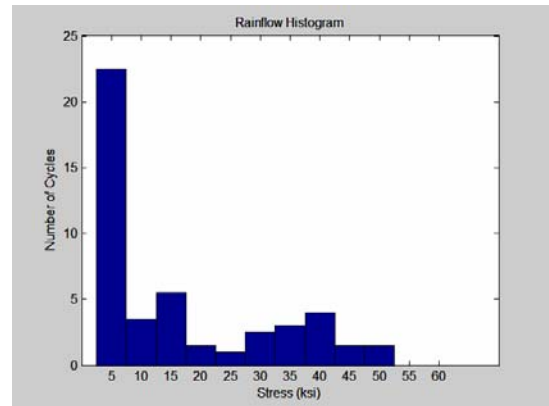
1<sup>st</sup> Mode



2<sup>nd</sup> Mode



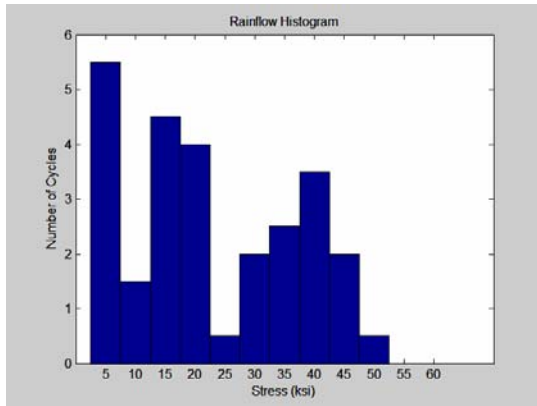
3<sup>rd</sup> Mode



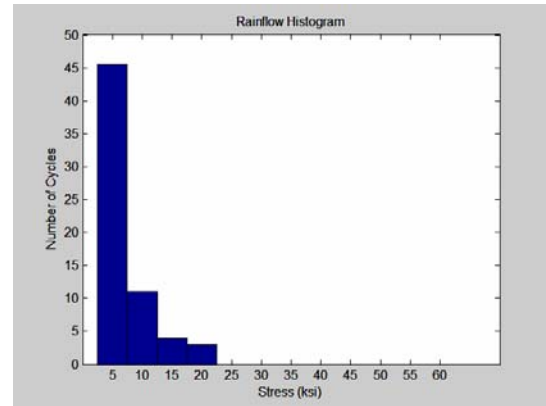
All Modes

Figure 5.15, continued: Rainflow histograms for beams of the ten-story building.

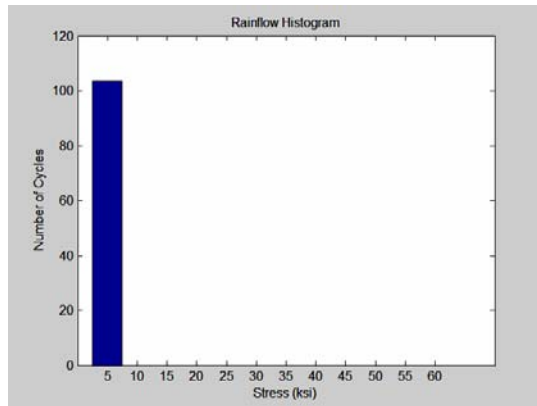
### 4<sup>th</sup> Floor Beam



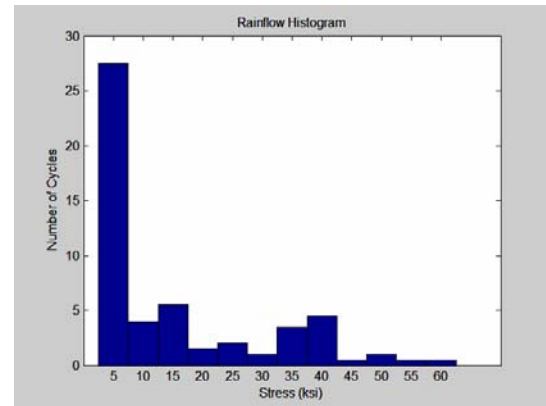
1<sup>st</sup> Mode



2<sup>nd</sup> Mode



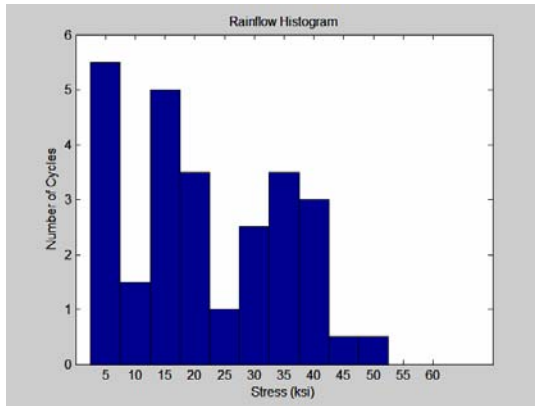
3<sup>rd</sup> Mode



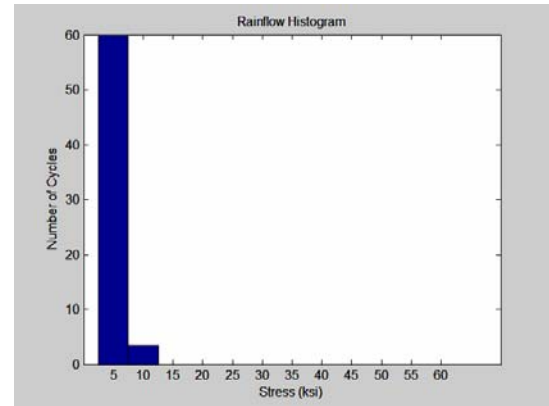
All Modes

Figure 5.15, continued: Rainflow histograms for beams of the ten-story building.

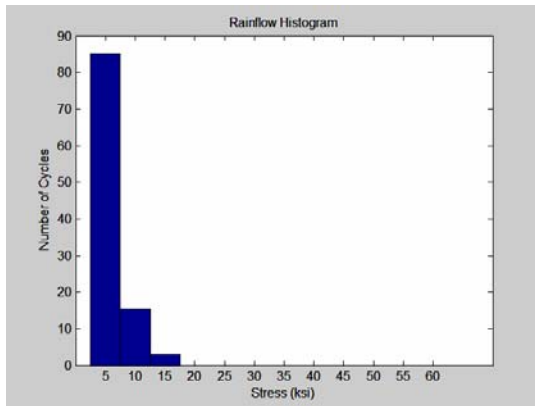
### 5<sup>th</sup> Floor Beam



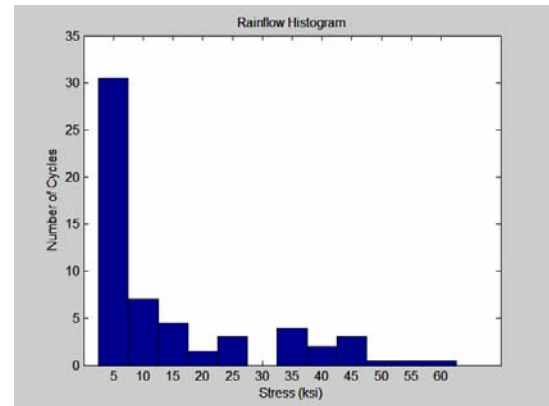
1<sup>st</sup> Mode



2<sup>nd</sup> Mode



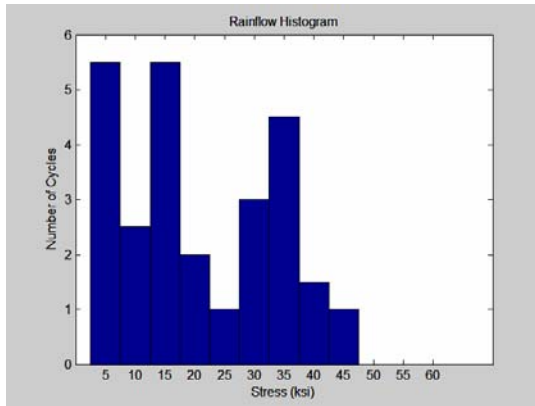
3<sup>rd</sup> Mode



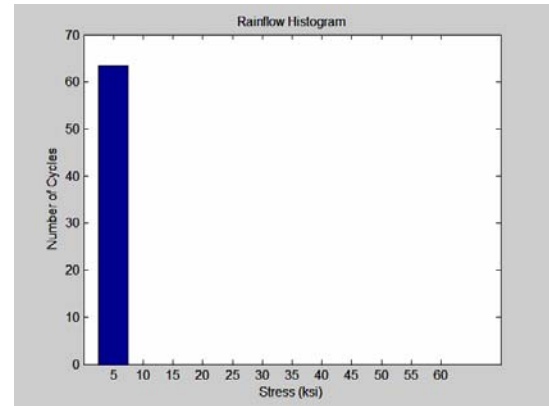
All Modes

Figure 5.15, continued: Rainflow histograms for beams of the ten-story building.

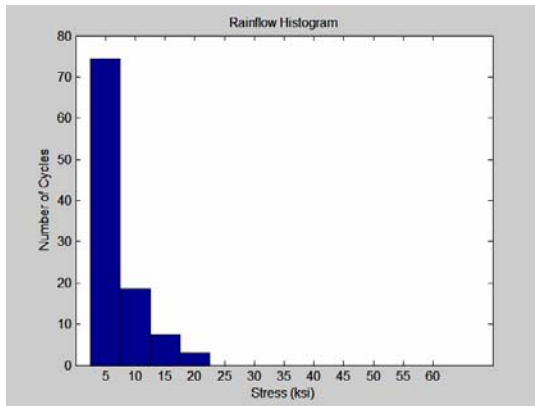
## 6<sup>th</sup> Floor Beam



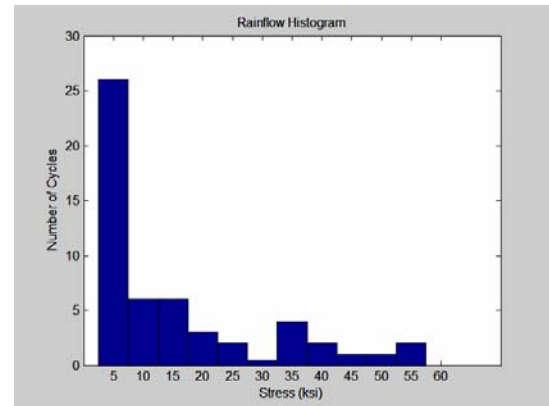
1<sup>st</sup> Mode



2<sup>nd</sup> Mode



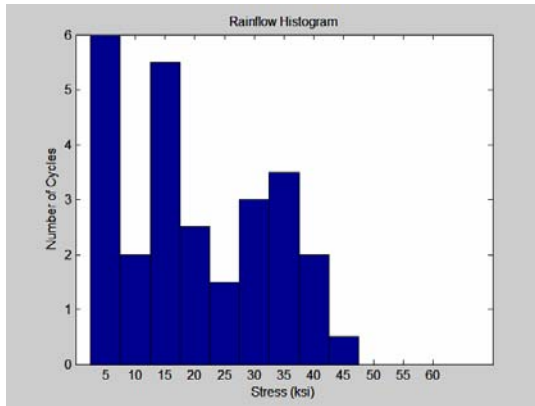
3<sup>rd</sup> Mode



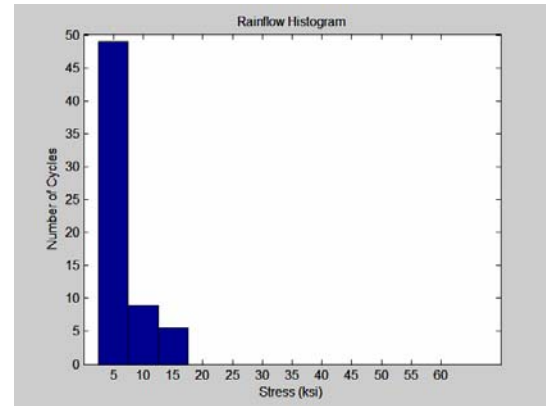
All Modes

Figure 5.15, continued: Rainflow histograms for beams of the ten-story building.

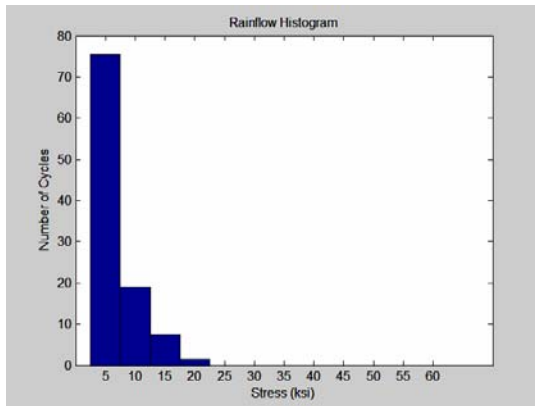
## 7<sup>th</sup> Floor Beam



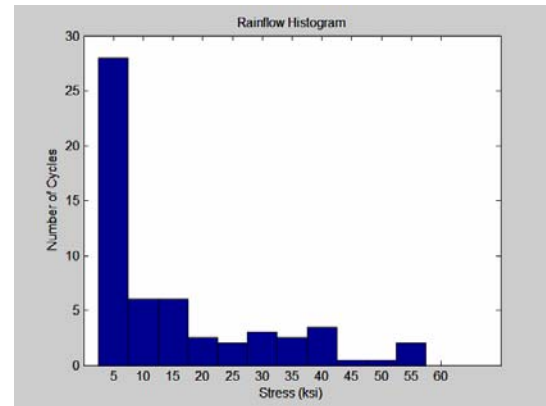
1<sup>st</sup> Mode



2<sup>nd</sup> Mode



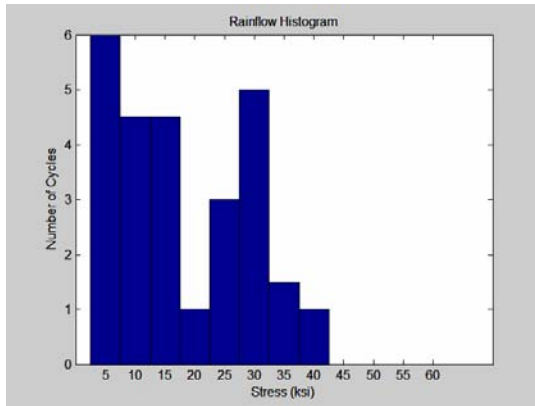
3<sup>rd</sup> Mode



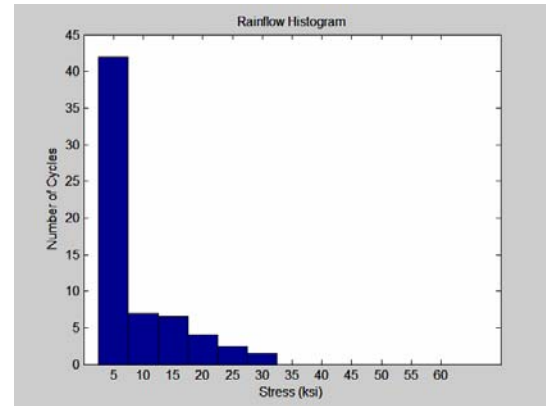
All Modes

Figure 5.15, continued: Rainflow histograms for beams of the ten-story building.

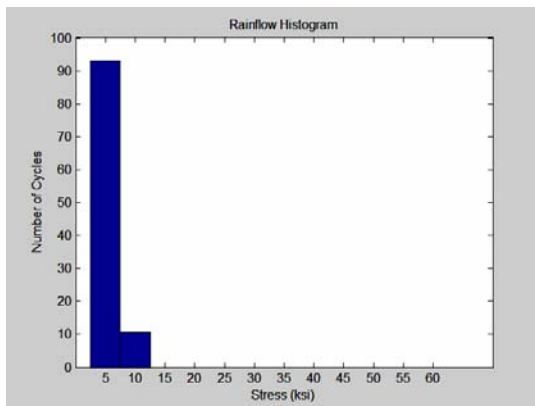
## 8<sup>th</sup> Floor Beam



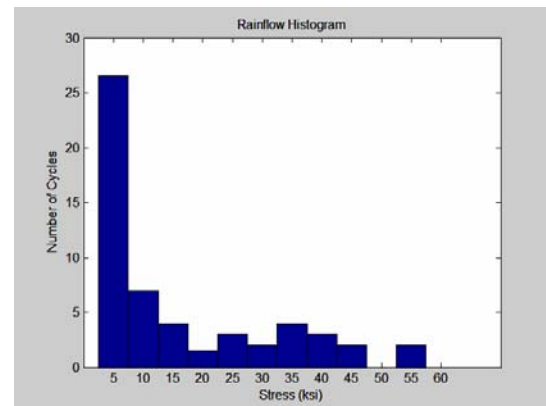
1<sup>st</sup> Mode



2<sup>nd</sup> Mode



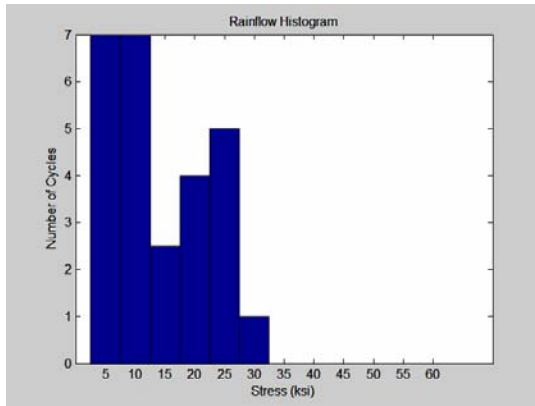
3<sup>rd</sup> Mode



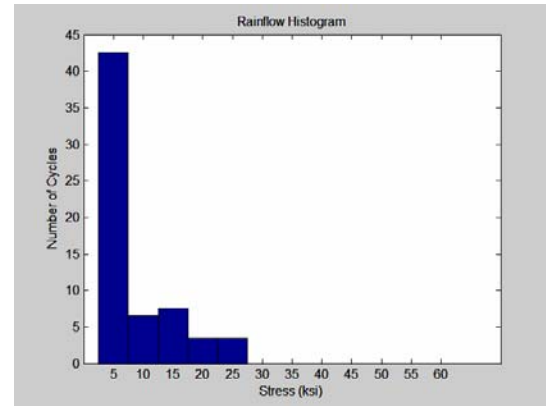
All Modes

Figure 5.15, continued: Rainflow histograms for beams of the ten-story building.

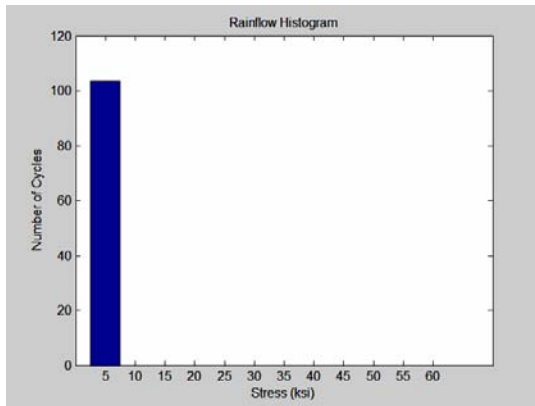
## 9<sup>th</sup> Floor Beam



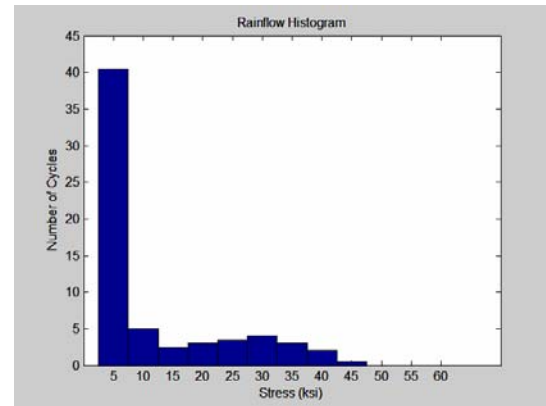
1<sup>st</sup> Mode



2<sup>nd</sup> Mode



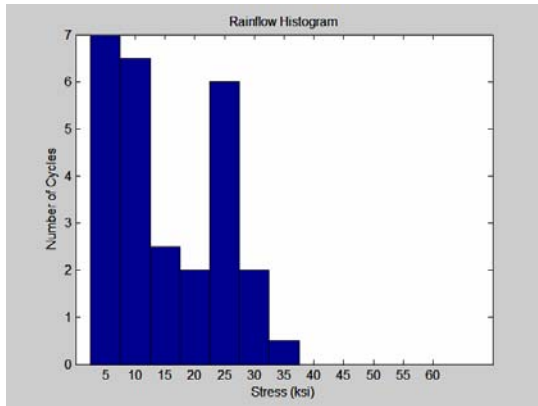
3<sup>rd</sup> Mode



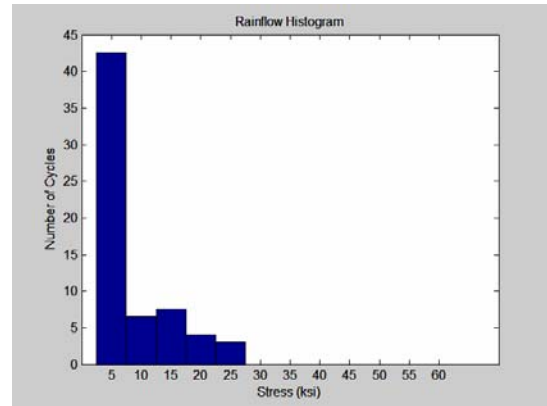
All Modes

Figure 5.15, continued: Rainflow histograms for beams of the ten-story building.

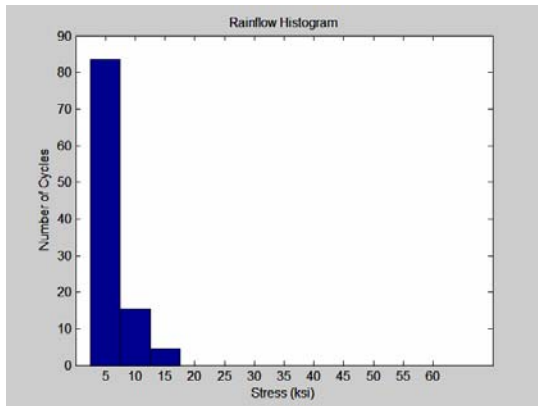
## 2<sup>nd</sup> Floor Column



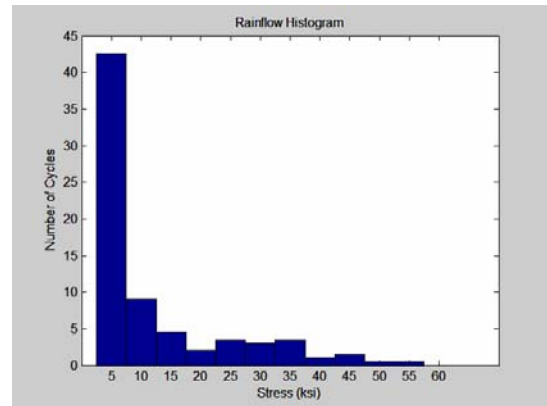
1<sup>st</sup> Mode



2<sup>nd</sup> Mode



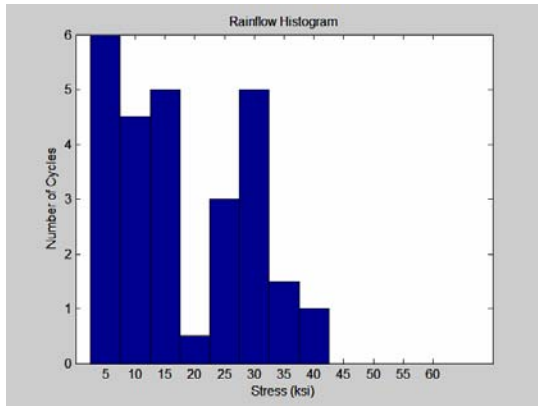
3<sup>rd</sup> Mode



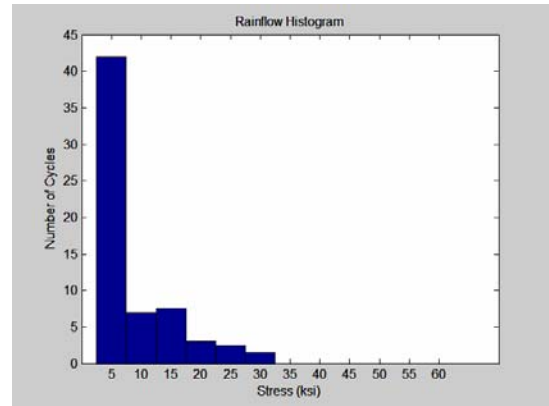
All Modes

Figure 5.16: Rainflow histograms for columns of the ten-story building.

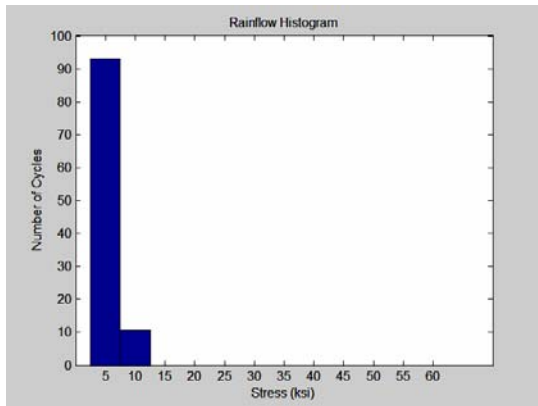
### 3<sup>rd</sup> Floor Column



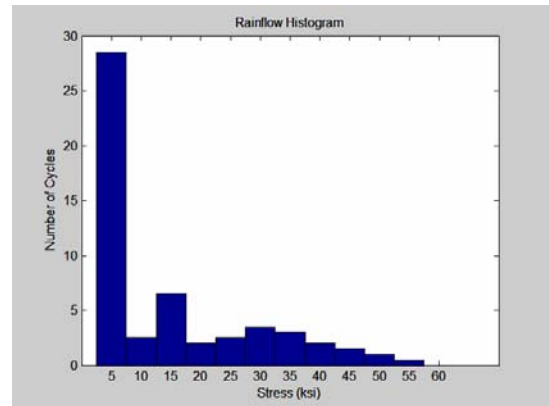
1<sup>st</sup> Mode



2<sup>nd</sup> Mode



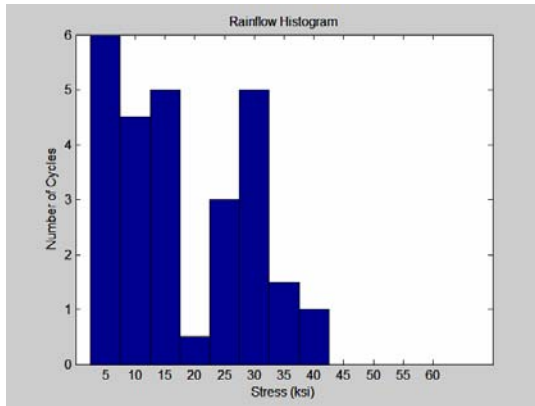
3<sup>rd</sup> Mode



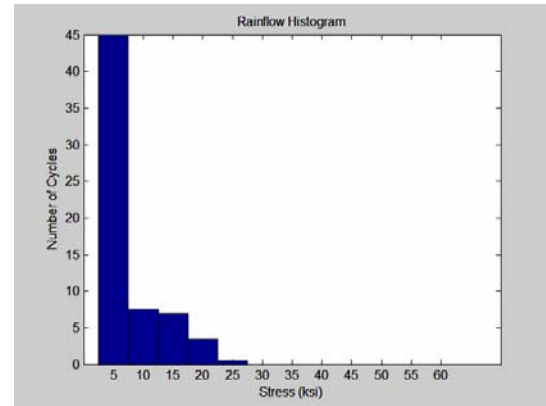
All Modes

Figure 5.16, continued: Rainflow histograms for columns of the ten-story building.

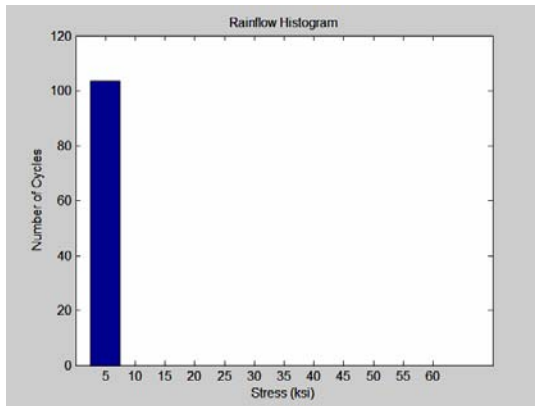
### 4<sup>th</sup> Floor Column



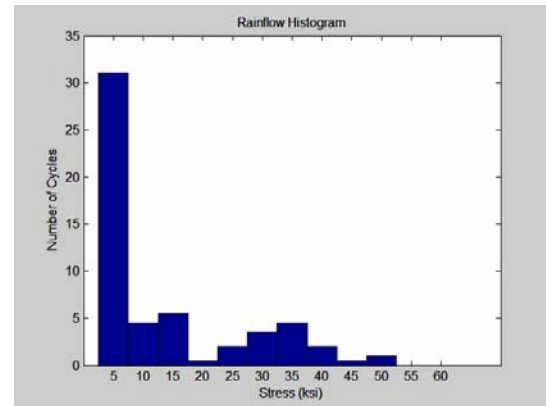
1<sup>st</sup> Mode



2<sup>nd</sup> Mode



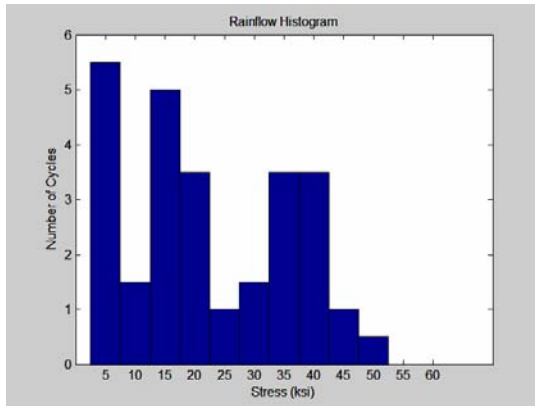
3<sup>rd</sup> Mode



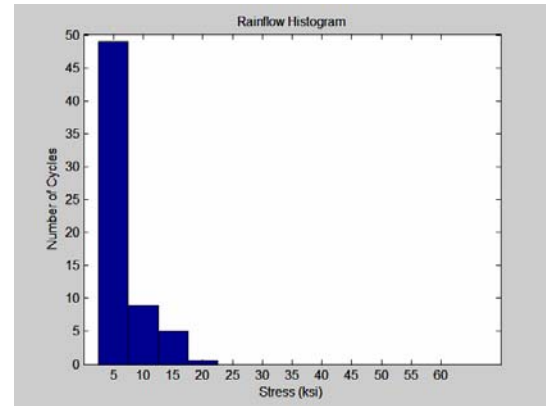
All Modes

Figure 5.16, continued: Rainflow histograms for columns of the ten-story building.

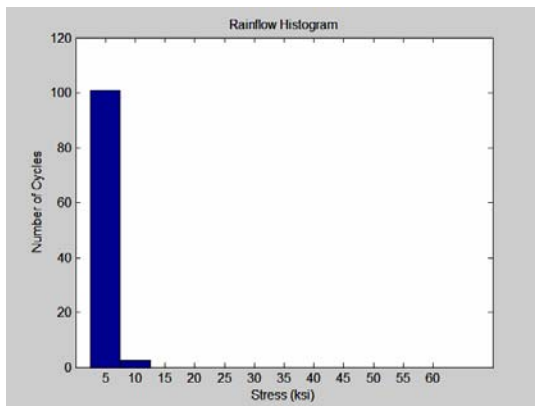
### 5<sup>th</sup> Floor Column



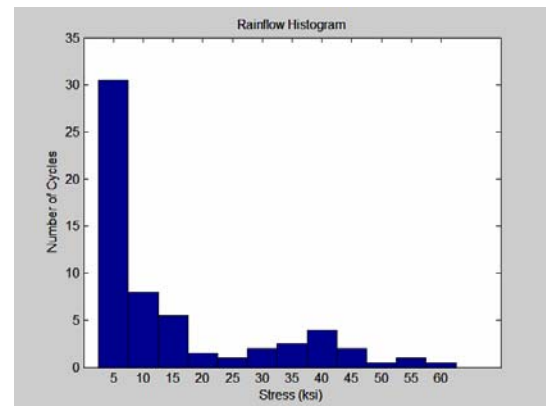
1<sup>st</sup> Mode



2<sup>nd</sup> Mode



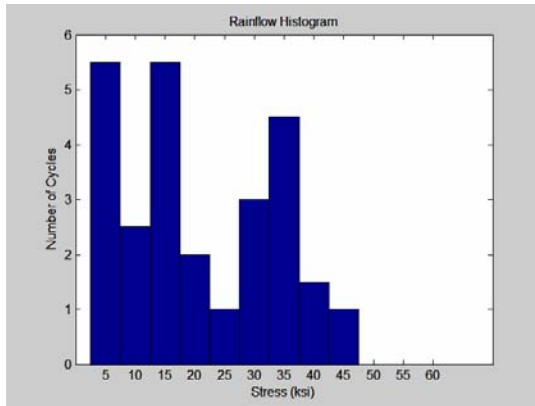
3<sup>rd</sup> Mode



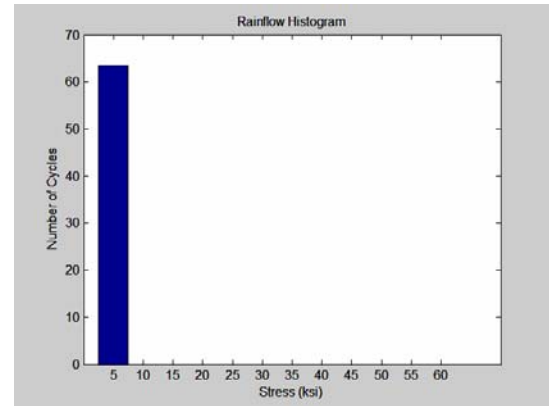
All Modes

Figure 5.16, continued: Rainflow histograms for columns of the ten-story building.

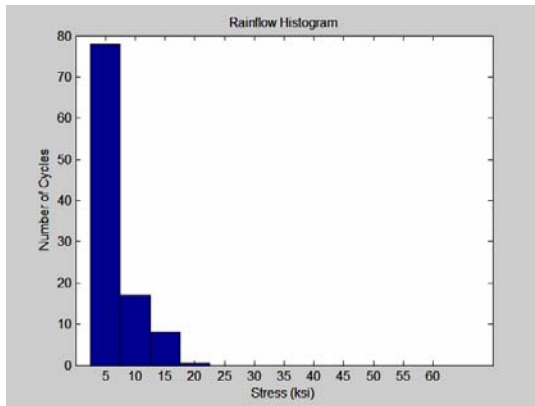
## 6<sup>th</sup> Floor Column



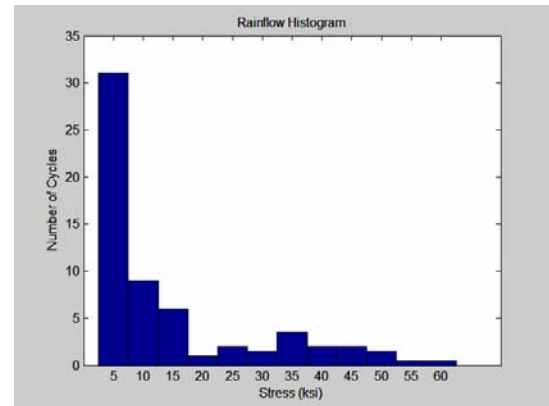
1<sup>st</sup> Mode



2<sup>nd</sup> Mode



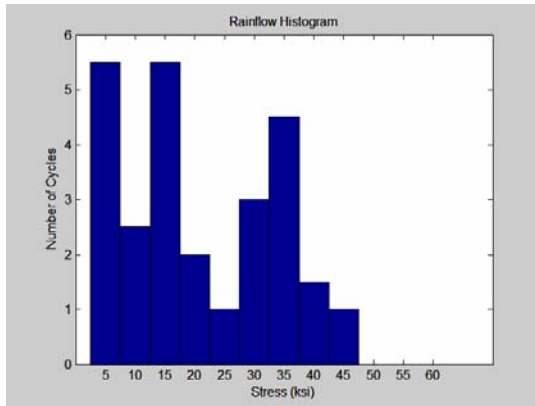
3<sup>rd</sup> Mode



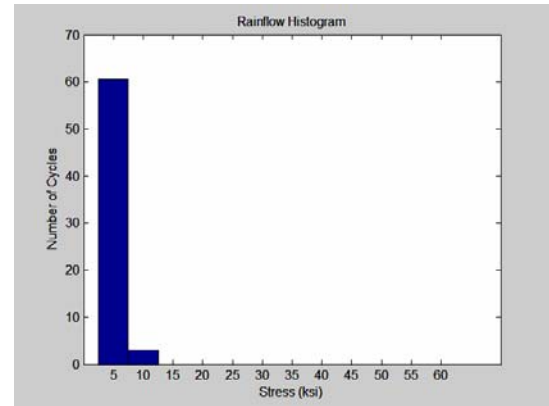
All Modes

Figure 5.16, continued: Rainflow histograms for columns of the ten-story building.

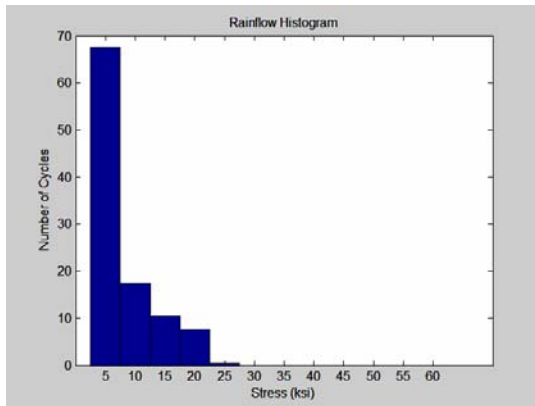
### 7<sup>th</sup> Floor Column



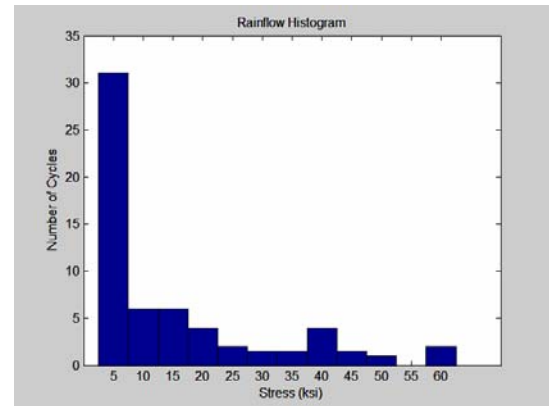
1<sup>st</sup> Mode



2<sup>nd</sup> Mode



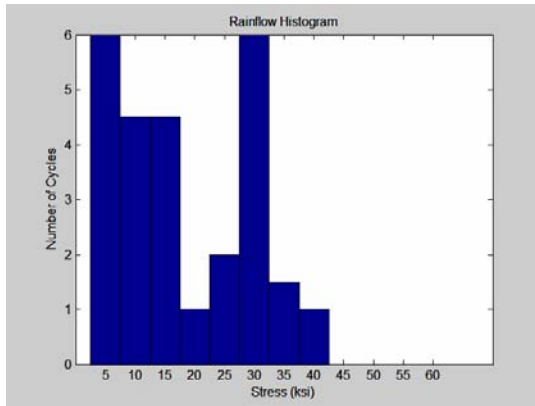
3<sup>rd</sup> Mode



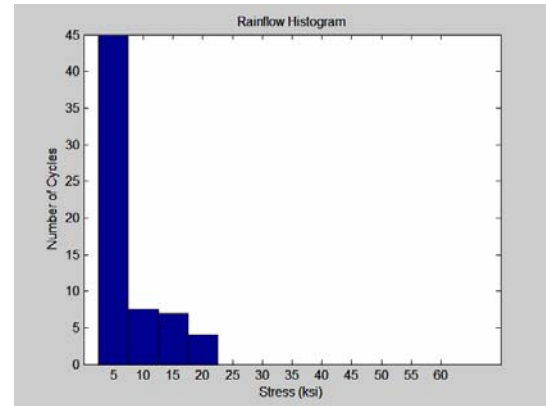
All Modes

Figure 5.16, continued: Rainflow histograms for columns of the ten-story building.

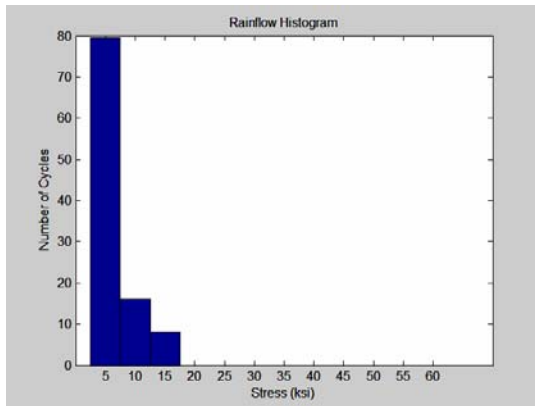
## 8<sup>th</sup> Floor Column



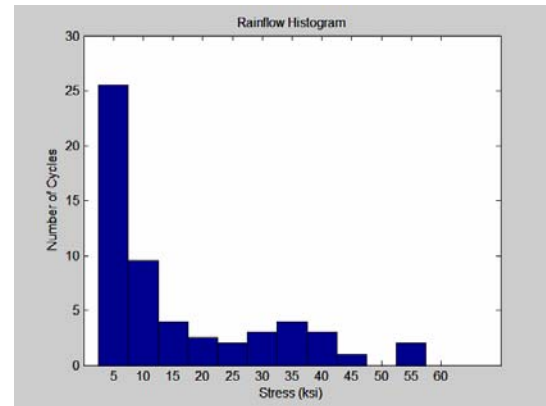
1<sup>st</sup> Mode



2<sup>nd</sup> Mode



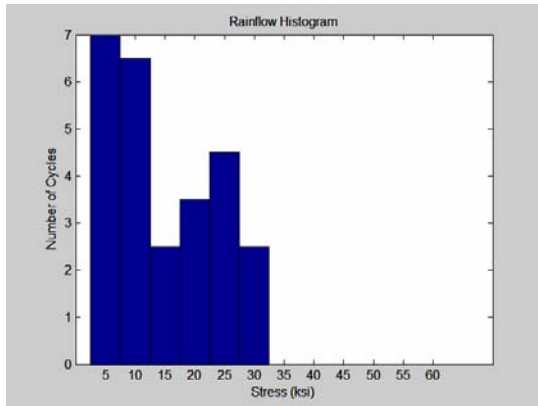
3<sup>rd</sup> Mode



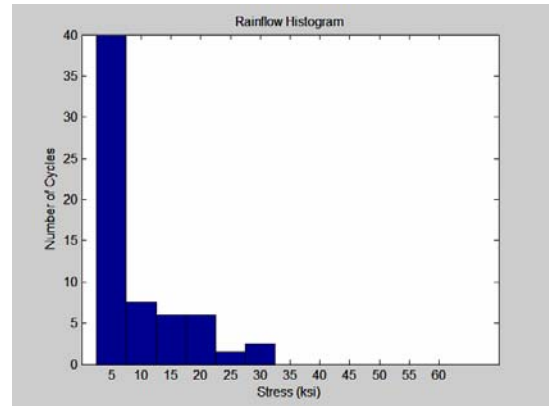
All Modes

Figure 5.16, continued: Rainflow histograms for columns of the ten-story building.

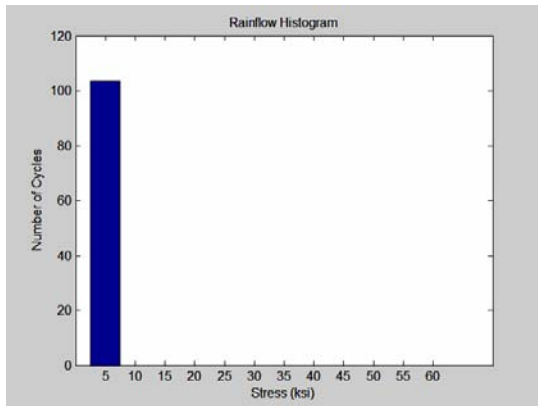
### 9<sup>th</sup> Floor Column



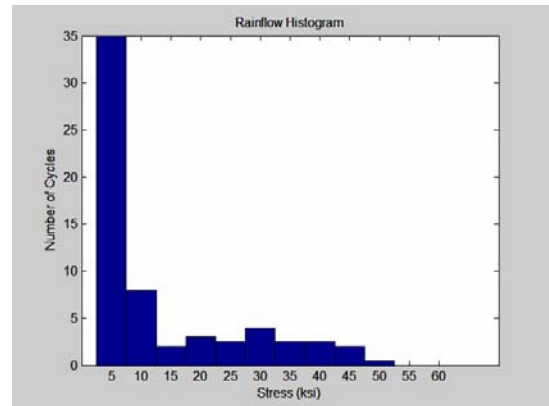
1<sup>st</sup> Mode



2<sup>nd</sup> Mode



3<sup>rd</sup> Mode



All Modes

Figure 5.16, continued: Rainflow histograms for columns of the ten-story building.

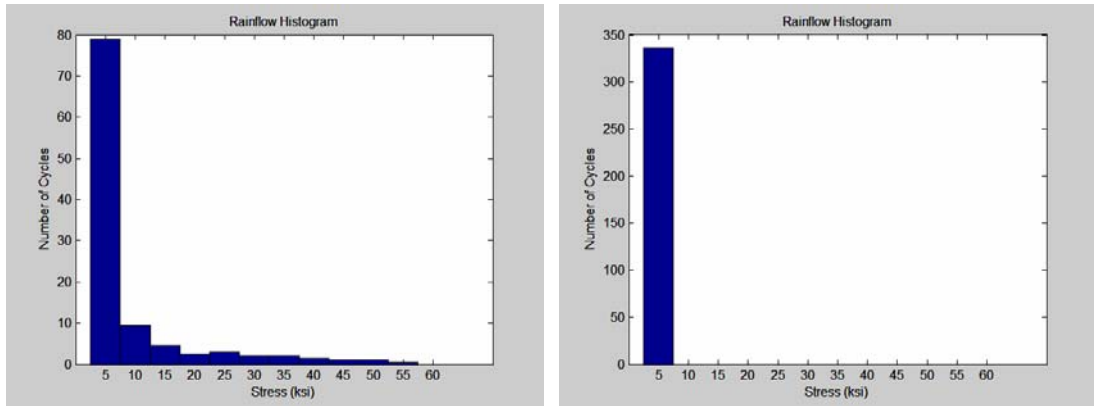
It can be seen that the higher modes of vibration enormously effect the cycle counting results and the histograms corresponding to the 1<sup>st</sup> mode are significantly different from the ones corresponding to all modes. This shows that the *higher mode effects* make a significant difference in the results of the fatigue analysis in this building. Figures 5.21 and 5.22 show a blowup of the histograms for the 6<sup>th</sup> floor beam and the 7<sup>th</sup> floor column and clearly illustrates the difference between the 1<sup>st</sup> mode and all mode histograms.

### **5.3.2 Two-Story Building**

The results of the *rainflow cycle counting* for the beams and columns of the two-story building have been shown in figures 5.17 and 5.18, respectively.

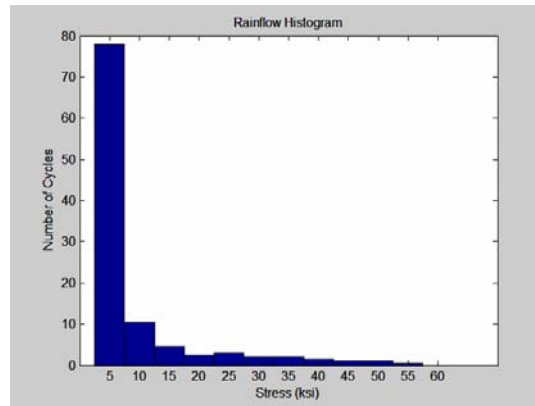
It can be observed from the histograms that the effect of 2<sup>nd</sup> mode of vibration is not significant. In other words, the histograms corresponding to the first mode and all modes are very similar. This observation is different from that of the ten-story building.

## 2<sup>nd</sup> Floor Beam



1<sup>st</sup> Mode

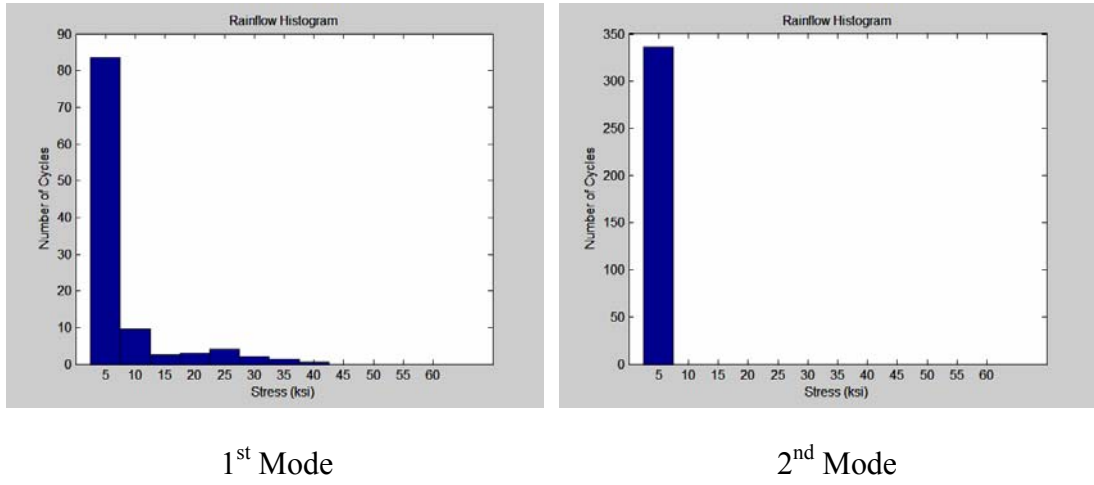
2<sup>nd</sup> Mode



All Modes

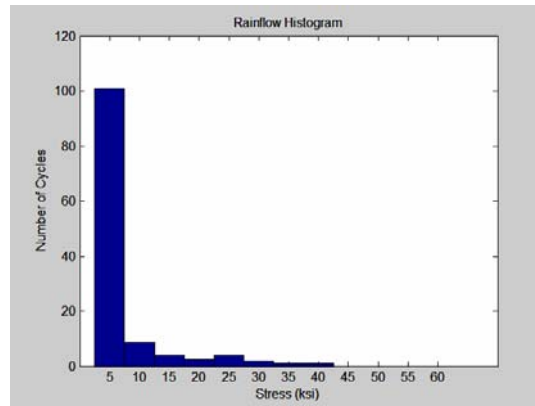
Figure 5.17: Rainflow histograms for beams of the two-story building.

## Roof Beam



1<sup>st</sup> Mode

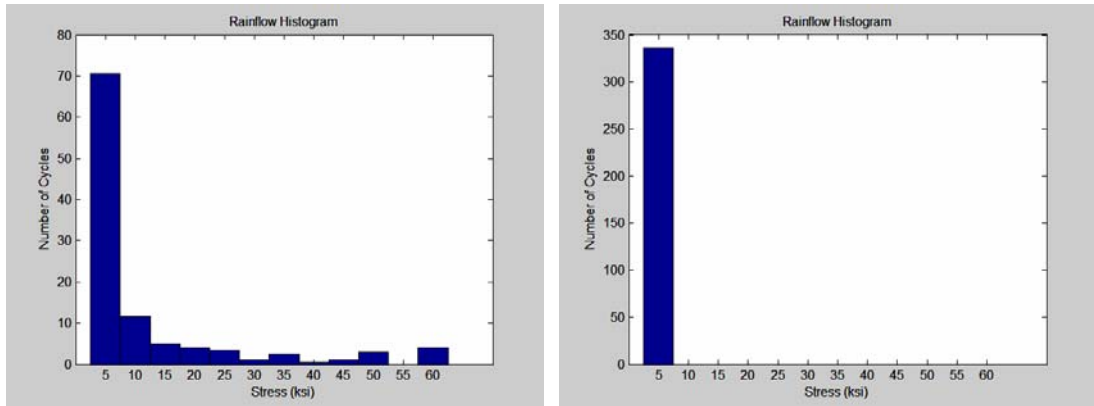
2<sup>nd</sup> Mode



All Modes

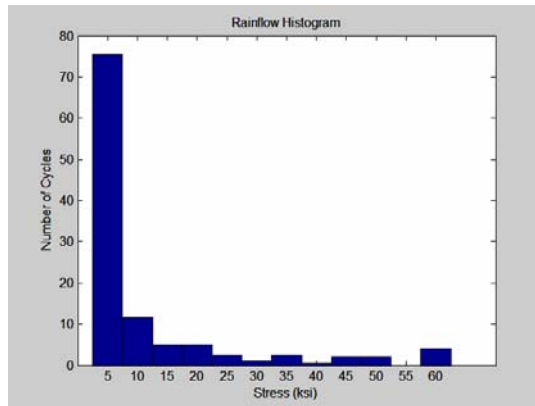
Figure 5.17, continued: Rainflow histograms for beams of the two-story building.

## 2<sup>nd</sup> Floor Column



1<sup>st</sup> Mode

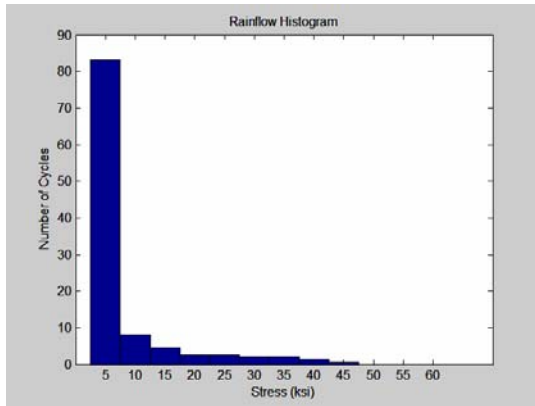
2<sup>nd</sup> Mode



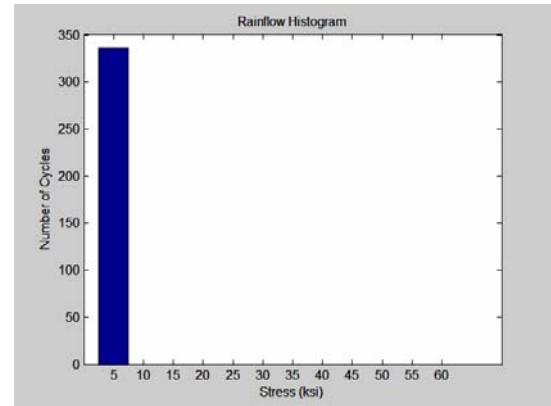
All Modes

Figure 5.18: Rainflow histograms for columns of the two-story building.

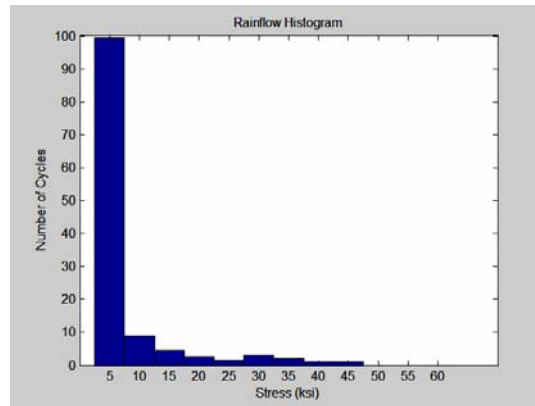
## Roof Column



1<sup>st</sup> Mode



2<sup>nd</sup> Mode



All Modes

Figure 5.18, continued: Rainflow histograms for columns of the two-story building.

## 5.4 Cumulative Fatigue Analysis

As explained earlier, the cumulative fatigue analysis is performed using *Palmgren-Miner rule*. This section summarizes the results of the cumulative fatigue analysis on the investigated beams and columns of the ten-story and two-story buildings.

### 5.4.1 Ten-Story Building

BEAM CUMULATIVE FATIGUE ANALYSES RESULTS

Ni (Cycles)												
5 ksi	10 ksi	15 ksi	20 ksi	25 ksi	30 ksi	35 ksi	40 ksi	45 ksi	50 ksi	55 ksi	60 ksi	
3173900	378607.9	109152.2	31991.6	4967.1	1084.3	299.46	98.23	36.75	15.25	6.88	3.33	

Floor	Mode	ni (Cycles)											SUM(ni/Ni)	
		5 ksi	10 ksi	15 ksi	20 ksi	25 ksi	30 ksi	35 ksi	40 ksi	45 ksi	50 ksi	55 ksi		60 ksi
2nd	1st Mode	7	4.5	4	1	4	3.5	2	0.5	0	0	0	0	0.01588
	2nd Mode	44	7	5.5	4	3	0	0	0	0	0	0	0	0.00081
	3rd Mode	93	10.5	0	0	0	0	0	0	0	0	0	0	0.00006
	All Modes	29.5	5	4	3.5	2	2.5	3.5	1.5	1.5	1.5	0	0	0.16901
3rd	1st Mode	5.5	2.5	5.5	2.5	1.5	3	3.5	2	0.5	0	0	0	0.04886
	2nd Mode	44	7	6	3.5	3	0	0	0	0	0	0	0	0.00080
	3rd Mode	103.5	0	0	0	0	0	0	0	0	0	0	0	0.00003
	All Modes	22.5	3.5	5.5	1.5	1	2.5	3	4	1.5	1.5	0	0	0.19254
4th	1st Mode	5.5	1.5	4.5	4	0.5	2	2.5	3.5	2	0.5	0	0	0.13330
	2nd Mode	45.5	11	4	3	0	0	0	0	0	0	0	0	0.00017
	3rd Mode	103.5	0	0	0	0	0	0	0	0	0	0	0	0.00003
	All Modes	27.5	4	5.5	1.5	2	1	3.5	4.5	0.5	1	0.5	0.5	0.36094
5th	1st Mode	5.5	1.5	5	3.5	1	2.5	3.5	3	0.5	0.5	0	0	0.09129
	2nd Mode	60	3.5	0	0	0	0	0	0	0	0	0	0	0.00003
	3rd Mode	85	15.5	3	0	0	0	0	0	0	0	0	0	0.00010
	All Modes	30.5	7	4.5	1.5	3	0	4	2	3	0.5	0.5	0.5	0.37168
6th	1st Mode	5.5	2.5	5.5	2	1	3	4.5	1.5	1	0	0	0	0.06060
	2nd Mode	63.5	0	0	0	0	0	0	0	0	0	0	0	0.00002
	3rd Mode	74.5	18.5	7.5	3	0	0	0	0	0	0	0	0	0.00023
	All Modes	26	6	6	3	2	0.5	4	2	1	1	2	0	0.41824
7th	1st Mode	6	2	5.5	2.5	1.5	3	3.5	2	0.5	0	0	0	0.04886
	2nd Mode	49	9	5.5	0	0	0	0	0	0	0	0	0	0.00009
	3rd Mode	75.5	19	7.5	1.5	0	0	0	0	0	0	0	0	0.00019
	All Modes	28	6	6	2.5	2	3	2.5	3.5	0.5	0.5	2	0	0.38440
8th	1st Mode	6	4.5	4.5	1	3	5	1.5	1	0	0	0	0	0.02049
	2nd Mode	42	7	6.5	4	2.5	1.5	0	0	0	0	0	0	0.00210
	3rd Mode	93	10.5	0	0	0	0	0	0	0	0	0	0	0.00006
	All Modes	26.5	7	4	1.5	3	2	4	3	2	0	2	0	0.39158
9th	1st Mode	7	7	2.5	4	5	1	0	0	0	0	0	0	0.00210
	2nd Mode	42.5	6.5	7.5	3.5	3.5	0	0	0	0	0	0	0	0.00091
	3rd Mode	103.5	0	0	0	0	0	0	0	0	0	0	0	0.00003
	All Modes	40.5	5	2.5	3	3.5	4	3	2	0.5	0	0	0	0.04852

Table 5.1: Results of the cumulative fatigue analyses on beams of the ten-story building.

Table 5.1 shows the results of the analysis on the beams of the ten-story building. It can be observed that the cumulative fatigue created by all modes is significantly

larger than the corresponding value for the 1<sup>st</sup> mode only. This comparison can be clearly seen in figure 5.19. Also table 5.2 and figure 5.20 confirm the same observations for the columns of the ten-story building.

Figures 5.21 and 5.22 show the blowup of the rainflow histograms for the most critical beam and column. It can be seen that effect of higher modes significantly increases the cumulative fatigue value at these members. Due to effect of potential defects and principal stresses that are not included this study, cumulative fatigue values of 0.41 and 0.75 are high enough to be considered the cause of observed damages. The observations from the fatigue analysis of the 7<sup>th</sup> floor column (most critical member) as shown in figure 5.22 can be summarized as follows:

- Comparison between cumulative fatigue analyses of 1<sup>st</sup> mode and all modes clearly indicate that *higher mode effects* are significant.
- Cumulative fatigue analysis of 1<sup>st</sup> mode only, indicates that the column has gone through only 6% of its fatigue life.
- Cumulative Fatigue Analysis of all modes, shows a significantly larger cumulative fatigue value in the column (75%). This is the result of higher modes.

- The contribution of higher modes of vibration significantly increases the cumulative fatigue in this column. This is because of the contribution of higher mode stresses than can increase the total stress significantly (relative to 1<sup>st</sup> mode stress only) at each point in time.
- Low-cycle fatigue is significant at this column and as expected high-cycle fatigue does not play a major role.

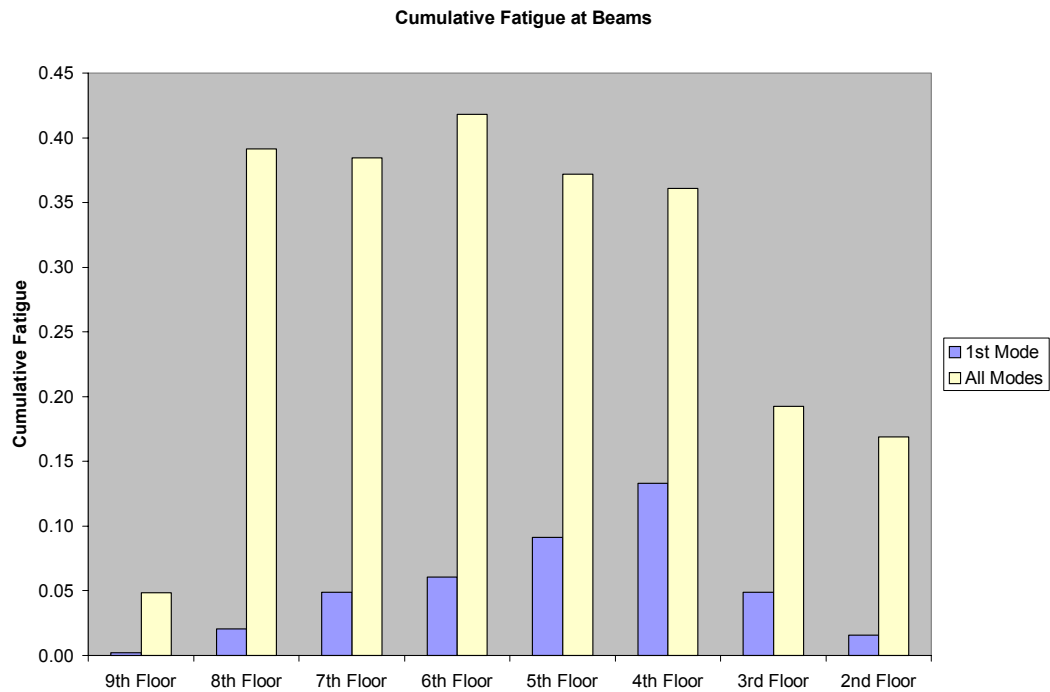


Figure 5.19: Cumulative fatigue at beams of the ten-story building (1<sup>st</sup> mode vs. all modes).

COLUMNS CUMULATIVE FATIGUE ANALYSES RESULTS

Ni (Cycles)											
5 ksi	10 ksi	15 ksi	20 ksi	25 ksi	30 ksi	35 ksi	40 ksi	45 ksi	50 ksi	55 ksi	60 ksi
3173900	378607.9	109152.2	31991.6	4967.1	1084.3	299.46	98.23	36.75	15.25	6.88	3.33

Floor	Mode	ni (Cycles)												SUM(ni/Ni)
		5 ksi	10 ksi	15 ksi	20 ksi	25 ksi	30 ksi	35 ksi	40 ksi	45 ksi	50 ksi	55 ksi	60 ksi	
2nd	1st Mode	7	6.5	2.5	2	6	2	0.5	0	0	0	0	0	0.00483
	2nd Mode	42.5	6.5	7.5	4	3	0	0	0	0	0	0	0	0.00083
	3rd Mode	83.5	15.5	4.5	0	0	0	0	0	0	0	0	0	0.00011
	All Modes	42.5	9	4.5	2	3.5	3	3.5	1	1.5	0.5	0.5	0	0.17176
3rd	1st Mode	6	4.5	5	0.5	3	5	1.5	1	0	0	0	0	0.02048
	2nd Mode	42	7	7.5	3	2.5	1.5	0	0	0	0	0	0	0.00208
	3rd Mode	93	10.5	0	0	0	0	0	0	0	0	0	0	0.00006
	All Modes	28.5	2.5	6.5	2	2.5	3.5	3	2	1.5	1	0.5	0	0.21331
4th	1st Mode	6	4.5	5	0.5	3	5	1.5	1	0	0	0	0	0.02048
	2nd Mode	45	7.5	7	3.5	0.5	0	0	0	0	0	0	0	0.00031
	3rd Mode	103.5	0	0	0	0	0	0	0	0	0	0	0	0.00003
	All Modes	31	4.5	5.5	0.5	2	3.5	4.5	2	0.5	1	0	0	0.11828
5th	1st Mode	5.5	1.5	5	3.5	1	1.5	3.5	3.5	1	0.5	0	0	0.10906
	2nd Mode	49	9	5	0.5	0	0	0	0	0	0	0	0	0.00010
	3rd Mode	101	2.5	0	0	0	0	0	0	0	0	0	0	0.00004
	All Modes	30.5	8	5.5	1.5	1	2	2.5	4	2	0.5	1	0.5	0.43395
6th	1st Mode	5.5	2.5	5.5	2	1	3	4.5	1.5	1	0	0	0	0.06060
	2nd Mode	63.5	0	0	0	0	0	0	0	0	0	0	0	0.00002
	3rd Mode	78	17	8	0.5	0	0	0	0	0	0	0	0	0.00016
	All Modes	31	9	6	1	2	1.5	3.5	2	2	1.5	0.5	0.5	0.40956
7th	1st Mode	5.5	2.5	5.5	2	1	3	4.5	1.5	1	0	0	0	0.06060
	2nd Mode	49	9	5.5	0	0	0	0	0	0	0	0	0	0.00009
	3rd Mode	75.5	19	7.5	1.5	0	0	0	0	0	0	0	0	0.00019
	All Modes	31	6	6	4	2	1.5	1.5	4	1.5	1	0	2	0.75471
8th	1st Mode	6	4.5	4.5	1	3	5	1.5	1	0	0	0	0	0.02049
	2nd Mode	42	7	6.5	4	2.5	1.5	0	0	0	0	0	0	0.00210
	3rd Mode	93	10.5	0	0	0	0	0	0	0	0	0	0	0.00006
	All Modes	25.5	9.5	4	2.5	2	3	4	3	1	0	2	0	0.36512
9th	1st Mode	7	7	2.5	4	5	1	0	0	0	0	0	0	0.00210
	2nd Mode	42.5	6.5	7.5	3.5	3.5	0	0	0	0	0	0	0	0.00091
	3rd Mode	103.5	0	0	0	0	0	0	0	0	0	0	0	0.00003
	All Modes	35	8	2	3	2.5	4	2.5	2.5	2	0.5	0	0	0.12534

Table 5.2: Results of the cumulative fatigue analyses on columns of the ten-story building.

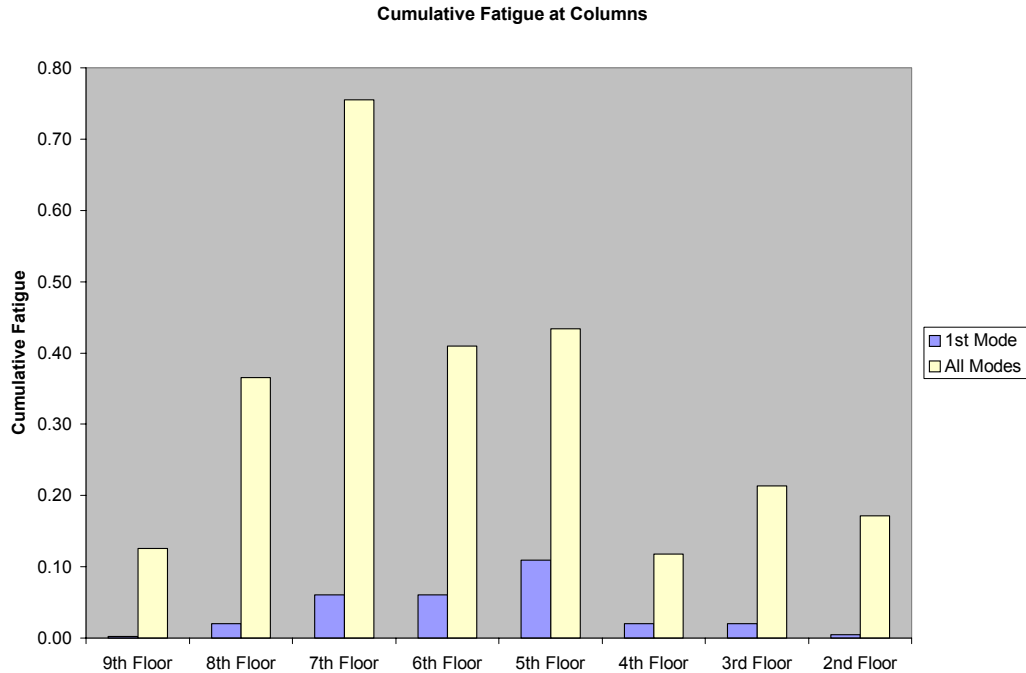
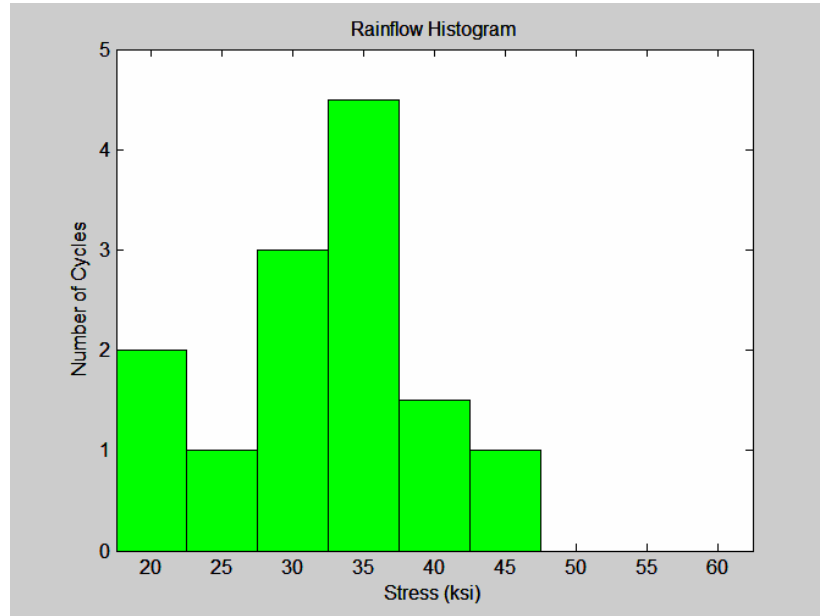
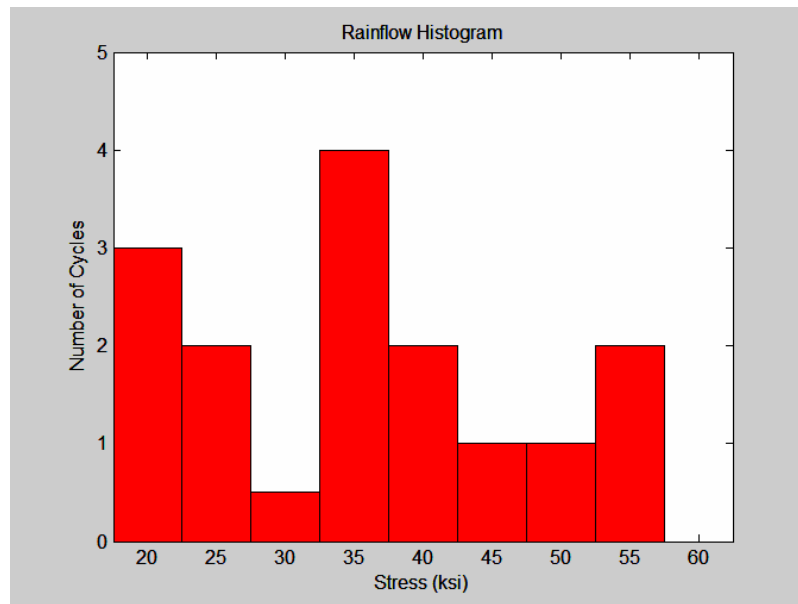


Figure 5.20: Cumulative fatigue at columns of the ten-story building (1<sup>st</sup> mode vs. all modes).

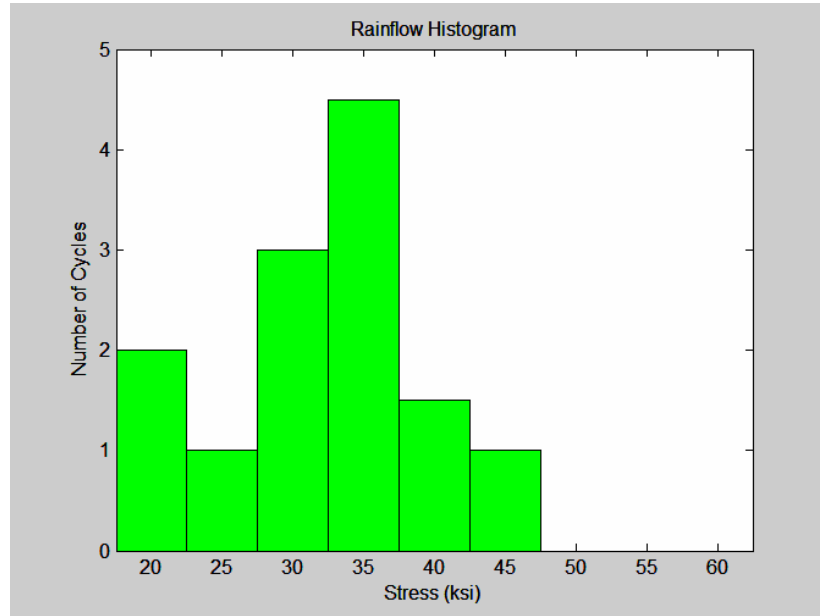


1<sup>st</sup> Mode ( $\sum \frac{n_i}{N_i} = 0.06$ ).

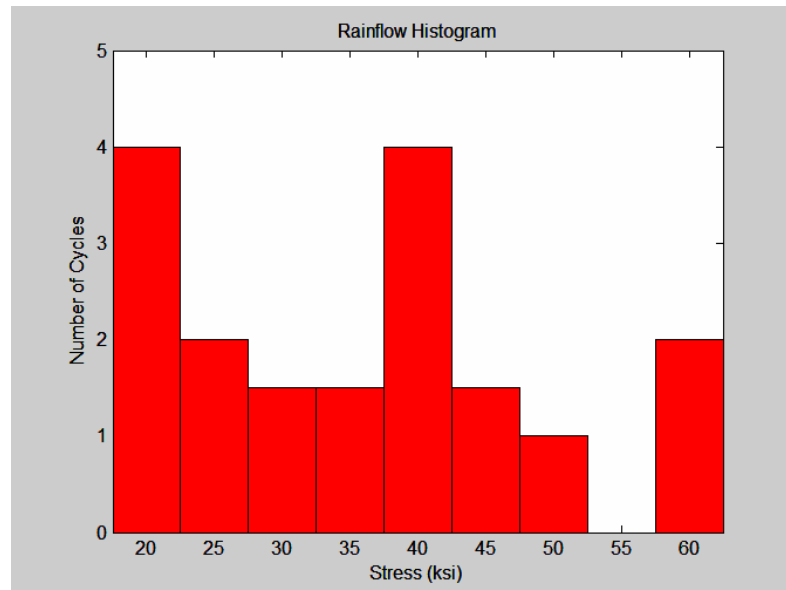


All Modes ( $\sum \frac{n_i}{N_i} = 0.41$ )

Figure 5.21: Rainflow histogram blow-up for the 6<sup>th</sup> floor beam.



$$1^{\text{st}} \text{ Mode } \left( \sum \frac{n_i}{N_i} = 0.06 \right)$$



$$\text{All Modes } \left( \sum \frac{n_i}{N_i} = 0.75 \right)$$

Figure 5.22: Rainflow histogram blow-up for the 7<sup>th</sup> floor column.

It is obvious that the cumulative fatigue at the column above, the column below, and the beam at each joint can contribute directly to the connection damage. Figure 5.23 and 5.24 illustrate the cumulative fatigue values at the column above, the column below, and the beam at each connection. It can be observed that the 5<sup>th</sup>, 6<sup>th</sup>, and 7<sup>th</sup> floors have the highest values in figure 5.24. As explained in chapter three, these floors are the floors the experienced significant connection damage during the Northridge Earthquake. Figure 5.25 shows the contribution of higher modes to the cumulative fatigue values and clearly indicate the role of higher modes of vibration in the observed connection damages.

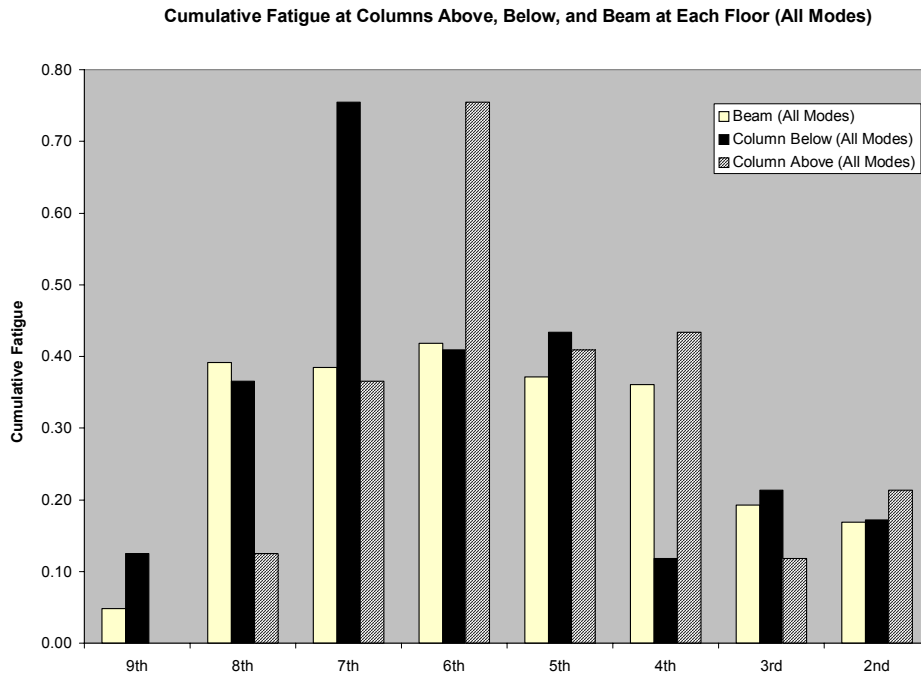


Figure 5.23: Cumulative fatigue at the column above, the column below and the beam at each floor (all modes).

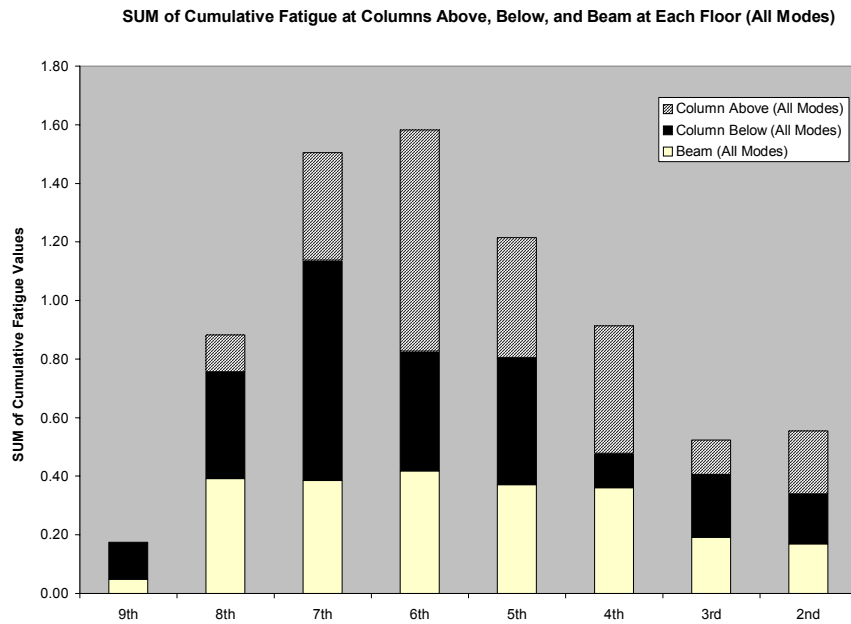


Figure 5.24: Sum of cumulative fatigue values at the column above, the column below and the beam at each floor (all modes).

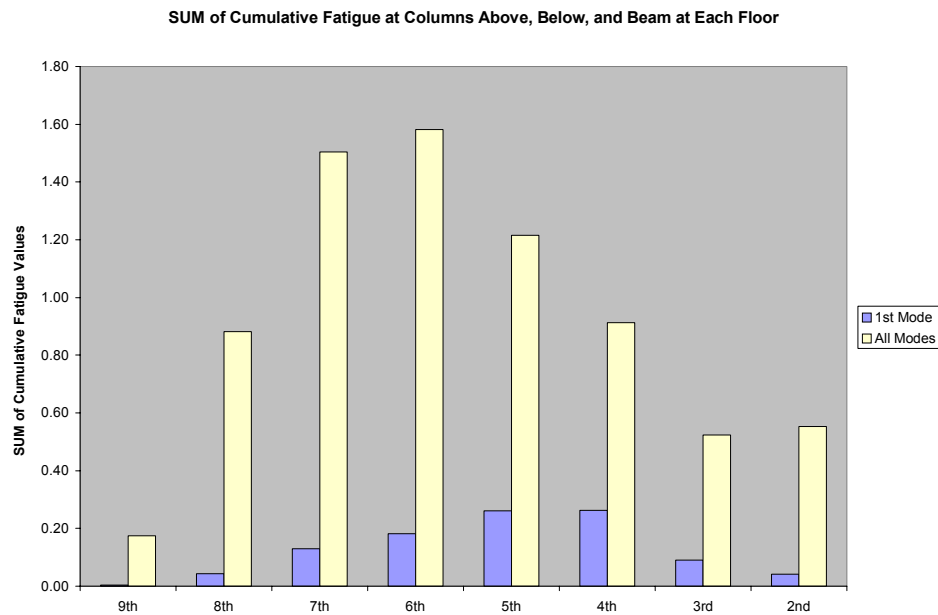


Figure 5.25: Sum of cumulative fatigue values at the column above, the column below and the beam at each floor (1<sup>st</sup> mode vs. all modes).

### 5.4.2 Two-Story Building

Table 5.3 shows the results of the analysis on the beams of the two-story building. It can be observed that the cumulative fatigue created by all modes and the cumulative fatigue created by only the first mode are not significantly different. This comparison can be clearly seen in figure 5.26. It can be observed that the cumulative fatigue created at the 2<sup>nd</sup> floor beam and column of the two story building are high enough to be considered the cause of the observed damages during the Northridge Earthquake. Table 5.4 and figure 5.27 confirm the same observations for the columns of the two-story building. It can be observed in table 5.4 that the *cumulative fatigue* in the 2<sup>nd</sup> floor column is over 1.4 (significantly larger than 1). This observation indicates that theoretically the fatigue life of the column is over and it justifies the observed crack in the flange and through the web of this column.

The above observation is different from what was previously seen in the case of the ten-story building. It is obvious that the cumulative fatigue at the column above, the column below, and the beam at each joint can contribute directly to the connection damage. Figure 5.28 illustrates the cumulative fatigue values at the column above, the column below, and the beam at each connection. It can be observed that the 2<sup>nd</sup> floor has a significantly high value in figure 5.28. As explained in chapter three, this floor is the floor that experienced significant connection damage during the Northridge Earthquake.

BEAM CUMULATIVE FATIGUE ANALYSES RESULTS

Ni (Cycles)													
5 ksi	10 ksi	15 ksi	20 ksi	25 ksi	30 ksi	35 ksi	40 ksi	45 ksi	50 ksi	55 ksi	60 ksi		
3173900	378607.9	109152.2	31991.6	4967.1	1084.3	299.46	98.23	36.75	15.25	6.88	3.33		

Floor	Mode	ni (Cycles)												SUM(ni/Ni)
		5 ksi	10 ksi	15 ksi	20 ksi	25 ksi	30 ksi	35 ksi	40 ksi	45 ksi	50 ksi	55 ksi	60 ksi	
2nd	1st Mode	79	9.5	4.5	2.5	3	2	2	1.5	1	1	0.5	0	0.19003
	2nd Mode	336	0	0	0	0	0	0	0	0	0	0	0	0.00011
	All Modes	78	10.5	4.5	2.5	3	2	2	1.5	1	1	0.5	0	0.19003
Roof	1st Mode	83.5	9.5	2.5	3	4	2	1.5	0.5	0	0	0	0	0.01292
	2nd Mode	336	0	0	0	0	0	0	0	0	0	0	0	0.00011
	All Modes	101	8.5	4	2.5	4	2	1	1	0	0	0	0	0.01634

Table 5.3: Results of the cumulative fatigue analyses on beams of the two-story building.

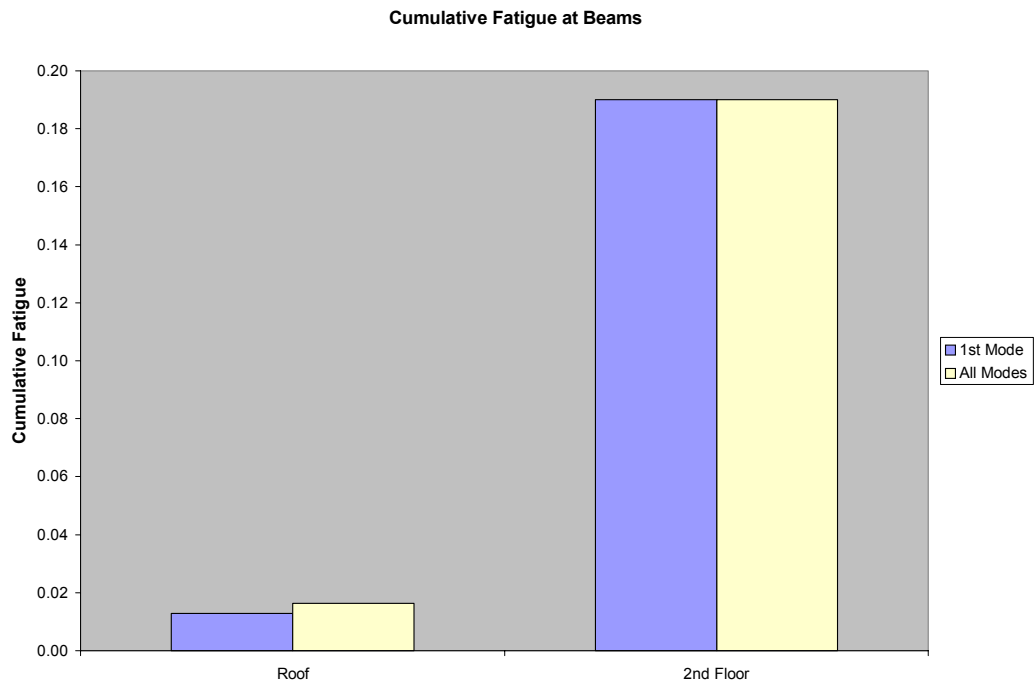


Figure 5.26: Cumulative fatigue at beams of the two-story building (1<sup>st</sup> mode vs. all modes).

COLUMNS CUMULATIVE FATIGUE ANALYSES RESULTS

Ni (Cycles)												
5 ksi	10 ksi	15 ksi	20 ksi	25 ksi	30 ksi	35 ksi	40 ksi	45 ksi	50 ksi	55 ksi	60 ksi	
3173900	378607.9	109152.2	31991.6	4967.1	1084.3	299.46	98.23	36.75	15.25	6.88	3.33	

Floor	Mode	ni (Cycles)											SUM(ni/Ni)	
		5 ksi	10 ksi	15 ksi	20 ksi	25 ksi	30 ksi	35 ksi	40 ksi	45 ksi	50 ksi	55 ksi		60 ksi
2nd	1st Mode	70.5	11.5	5	4	3.5	1	2.5	0.5	1	3	0	4	1.44042
	2nd Mode	336	0	0	0	0	0	0	0	0	0	0	0	0.00011
	All Modes	75.5	11.5	5	5	2.5	1	2.5	0.5	2	2	0	4	1.40189
Roof	1st Mode	83	8	4.5	2.5	2.5	2	2	1.5	0.5	0	0	0	0.03807
	2nd Mode	336	0	0	0	0	0	0	0	0	0	0	0	0.00011
	All Modes	99.5	9	4.5	2.5	1.5	3	2	1	1	0	0	0	0.04731

Table 5.4: Results of the cumulative fatigue analyses on columns of the two-story building.

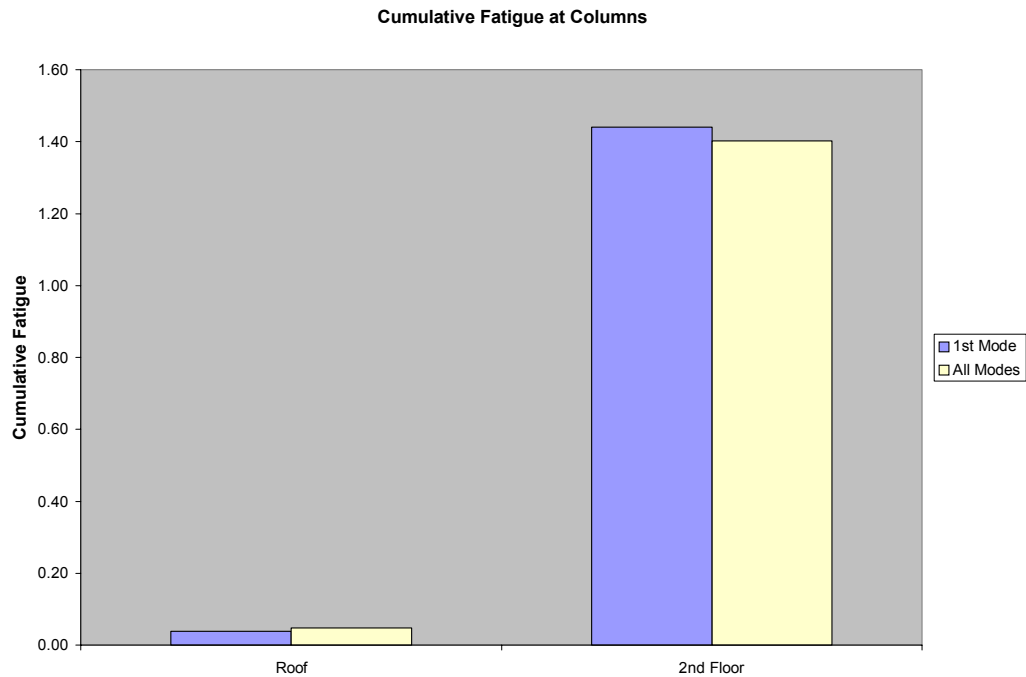


Figure 5.27: Cumulative fatigue at columns of the two-story building (1<sup>st</sup> mode vs. all modes).

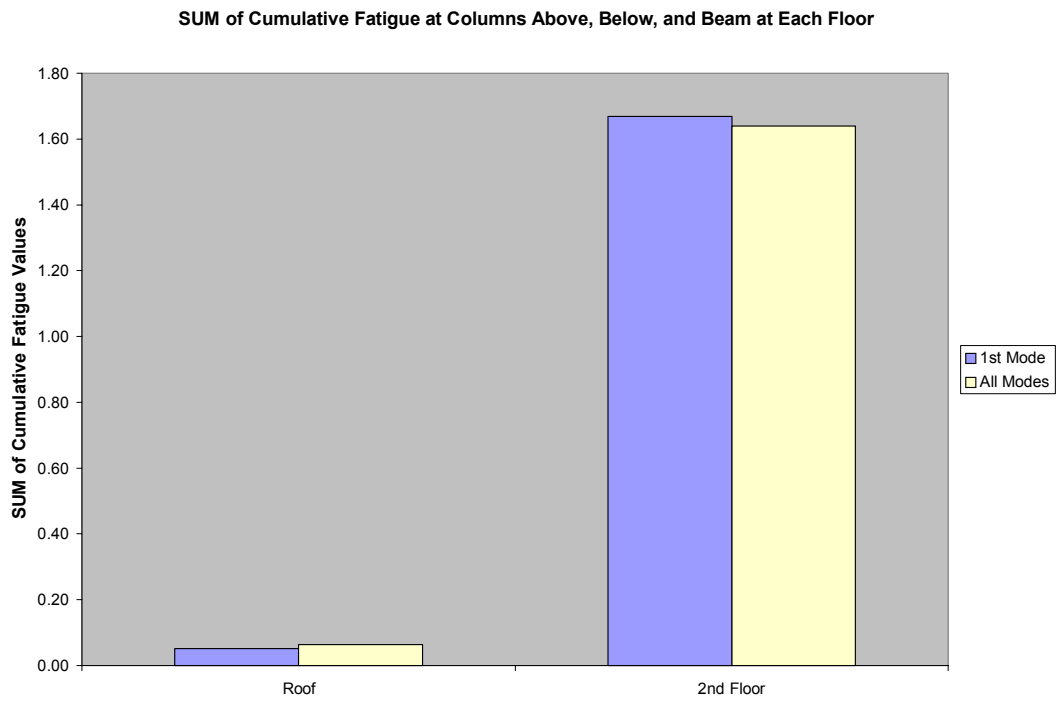


Figure 5.28: Sum of cumulative fatigue values at the column above, the column below and the beam at each floor (1<sup>st</sup> mode vs. all modes).

## CHAPTER 6: CONCLUSIONS

As described in the previous chapter, the result of the analytical study on the two-story building indicates that the first mode created a high percentage of cumulative fatigue in the connections of the investigated frame. However, the study of the ten-story building clearly shows that the contribution of higher modes of vibration in the beam and column stress histories significantly increased the cumulative fatigue relative to that created by the first mode alone. Investigations of the damage pattern in the investigated ten-story building indicate that the effect of higher modes of vibration was significant in the connection damage observed after the Northridge Earthquake.

Figure 6.1 illustrates the damage in the ten-story building. It can be observed that the cumulative fatigue distribution at the investigated connections match the observed damage during the Northridge Earthquake. However, the cumulative fatigue created by the 1<sup>st</sup> mode only (as shown in figure 6.1) does not appear to match the observed damage distribution. This observation indicates that the higher mode effects are significant in this building. The damage indicator used in this comparison for quantifying the connection damage in the ten-story building shows the number of damaged locations in the beams on both sides of the joints and columns above and below the joints at each level in all the moment frames in the investigated direction (East-West).

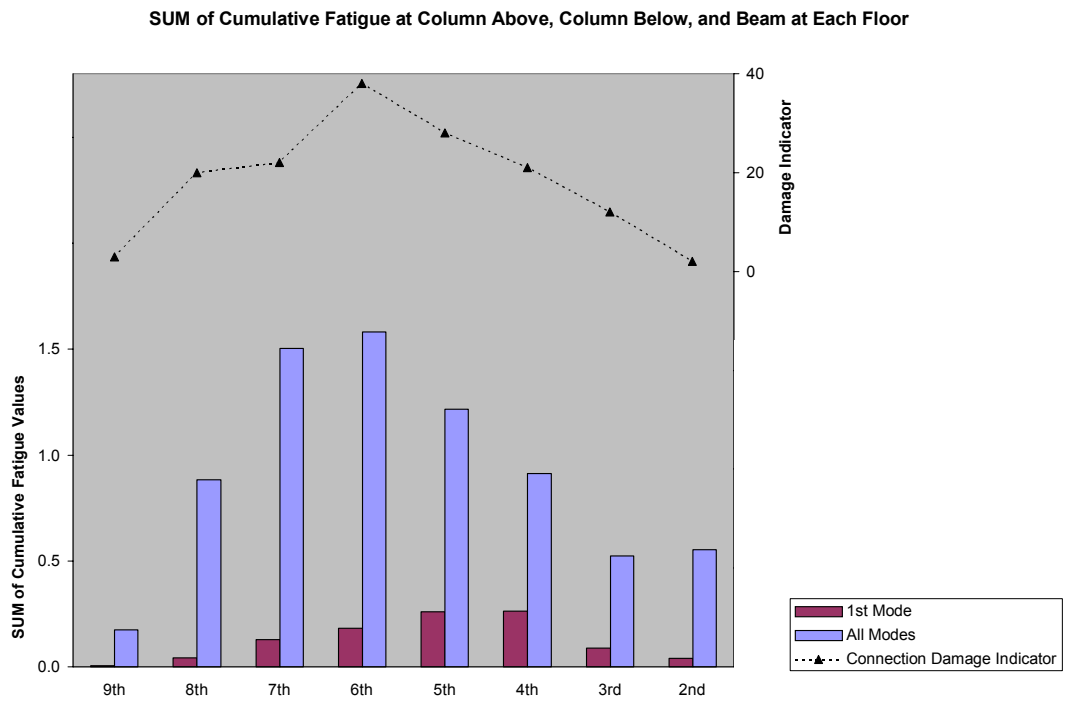


Figure 6.1: Comparison between cumulative fatigue distribution and observed damage in the ten-story building.

## 6.1 Conclusions

The general conclusions of this study can be summarized as follows:

1. Comparison between cumulative fatigue analyses of first mode and all modes clearly indicates that *higher mode effects* are significant in the ten-story building.

2. Comparison between the cumulative fatigue caused by the *first mode* only and cumulative fatigue caused by *all modes* of vibration indicates that the latter is significantly larger at each beam and column in the ten-story building. This is the result of *higher mode effects*.
3. In the investigated ten-story building, the contribution of the higher modes of vibration significantly increases the cumulative fatigue at the end of each member. This is because of the contribution of higher mode stresses that can increase the total stress significantly (relative to 1st mode stress only) at each point in time.
4. In both buildings, *low-cycle fatigue* is significant at all the investigated members. As expected, *high-cycle fatigue* was not important during the Northridge Earthquake.
5. In both buildings, cumulative fatigue distribution at the investigated beams and columns matches observed damage during the Northridge Earthquake.
6. Distribution of the sum of cumulative fatigue values at the column above, the column below, and the beam at each connection matches the distribution of connection damage indicator introduced earlier in this chapter.

7. This study shows that the following wording from the “AISC Steel Construction Manual” [2], appears to be incorrect:

“*Fatigue* shall be considered in accordance with Appendix 3, Design for Fatigue, for members and their *connections* subject to repeated *loading*. Fatigue need not be considered for seismic effects or for the effects of wind loading on normal building *lateral load resisting systems* and building enclosure components.”

Fatigue can play a major role in the behavior of structures during seismic events and needs to be further investigated and carefully considered in the seismic design of certain structures. The result of the current research emphasizes that *low-cycle fatigue* appears to be the cause of connection fatigue failures in both of the investigated buildings similar to that observed during the Northridge Earthquake.

8. As described earlier, *low damping* and *vertical irregularity* (set-back) are the characteristics of the investigated ten-story building which contributed to the results. It appears that other steel buildings having these characteristics might need some additional analyses.
9. The *low damping* may be important in the results of this study. One way to improve this is to include supplemental damping [3].

10. Response data does not support the existence of plastic hinges at failure locations. Recorded data and calculations indicate pre-dominate elastic response. Hence, fatigue (low-cycle) must be significant in explaining the overall behavior (damage).
  
11. The buildings used in this study have experienced only one earthquake. Since the cumulative fatigue created by past events is remembered by the connection, it appears that *low-cycle fatigue* damage will be more significant for the buildings that have experienced two or more earthquakes in their life. In other words, the behavior of the building during an earthquake depends on the fatigue accumulated in the connections from all the past major seismic events.

## **6.2 Future Studies**

As discussed earlier in this document, the current study tried to establish the link between existing research on fatigue and fracture mechanics in the area of material science and apply it to the structural engineering field in general and to beam-column moment connection applications in particular.

The current research tried to use all applicable technical resources and fatigue test results available at the time of this work. Since the available fatigue tests for the investigated beam-column connection detail are limited, a probabilistic approach is not possible. Therefore, the developed S-N curve, and consequently the fatigue analyses results, are based on the available test data at the time of this study. Obviously, performing more fatigue tests especially in the low-cycle region and creating more data points on the S-N curve could be an interesting topic for future research. Also, further empirical study on the area of the S-N curve that falls between the low-cycle and high-cycle regions (mid-cycle) could be a major focus of future studies. In addition, analyzing more instrumented buildings will be useful in better understanding of the problem.

Furthermore, studying the effect of *defects* on fatigue life of the connection will be an interesting topic for future research. The current study was primarily focused on stresses at the beams and columns. As a result, the effect of principal stresses at the connection was never investigated. This appears to be an interesting topic for further research.

## BIBLIOGRAPHY

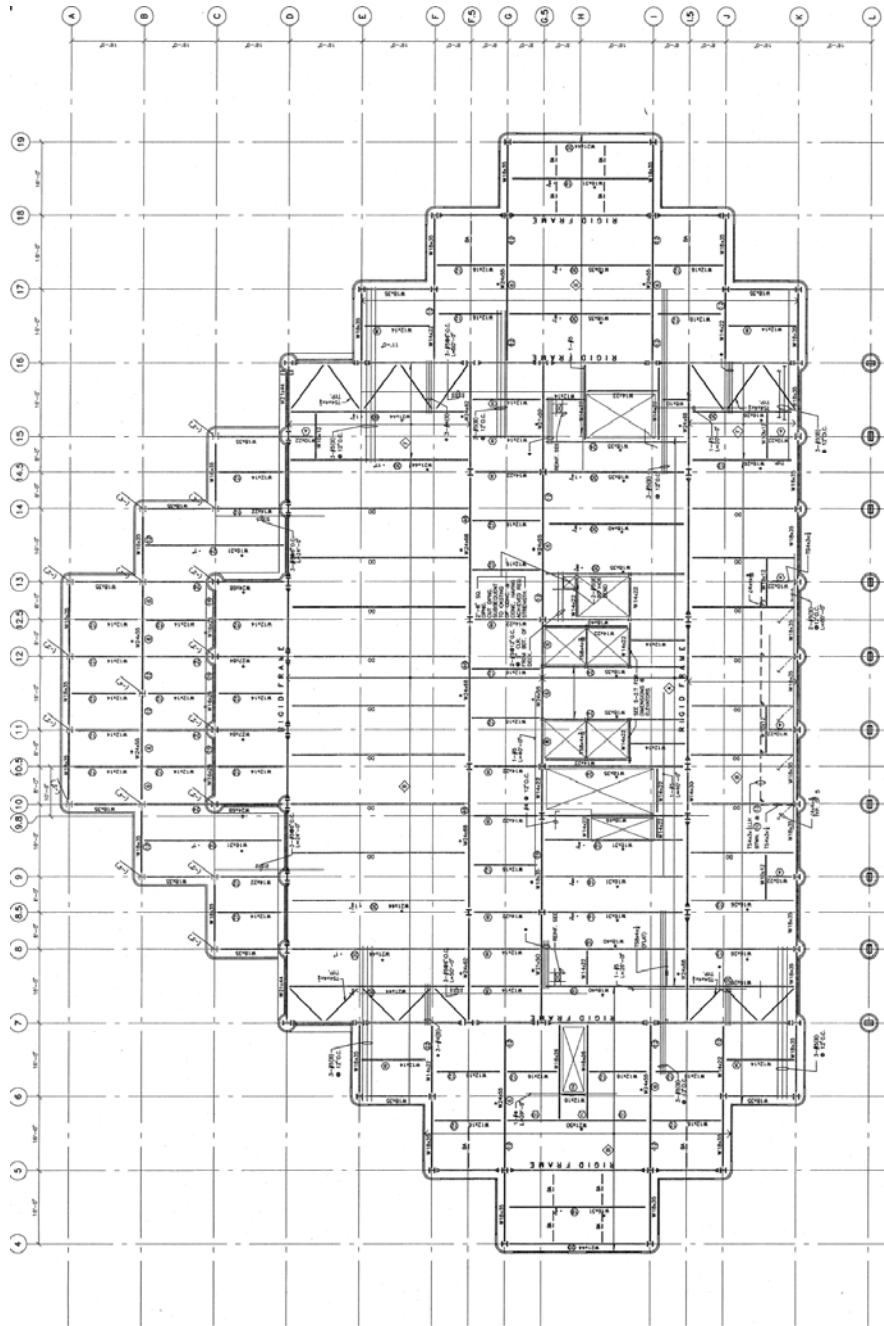
1. American Association of State Highway and Transportation Officials (1990). *Guide Specifications for Fatigue Evaluation of Existing Steel Bridges*. Washington, D.C.: AASHTO.
2. American Institute of Steel Construction (2006). *Steel Construction Manual*. Thirteenth Edition. Chicago, Illinois: AISC.
3. Anderson, J.C., & Bertero, V.V. (1998). *Seismic response of a 42-story steel building*. The Loma Prieta, California, Earthquake of October 17, 1989, Building Structures. U.S. Geological Survey Professional Paper 1552-C, C113-C139.
4. Anderson, J.C., & Duan, X. (1998, May). *Repair/Update procedures for welded beam to column connections*. Pacific Earthquake Engineering Research Center, PEER 98/03.
5. ATC 24 (1992). *Guidelines for cyclic seismic testing of components of steel structures*. Applied Technology Council.
6. Barsom, J.M. (2000, May 1). *Development of fracture toughness requirements for weld metals in seismic applications*. SAC steel project task 7.1.3.
7. Barsom, J.M., & Rolfe, S.T. (1977). *Fracture and fatigue control in structures: Applications of fracture mechanics*. New Jersey: Prentice Hall.
8. Bertero, V.V., & Popov, E. (1965, February). Effect of large alternating strains of steel beams. *Proceedings of the American Society of Civil Engineers, Journal of structural division*. 1-12.
9. Dowling, Norman E. (1993). *Mechanical behavior of materials: Engineering methods for deformation, fracture, and fatigue*. New Jersey: Prentice Hall.
10. FEMA 267 (1995, August). *Interim Guidelines: Evaluation, Repair, Modification and Design of Welded Steel Moment Frame Structures*.
11. FEMA 267A (1997, January). *Interim Guidelines Advisory No. 1, Supplement to FEMA 267*.
12. FEMA 274 (1997, October). *NEHRP Commentary on the Guidelines for the Seismic Rehabilitation of Buildings*.

13. FEMA 350 (2000, July) and Errata (2001, March). *Recommended Seismic Design Criteria for New Steel Moment-Frame Buildings*.
14. FEMA 351 (2000, July). *Recommended Seismic Evaluation and Upgrade Criteria for Existing Welded Steel Moment-Frame Buildings*.
15. FEMA 352 (2000, July). *Recommended Post-Earthquake Evaluation and Repair Criteria for Welded Steel Moment-Frame Buildings*.
16. FEMA 353 (2000, July). *Recommended Specifications and Quality Assurance Guidelines for Steel Moment Frame Construction for Seismic Applications*.
17. FEMA 355A (2000). *State of the Art Report on Base Metals and Fracture*.
18. FEMA 355B (2000). *State of the Art Report on Welding and Inspection*.
19. FEMA 355D (2000). *State of the Art Report on Connection Performance*.
20. FEMA 355F (2000). *State of the Art Report on Performance Prediction and Evaluation of Steel Moment-Frame Buildings*.
21. Fisher, J.W. (1984). *Fatigue and Fracture in Steel Bridges, Case Studies*. John Wiley & Sons, Inc.
22. Fisher, J.W., & Yen, B.T. (1977). Fatigue Strength of Steel Members with Welded Details. *Engineering Journal, American Institute of Steel Construction*. Fourth Quarter, 1977.
23. Fisher, J.W., Kulak, G.L., & Smith, I.F.C. (1998, May). *A Fatigue Primer for Structural Engineers*. National Steel Bridge Alliance.
24. Irwin, G.R., 1948. *Fracture dynamics*. In: Jonassen, F., Roop, W.P., Bayless, R.T. (Eds.), *Fracturing of Metals*. American Society for Metals, Cleveland, pp. 147–166.
25. Krawinkler, H., Zohrei, M., Lashkari-Irvani, B., Cofie, N.G., & Hadidi-Tamjed, H. (1983, September). *Recommendations for experimental studies on the seismic behavior of steel components and materials*. Report No. 61, The John A. Blume Earthquake Engineering Center, Department of Civil Engineering, Stanford University.

26. Kuwamura, H., & Suzuki, T. (1992). Low-Cycle fatigue resistance of welded joints of high-strength steel under earthquake loading. *Proceedings of the Tenth World Conference on Earthquake Engineering*. 19-24 July 1992, Madrid, Spain, 2851-2856.
27. Maranian, P., Metzger, A., & Stovner, E. (have not yet been published at the time this dissertation was written). *Considerations on reducing brittle and fatigue failures in steel structures (Draft Version)*. Technical Council on Forensic Engineering of the American Society of Civil Engineers.
28. Orowan, E., 1945. Notch brittleness and the strength of metals. *Proceedings of the Society of Engineers and Shipbuilders*, Paper No. 1063, Scotland.
29. Owens, G.W., & Knowles, P.R. (Editors). *Steel Designers' Manual*. Fifth Edition. The Steel Construction Institute. Blackwell Science.
30. Partridge, J.E., Allen, J., & Richard, R.M. (2002). *Failure analysis of structural steel connections in the Northridge and Loma Preita, California earthquakes*.
31. Partridge, J.E., Paterson, S.R., & Richard, R.M. (2000). Low cycle fatigue tests and fracture analyses of bolted-welded seismic moment frame connections. *STESSA 2000, Third International Conference*. August 21-24, 2000, Montreal, Canada.
32. Partridge, J.E., Paterson, S.R., & Richard, R.M. (2003). ATC-24 cumulative damage tests and fracture analyses of bolted-welded seismic moment frame connections. *Proceedings of the Third Congress, Oct. 19-21, 2003, San Diego, CA*. Technical Council on Forensic Engineering of the American Society of Civil Engineers. 142-157.
33. Popov, E.P., & Pinkney, R.B. (1969, March). Cyclic yield reversal in steel building connections. *Proceedings of the American Society of Civil Engineers, Journal of structural division*. 327-353.
34. Richard, R.M., Allen, J., & Partridge, J.E. (2001). Accumulated seismic connection damage based upon low cycle fatigue connection tests. *Proceedings of SEAOC 2001 70<sup>th</sup> Annual Convention*.
35. Richard, R.M., Partridge, J.E., & Allen, J. *Low cycle fatigue and seismic performance of steel connections*.

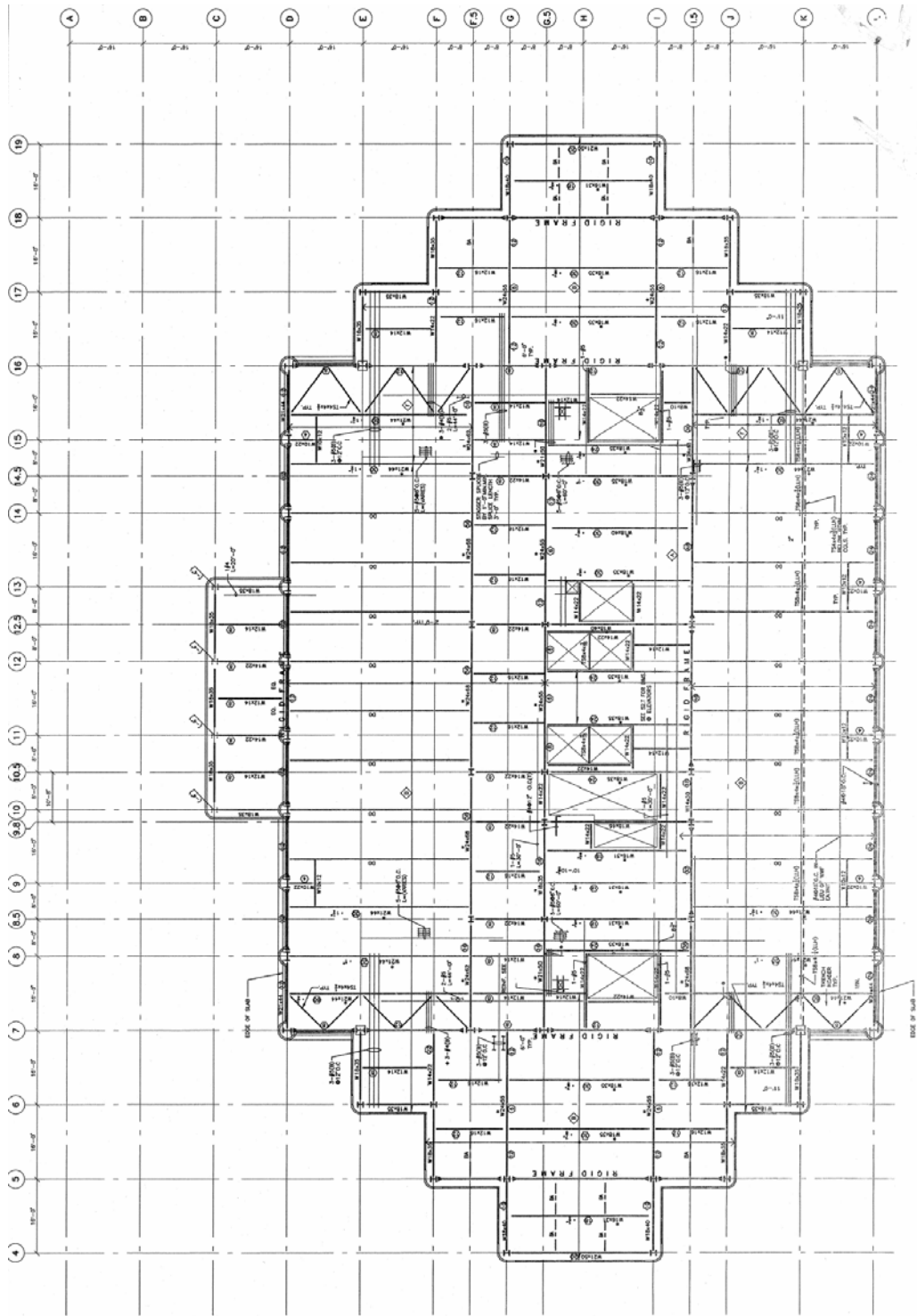
36. Richard, R.M., Partridge, J.E., Allen, J., & Radau, S. (1995, October). Finite element analysis and tests of beam-to-column connections. *Modern Steel Construction*. 44-47.
37. Ricles, J.M., Mao, C., Lu, L.W., & Fisher, J.W. (2000, August). *Development and evaluation of improved details for ductile welded unreinforced flange connections*. Final report, SAC Task 7.05. ATLSS Report No. 00-04.
38. SEAOC Seismology Committee, FEMA 350 Task Group (2002, January). *Commentary and recommendations on FEMA 350*.
39. Ts'ao, H.S., & Werner, S.D. (1975, May). *Determination of Equivalent Response Cycles for Use in Earthquake-Induced Fatigue Analyses*. Technical Information Center, Energy Research and Development Administration. El Segundo, California: Agbabian Associates.

## APPENDIX A: TEN-STORY BUILDING DRAWINGS



a. 2<sup>nd</sup> floor framing plan.

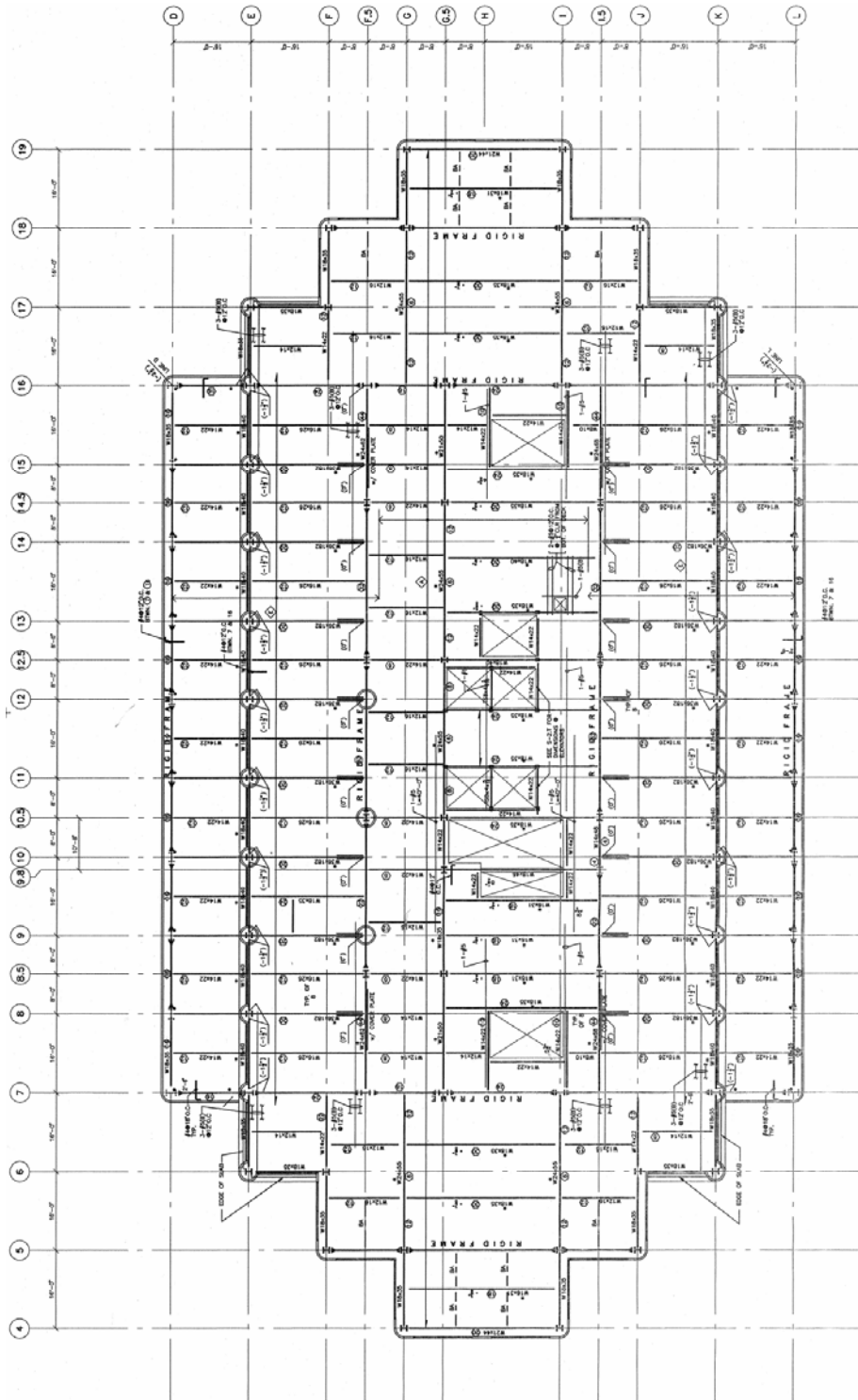
Figure A.1: Ten-story building framing plans.  
[Brandow and Johnston, Inc. drawings]



b. 3<sup>rd</sup> floor framing plan.

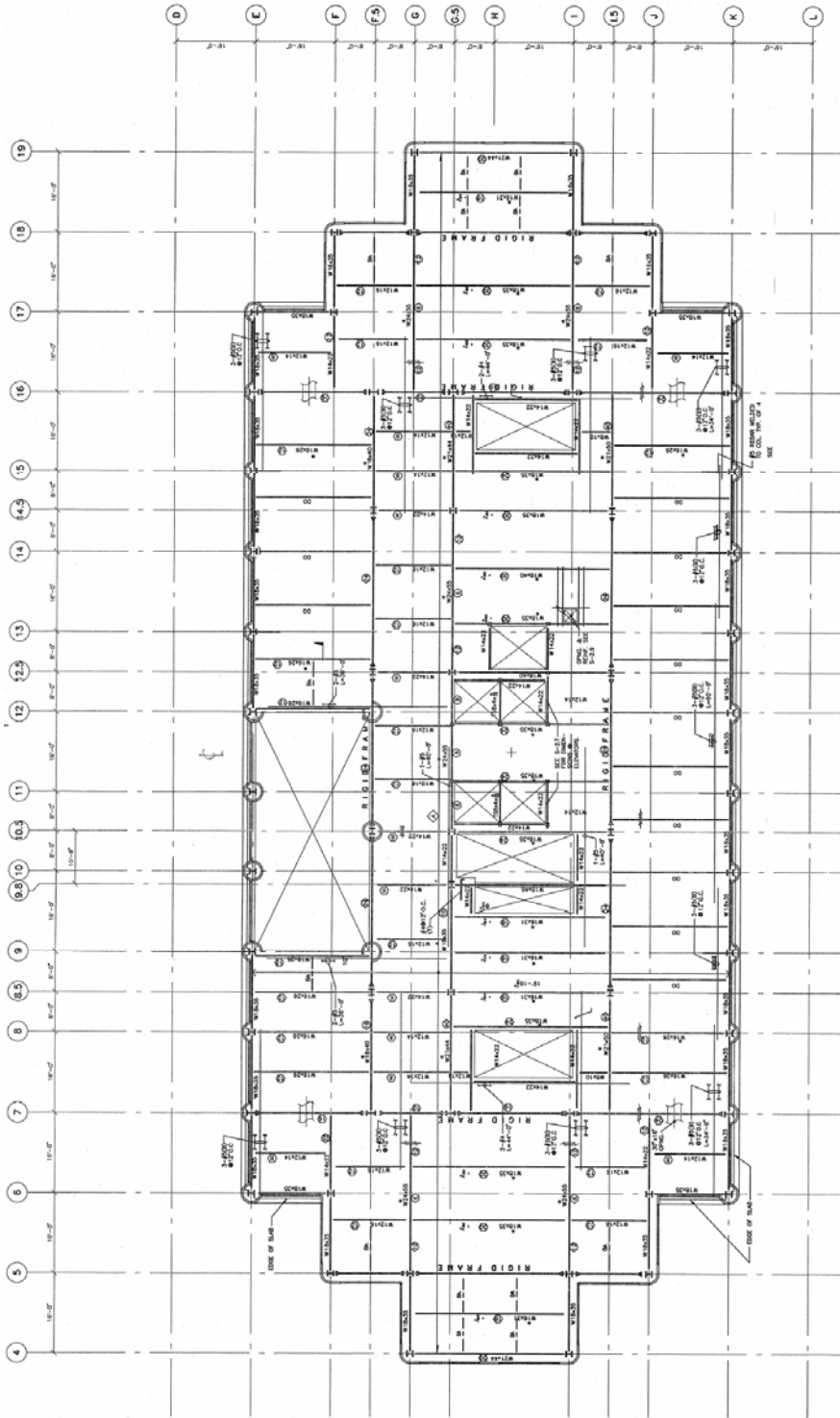
Figure A.1, Continued: Ten-story building framing plans.





d. 9<sup>th</sup> floor framing plan.

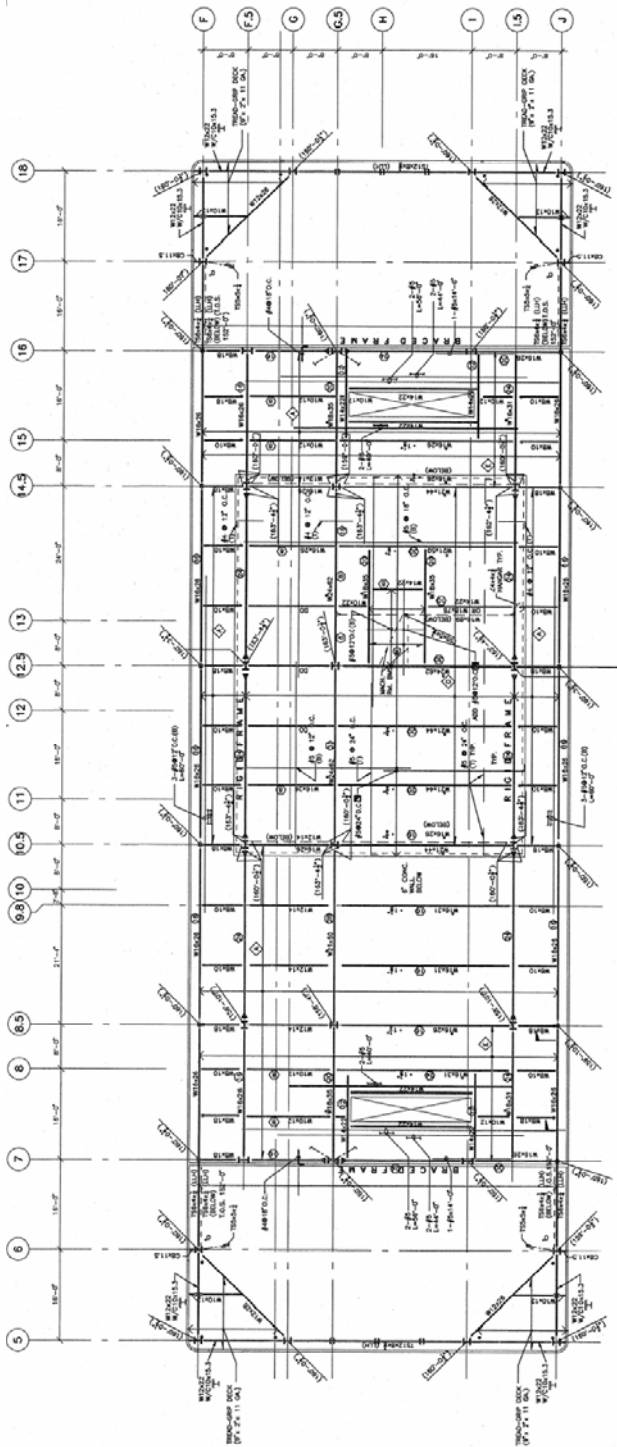
Figure A.1, Continued: Ten-story building framing plans.



e. 10<sup>th</sup> floor framing plan.

Figure A.1, Continued: Ten-story building framing plans.





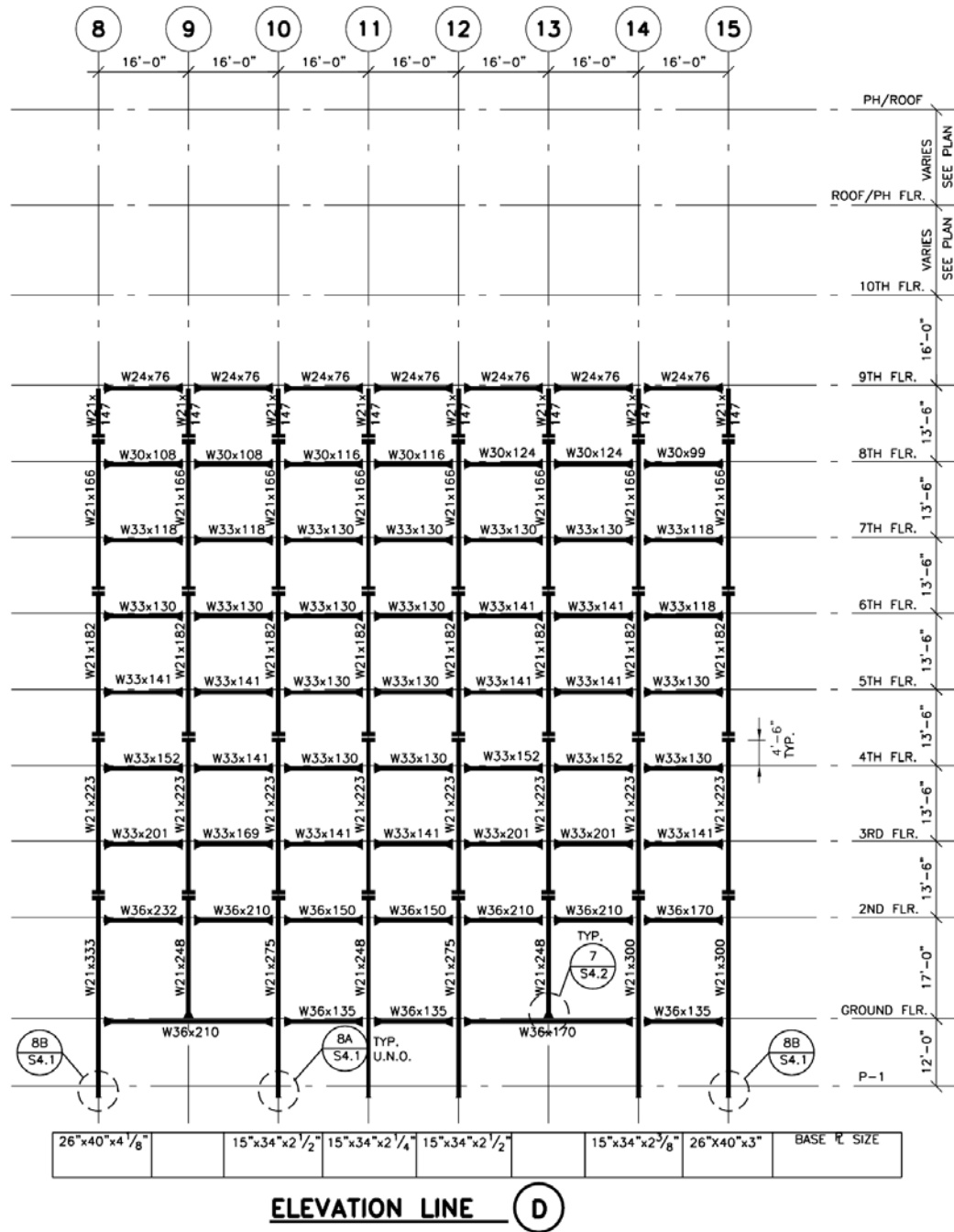


Figure A.2: Ten-story building frame elevations.  
[Brandow and Johnston, Inc. drawings]

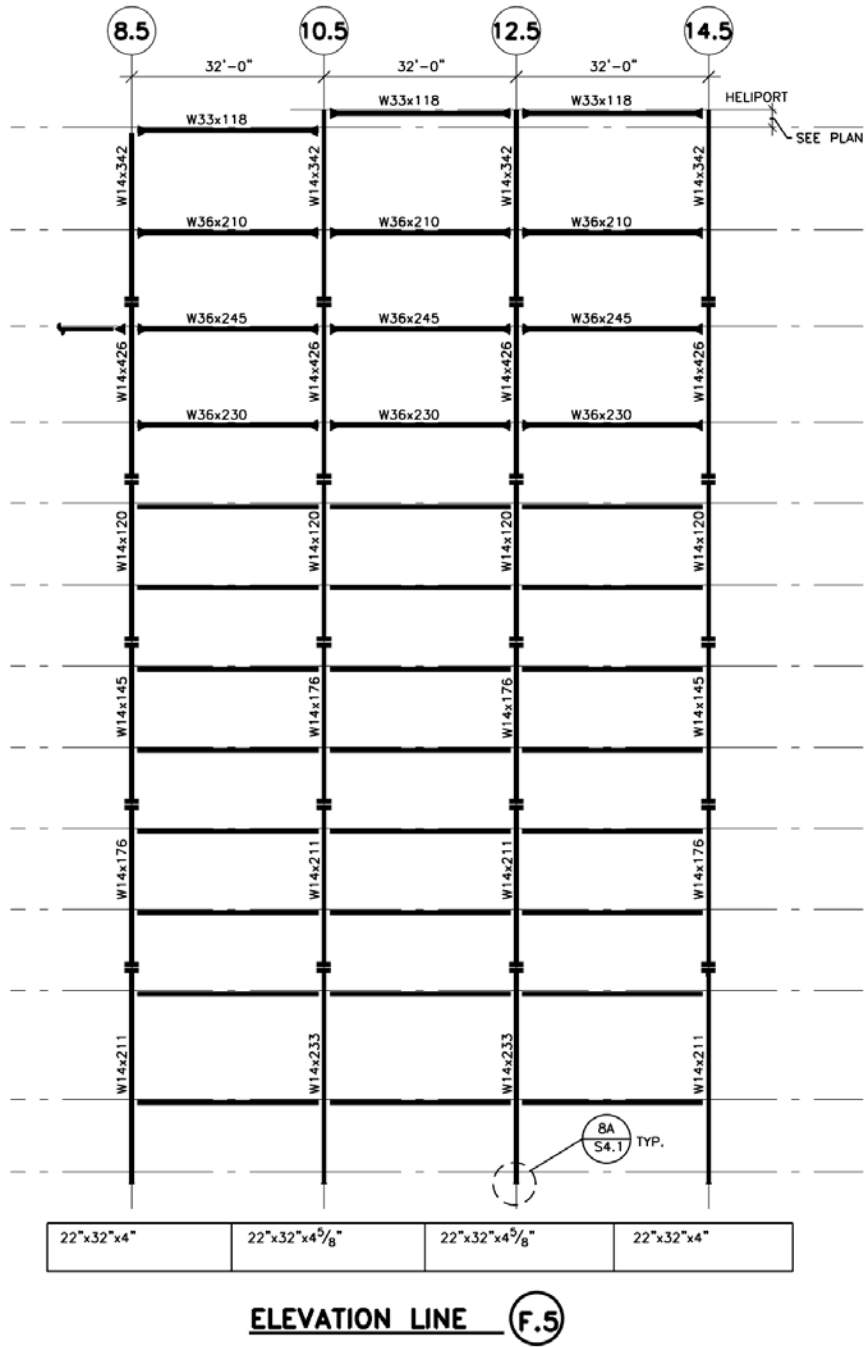


Figure A.2, Continued: Ten-story building frame elevations.



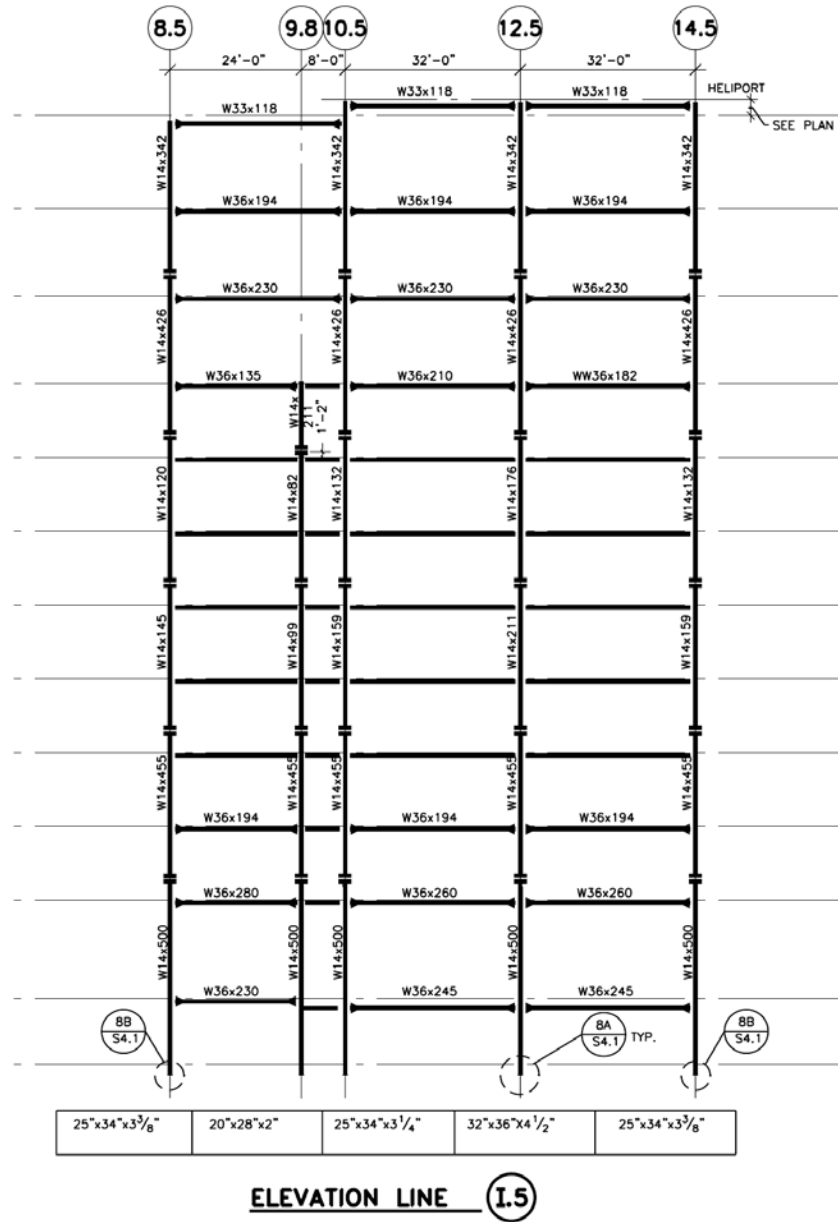


Figure A.2, Continued: Ten-story building frame elevations.

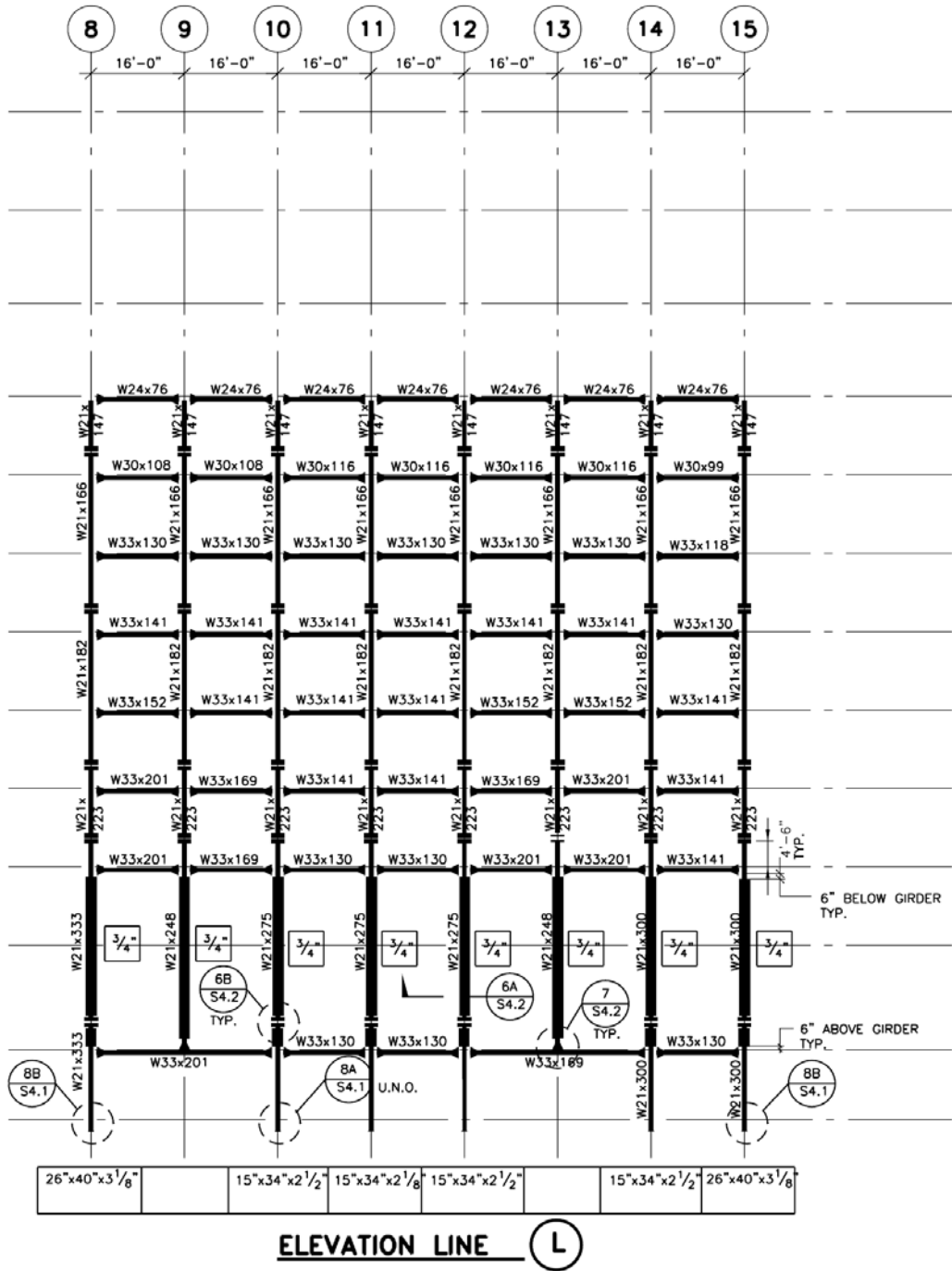


Figure A.2, Continued: Ten-story building frame elevations.

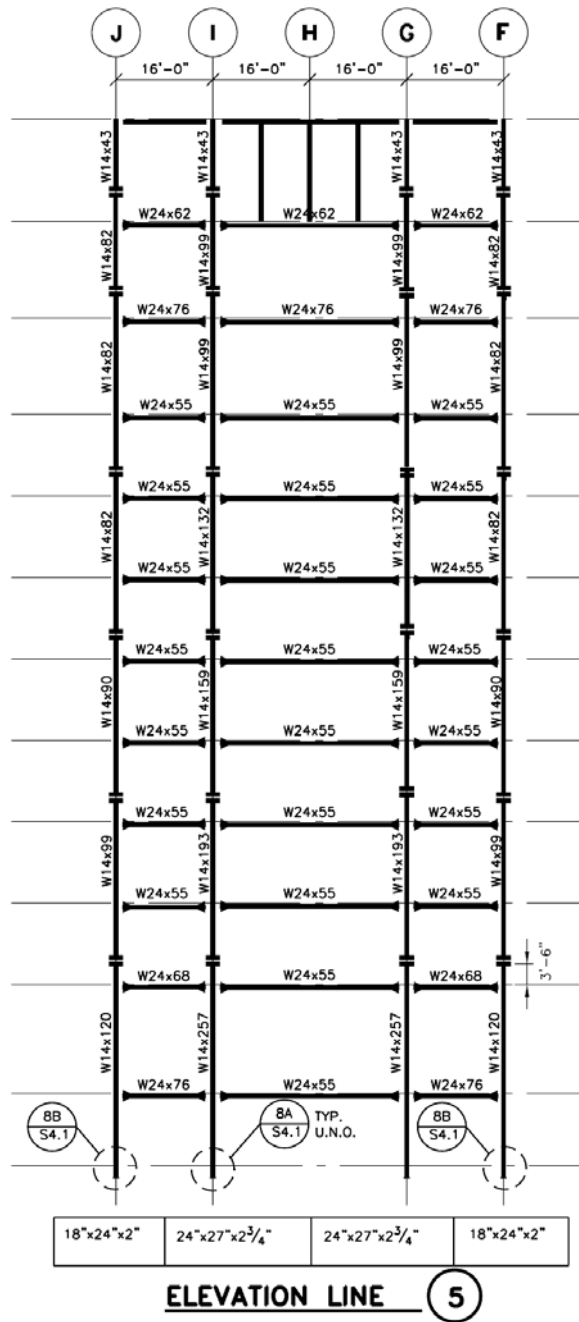


Figure A.2, Continued: Ten-story building frame elevations.

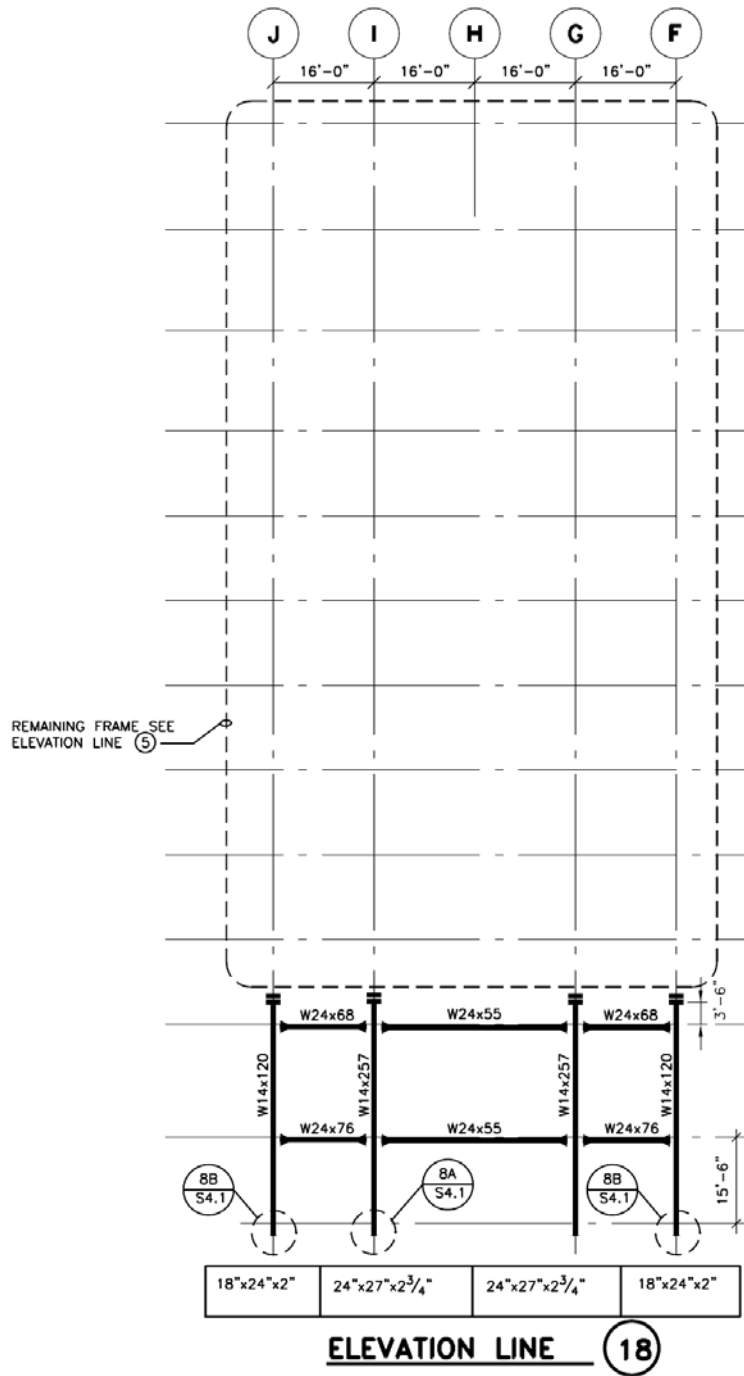


Figure A.2, Continued: Ten-story building frame elevations.

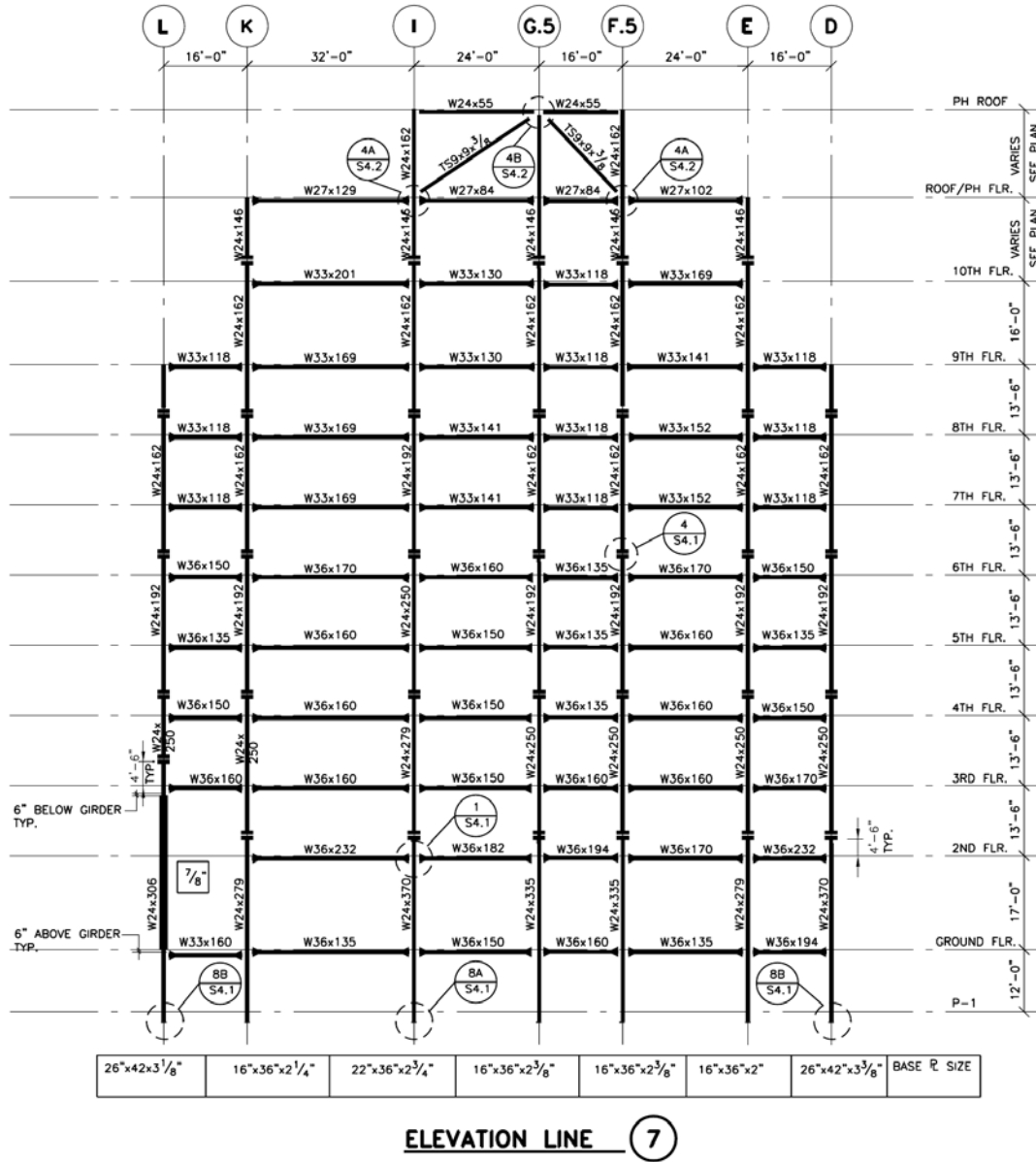
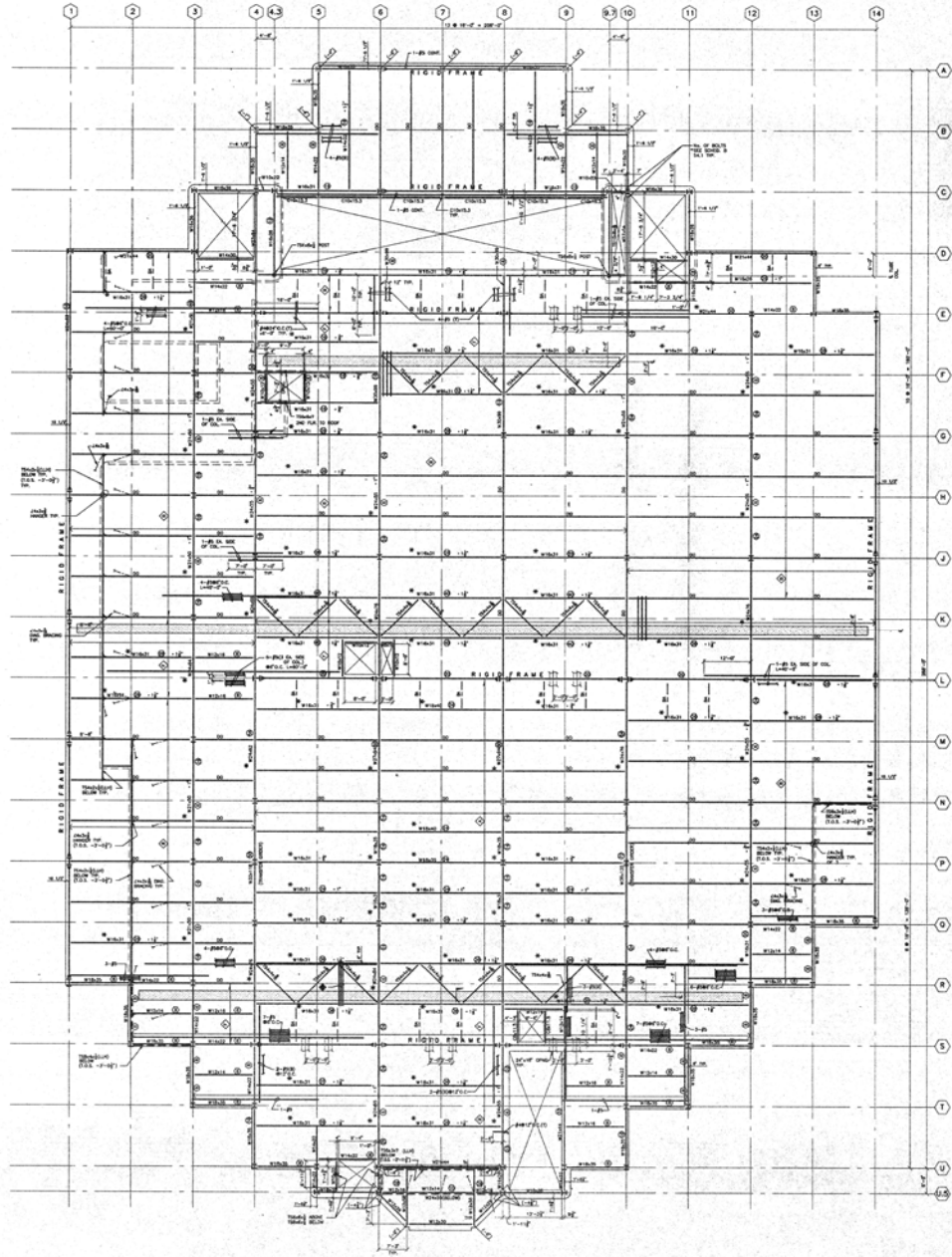


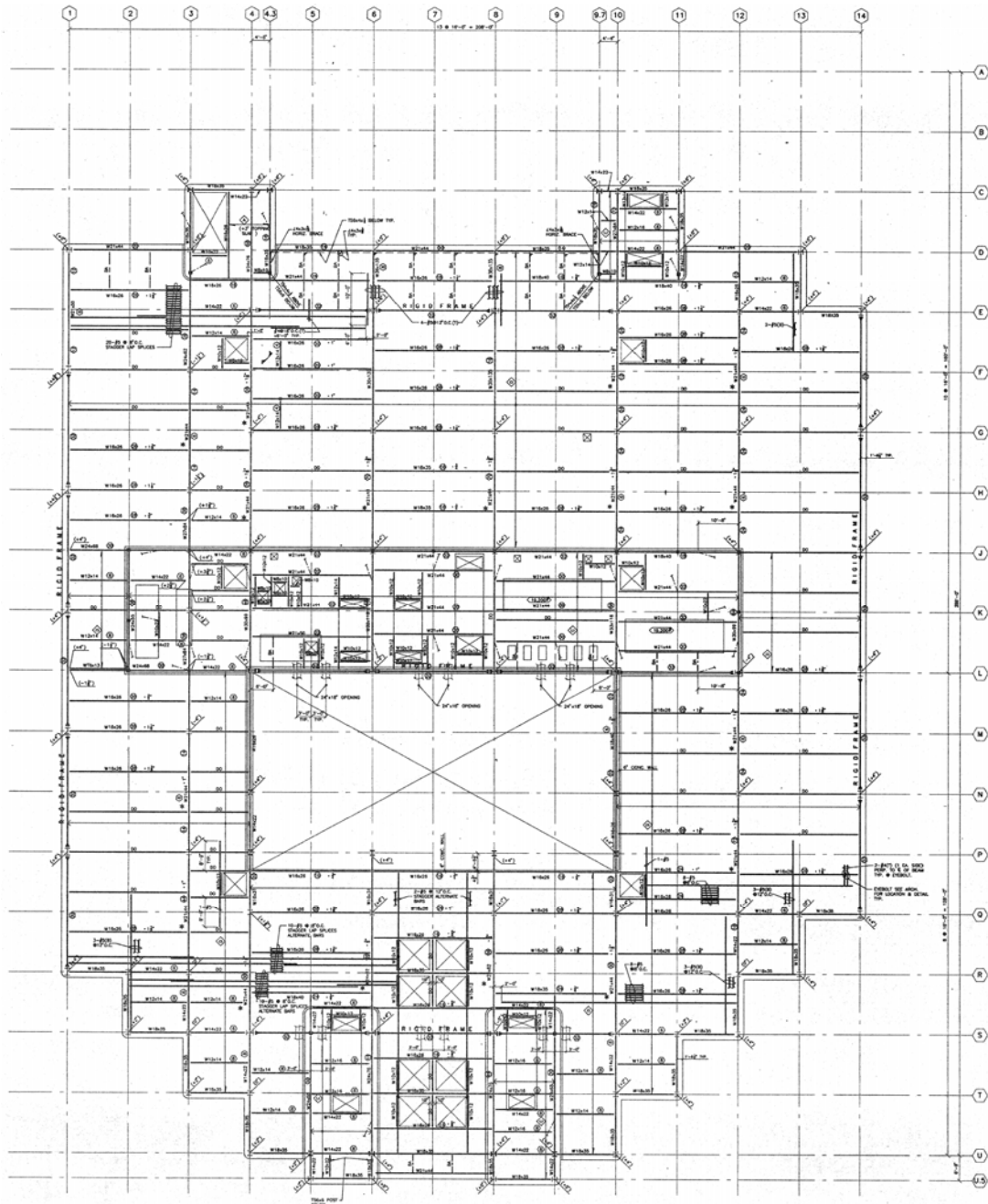
Figure A.2, Continued: Ten-story building frame elevations.

## APPENDIX B: TWO-STORY BUILDING DRAWINGS



a. 2<sup>nd</sup> floor framing plan.

Figure B.1: Two-story building framing plans.  
[Brandow and Johnston, Inc. drawings]



b. Roof framing plan

Figure B.1, Continued: Two-story building framing plans.

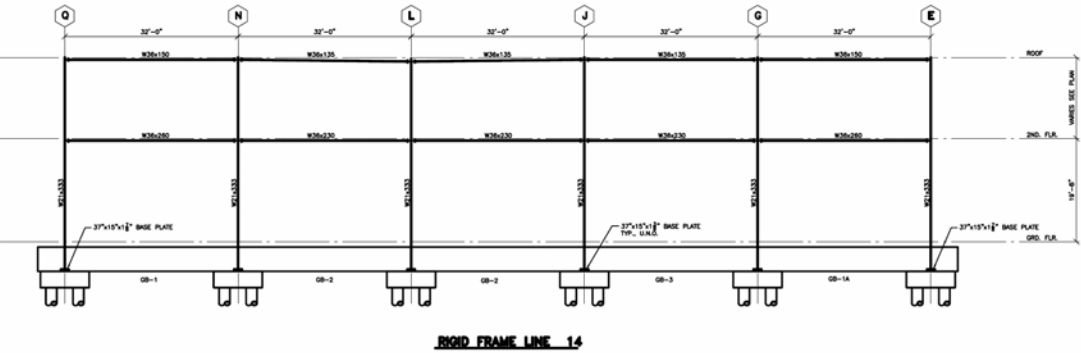
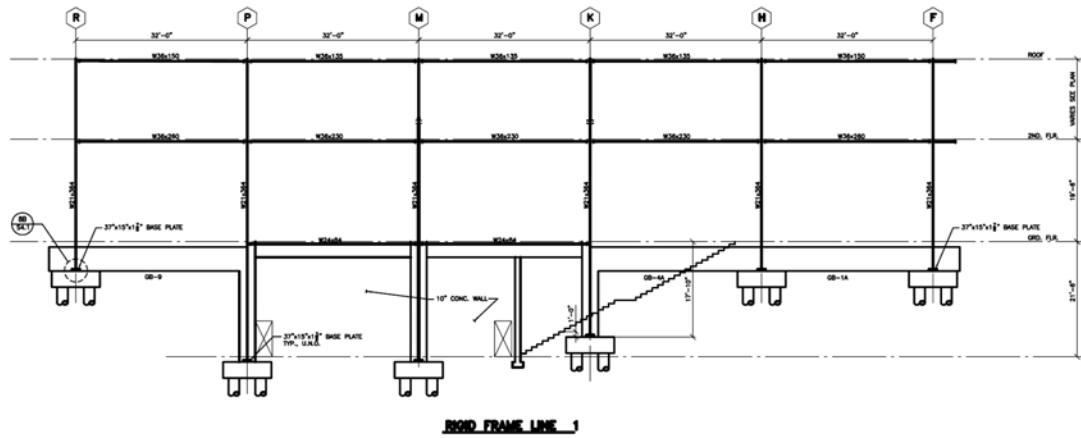


Figure B.2: Two-story building frame elevations.  
 [Brandow and Johnston, Inc. drawings]

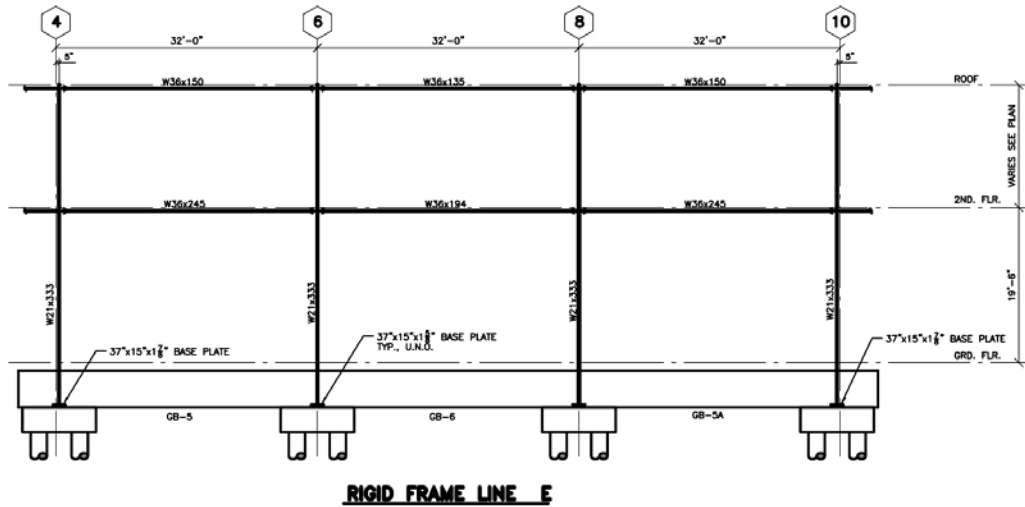
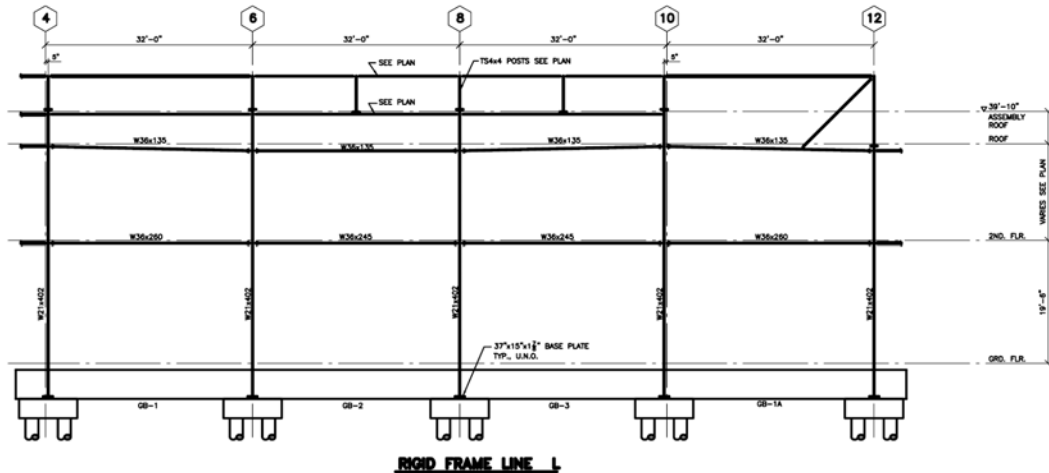


Figure B.2, Continued: Two-story building frame elevations.

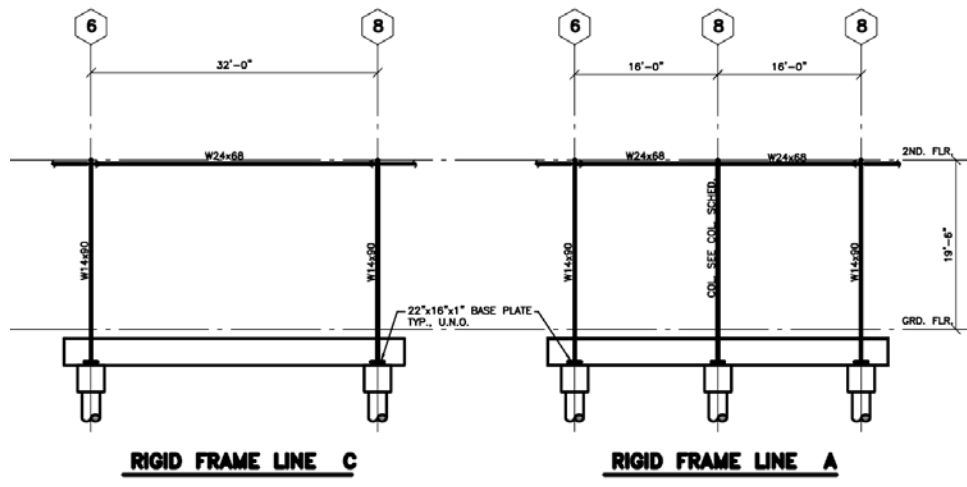
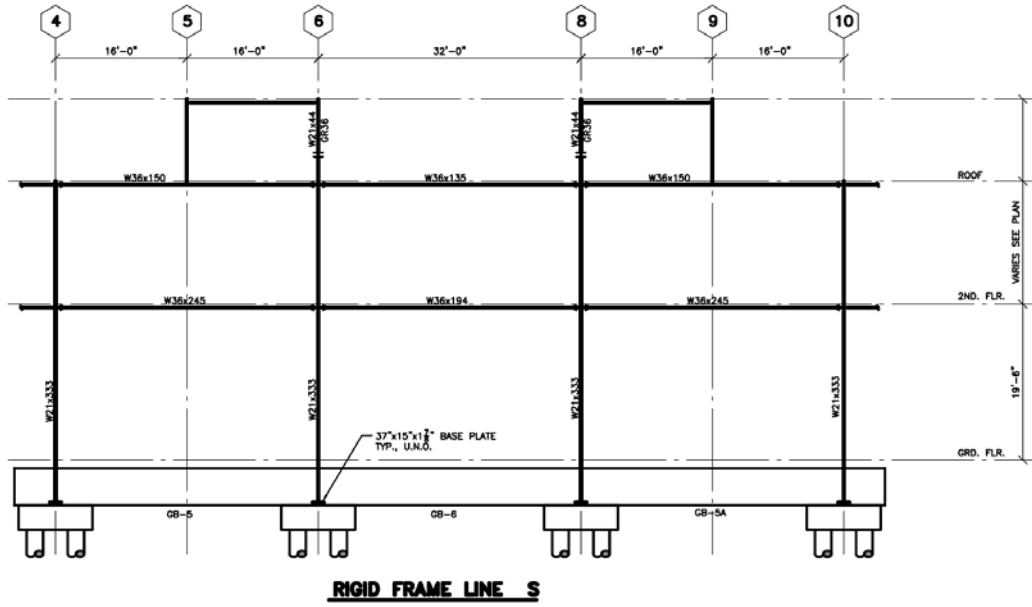


Figure B.2, Continued: Two-story building frame elevations.